Developing computational frameworks for multi-scale optimisation in multi-energy systems

Ruiqiu Yao

Supervisors:

Dr Yukun Hu

Prof Liz Varga

A thesis submitted in partial fulfilment of

the requirements for the degree of

Doctor of Philosophy

Department of Civil, Environmental and Geomatic Engineering

University College London

December 2025

Declaration

I, Ruiqiu Yao, confirm that the work presented in this thesis is my own. Where information has been derived from other sources, I confirm that this has been indicated in the thesis.

Signed:

Date:

Abstract

This thesis addresses the critical need to develop computational frameworks to manage the nested hierarchy of decision-making complexities that emerge across the operational, transactional, and strategic scales of multi-energy systems (MES), driven by the global transition towards sustainable and resilient energy infrastructures. The global transition towards the sustainable MES is driving fundamental shifts in uncertainty, decentralisation, and strategic evaluation.

Three significant research gaps are identified. First, at the operational scale, existing optimisation methods lack the capacity to manage deep uncertainty associated with novel assets like Liquid Air Energy Storage (LAES) under volatile market conditions. Second, at the transactional scale, current aggregation models lack consideration of dynamic competitive interactions among multiple aggregators and prosumers, particularly concerning computational efficiency and data privacy. Third, at the strategic scale, there is a lack of integrated Multi-Criteria Decision-Making (MCDM) frameworks for international hydrogen supply chains that simultaneously account for discounted techno-economic performance, life-cycle environmental impacts, and carrier efficiencies.

This thesis systematically addresses these gaps through novel methodological contributions and case studies. First, a novel hybrid optimisation method combining Information Gap Decision Theory (IGDT) and State Transition Algorithm (STA) within a multi-agent framework is proposed to enable risk-aware scheduling of LAES-equipped micro-grids. Second, a novel decentralised aggregation framework employing multi-leader-multi-follower game theory is developed. The proposed aggregation framework is solved by a computationally efficient and privacy-preserving graph-based consensus algorithm using edge computing. Lastly, an integrated MCDM framework that includes techno-economic, environmental, and efficiency criteria assessments is

developed and applied to an unexplored South Africa–UK green hydrogen supply corridor.

The methodological advancements introduced in this thesis offer novel computational frameworks that provide a theoretical basis for future decision-support tools. The results offer quantitative insights relevant to micro-grid operators, aggregators, policymakers, and investors.

Impact Statement

The global energy transition is driving fundamental shifts in how energy systems are operated, coordinated, and evaluated. The increasing penetration of intermittent renewable resources, the decentralisation of market actors, and the emergence of international green hydrogen trade create a nested hierarchy of decision-making complexities. This thesis contributes to addressing these challenges through three methodological advancements: (1) a hybrid optimisation framework for managing deep operational uncertainty; (2) a decentralised intelligent aggregation architecture for coordinating competitive market interactions; and (3) an integrated multi-criteria evaluation framework for strategic hydrogen supply chain selection.

Within the academic and research fields, this thesis advances multi-energy systems engineering by bridging the gap between computational frameworks and the emerging complexities of the energy transition. This thesis introduces novel framework hybridisation, specifically the coupling of IGDT with the STA, and a novel graph-based consensus algorithm for Multi-Leader Multi-Follower Games (MLMFG). Furthermore, it provides comprehensive quantitative datasets, particularly on the techno-economic and environmental performance of the South Africa–UK green hydrogen corridor, supporting future research on green hydrogen innovations.

Beyond academia, the computational frameworks developed in this thesis offer potential to inform the development of future decision-support systems. At the operational scale, the proposed IGDT-STA framework demonstrates how micro-grid operators could quantify and manage risks associated with price volatility and novel storage assets such as LAES, thereby offering a theoretical basis for resilient scheduling. At the transactional scale, the decentralised aggregation framework illustrates the feasibility of coordinating competitive markets while preserving prosumer privacy, providing a computational blueprint for future smart grid architectures. At the strategic scale, the integrated MCDM framework provides policymakers and investors with a

transparent mechanism for navigating the complex trade-offs among economic viability, environmental impact, and energy efficiency in hydrogen infrastructure planning. Collectively, these contributions developed the computational framework for MES, from local micro-grids to international hydrogen supply chains.

UCL Research Paper Declaration Form: referencing the doctoral candidate's own published work(s)

1. For a research manuscript that has already been published (if not yet published, please skip to section 2):

(a) What is the title of the manuscript?

Applications of Agent-Based Methods in Multi-Energy Systems—A Systematic Literature Review

(b) Please include a link to or doi for the work:

https://doi.org/10.3390/en16052456

(c) Where was the work published?

Energies

(d) Who published the work?

MDPI

(e) When was the work published?

2023

(f) List the manuscript's authors in the order they appear on the publication:

Ruiqiu Yao, Yukun Hu and Liz Varga

(g) Was the work peer reviewed?

Yes

(h) Have you retained the copyright

Yes

(i) Was an earlier form of the manuscript uploaded to a preprint server (e.g. medRxiv)? If 'Yes', please give a link or doi

No

If 'No', please seek permission from the relevant publisher and check the box next to the below statement:

☑ I acknowledge permission of the publisher named under 1d to include in this thesis portions of the publication named as included in 1c

2. For a research manuscript prepared for publication but that has not yet been published (if already published, please skip to section 3):

(a) What is the current title of the manuscript?

(b) Has the manuscript been uploaded to a preprint server e.g. medRxiv'?

If 'Yes', please give a link or doi:

(c) Where is the work intended to be published?

(d) List the manuscript's authors in the intended authorship order:

(e) Stage of publication:

3. For multi-authored work, please give a statement of contribution covering all authors (if single-author, please skip to section 4):

Ruiqiu Yao: Conceptualization, Methodology, Investigation, Writing—Original Draft, Visualization**. Yukun Hu**: Project administration, Investigation, Supervision, Writing—Review and Editing. **Liz Varga**: Investigation, Supervision, Writing—Review and Editing.

4. In which chapter(s) of your thesis can this material be found?

Chapter 2

5.e-Signatures confirming that the information above is accurate (this form should be co-signed by the supervisor/ senior author unless this is not appropriate, e.g. if the paper was a single-author work):

Candidate:

Date:

Supervisor/Senior Author signature (where appropriate):

Date:

UCL Research Paper Declaration Form: referencing the doctoral candidate's own published work(s)

1. For a research manuscript that has already been published (if not yet published, please skip to section 2):

(a) What is the title of the manuscript?

A multi-agent-based micro-grid day-ahead optimal operation framework with liquid air energy storage by hybrid IGDT-STA

(b) Please include a link to or doi for the work:

https://doi.org/10.1016/j.est.2024.111318

(c) Where was the work published?

Journal of Energy Storage

(d) Who published the work?

Elsevier

(e) When was the work published?

2024

(f) List the manuscript's authors in the order they appear on the publication:

Ruiqiu Yao, Hao Xie, Chunsheng Wang, Xiandong Xu, Dajun Du, Liz Varga, Yukun Hu

(g) Was the work peer reviewed?

Yes

(h) Have you retained the copyright

Yes

(ii) Was an earlier form of the manuscript uploaded to a preprint server (e.g. medRxiv)? If 'Yes', please give a link or doi

No

If 'No', please seek permission from the relevant publisher and check the box next to the below statement:

☑ I acknowledge permission of the publisher named under 1d to include in this thesis portions of the publication named as included in 1c

2. For a research manuscript prepared for publication but that has not yet been published (if already published, please skip to section 3):

(a) What is the current title of the manuscript?

(b) Has the manuscript been uploaded to a preprint server e.g. medRxiv'?

If 'Yes', please give a link or doi:

(c) Where is the work intended to be published?

(d) List the manuscript's authors in the intended authorship order:

(e) Stage of publication:

3. For multi-authored work, please give a statement of contribution covering all authors (if single-author, please skip to section 4):

Ruiqiu Yao: Conceptualization, Methodology, Writing – original draft. **Hao Xie**: Conceptualization, Methodology, Writing – original draft. **Chunsheng Wang**: Supervision, Writing – review & editing. **Xiandong Xu**: Data curation, Investigation. **Dajun Du**: Data curation, Investigation. **Liz Varga**: Project administration, Supervision. **Yukun Hu**: Funding acquisition, Project administration, Supervision, Writing – review & editing.

4. In which chapter(s) of your thesis can this material be found?

Chapter 4

5.e-Signatures confirming that the information above is accurate (this form should be co-signed by the supervisor/ senior author unless this is not appropriate, e.g. if the paper was a single-author work):

Candidate:

Date:

Supervisor/Senior Author signature (where appropriate):

Date:

UCL Research Paper Declaration Form: referencing the doctoral candidate's own published work(s)

1. For a research manuscript that has already been published (if not yet published, please skip to section 2):

(a) What is the title of the manuscript?

Decentralized intelligent multi-party competitive aggregation framework for electricity prosumers

(b) Please include a link to or doi for the work:

https://doi.org/10.1016/j.apenergy.2024.123860

(c) Where was the work published?

Applied Energy

(d) Who published the work?

Elsevier

(e) When was the work published?

2024

(f) List the manuscript's authors in the order they appear on the publication:

Xiaoyuan Cheng[†], Ruiqiu Yao[†], Andrey Postnikov, Yukun Hu, Liz Varga

[†]Authors have equal contributions

(g) Was the work peer reviewed?

Yes

(h) Have you retained the copyright

Yes

(iii) Was an earlier form of the manuscript uploaded to a preprint server (e.g. medRxiv)? If 'Yes', please give a link or doi

No

If 'No', please seek permission from the relevant publisher and check the box next to the below statement:

☑ I acknowledge permission of the publisher named under 1d to include in this thesis portions of the publication named as included in 1c

2. For a research manuscript prepared for publication but that has not yet been published (if already published, please skip to section 3):

(a) What is the current title of the manuscript?

(b) Has the manuscript been uploaded to a preprint server e.g. medRxiv'?

If 'Yes', please give a link or doi:

(c) Where is the work intended to be published?

(d) List the manuscript's authors in the intended authorship order:

(e) Stage of publication:

3. For multi-authored work, please give a statement of contribution covering all authors (if single-author, please skip to section 4):

Xiaoyuan Cheng: Conceptualization, Methodology, Writing – Original Draft, Software. **Ruiqiu Yao**: Conceptualization, Methodology, Writing – Original Draft, Software. **Andrey Postnikov**: Resources, Investigation, Writing - Review & Editing. **Yukun Hu**: Writing - Review & Editing, Project administration, Funding acquisition. **Liz Varga**: Writing - Review & Editing, Project administration, Funding acquisition.

4. In which chapter(s) of your thesis can this material be found?

Chapter 5

5.e-Signatures confirming that the information above is accurate (this form should be co-signed by the supervisor/ senior author unless this is not appropriate, e.g. if the paper was a single-author work):

Candidate:

Date:

Supervisor/Senior Author signature (where appropriate):

Date:

UCL Research Paper Declaration Form: referencing the doctoral candidate's own published work(s)

1. For a research manuscript that has already been published (if not yet published, please skip to section 2):

(a) What is the title of the manuscript?

A multi-criteria analysis framework for hydrogen carrier evaluation in large-scale intercontinental hydrogen exports

(b) Please include a link to or doi for the work:

https://doi.org/10.1016/j.enpol.2025.115040

(c) Where was the work published?

Energy Policy

(d) Who published the work?

Elsevier

(e) When was the work published?

2025

(f) List the manuscript's authors in the order they appear on the publication:

Ruiqiu Yao, Yutao Li, Liz Varga, Yukun Hu*

(g) Was the work peer reviewed?

Yes

(h) Have you retained the copyright

Yes

(iv) Was an earlier form of the manuscript uploaded to a preprint server (e.g. medRxiv)? If 'Yes', please give a link or doi

If ‘No’, please seek permission from the relevant publisher and check the box next to the below statement:

☑ I acknowledge permission of the publisher named under 1d to include in this thesis portions of the publication named as included in 1c

2. For a research manuscript prepared for publication but that has not yet been published (if already published, please skip to section 3):

(a) What is the current title of the manuscript?

(b) Has the manuscript been uploaded to a preprint server e.g. medRxiv’?

If ‘Yes’, please give a link or doi:

(c) Where is the work intended to be published?

(d) List the manuscript’s authors in the intended authorship order:

(e) Stage of publication:

3. For multi-authored work, please give a statement of contribution covering all authors (if single-author, please skip to section 4):

Ruiqiu Yao: Conceptualisation, Methodology, Writing – original draft. **Yutao Li**: Conceptualisation, Methodology, Writing – original draft. **Liz Varga**: Project administration, Supervision, Funding acquisition. **Yukun Hu**: Project administration, Supervision, Writing – review & editing, Funding acquisition.

4. In which chapter(s) of your thesis can this material be found?

Chapter 6

5.e-Signatures confirming that the information above is accurate (this form should be co-signed by the supervisor/ senior author unless this is not appropriate, e.g. if the paper was a single-author work):

Candidate:

Date:

Supervisor/Senior Author signature (where appropriate):

Date:

Acknowledgement

I am profoundly grateful to my principal supervisor, Dr. Yukun Hu, for the invaluable opportunity to pursue my PhD at UCL. The platform, resources, and vibrant community here exceeded anything I could have imagined before beginning this journey. Our work together began during the uncertain times of COVID-19. Throughout those challenging early days and the many challenges that followed, Dr. Hu's guidance, patience, and encouragement made a significant difference. I am especially appreciative of the research opportunities he provided and the confidence he entrusted in me. My sincere thanks also go to my second supervisor, Professor Liz Varga, whose mentorship has been a model of professionalism and integrity. Her thoughtful feedback consistently sharpened my thinking and improved my work.

I am thankful to my co-authors for their valuable contributions and collaboration, which led to a series of publications and strengthened the research that underpins this thesis. I also gratefully acknowledge the funders whose support made this work possible. I would like to thank the examiners, Professor Hailong Li and Dr Melanie King, for their critical comments that helped improve this thesis tremendously.

Finally, I owe my deepest thanks to my family for their unwavering love, patience, and belief in me, which sustained me throughout the PhD. And to Lucy for your unconditional love and support at every step of this journey.

Ruiqiu Yao

University College London

London UK

Dec 2025

Contents

List of Figures

List of Tables

List of Acronyms

ADMM	Alternating direction method of multipliers
AHP	Analytical hierarchy process
ASU	Air separation unit
BLTN	Bidirectional low-temperature networks
CAES	Compressed air energy storage
CAPEX	Capital Expenditure
CCHP	Combined cooling, heating, and power
DBT	Dibenzyltoluene
DER	Distributed energy resources
DR	Demand response
DSM	Demand side management
EV	Electric vehicle
FC	Fuel cells
GA	Genetic algorithm
GHC	Green hydrogen carrier
GWP	Global warming potential
HP	Heat Pump
HVAC	Heating, ventilation, and air conditioning
IGDT	Information gap decision theory
IoT	Internet of Things
LAES	Liquid air energy storage
LCA	Life cycle assessment
LCOH	Levelised cost of hydrogen
LH_2	Liquid hydrogen
LOHC	Liquid organic hydrogen carriers
MAS	Multi-agent systems
MCDM	Multi-criteria decision-making
MCH	Methylcyclohexane
MeOH	Methanol
MES	Multi-energy systems
MILP	Mixed integer linear programming
MLMFG	Multi-leader-multi-follower game
NH_3	Ammonia
NOCT	Nominal operating cell temperature

NPV	Net Present Value
OPEX	Operation Expense
PEM	Polymer electrolyte membrane
PSO	Particle swarm optimisation
PV	Photovoltaics
RL	Reinforcement learning
SOC	State of charge
STA	State Transition Algorithm
TCL	Thermostatically controlled loads
TOL	Toluene
V2G	Vehicle-to-grid
VPP	Virtual power plant

List of Symbols

Chapter 2

$\mathcal{L}(\cdot)$	Lagrangian function [-]
$\mathcal{g}(\cdot)$	Lagrangian dual function [-]
p^*	optimal value for primal problem [-]
d^*	global optimizer [-]
$p^{(1)}, p^{(2)}$	parents of genetic algorithm [-]
$q^{(1)}, q^{(2)}$	offspring of genetic algorithm [-]
$v_{i,t}$	velocity of particle i and time t [-]
$x_{i,t}$	position of particle i and time t [-]
r^k	primal residual [-]
s^k	dual residual [-]

Chapter 3

λ	actual value of the uncertain parameter [-]
$\hat{\lambda}_t$	predicted value of the uncertainty parameter [-]
α	bound for system uncertainty levels [-]
C_{averse}	target system cost that for risk-averse decision-makers [$]
C_{taking}	target system cost that for risk-taking decision-makers [$]
P_{WT}^t	WT output power at time t [kW]
G_T	solar radiation incident on the PV [Wm^{-2}]
T_c	PV cell temperature [°C]
P_{MT}^t	output power of micro-turbine at time t [kW]
P_{WT}^t	output power of wind power generation at time t [kW]
P_{PV}^t	output power of photovoltaic power generation at time t [kW]
P_{LAES}^t	charge and discharge power of LAES at time t [kW]
P_{gird}^t	tie line transition power at time t [kW]
ω	rotation operator [-]
β	translation operator [-]
γ	expansion operator [-]
δ	axesion operator [-]

Ψ_{SE}	search enforcement constant [-]
ω_{in}^{cut}	cut-in wind speed [ms^{-1}]
ω_{out}^{cut}	cut-out wind speed [ms^{-1}]
ω_{rate}	rated speed WT [kW]
P_{WT}^{rated}	Rated power of WT [kW]
P_{PV}^{rated}	rated power of PV [kW]
f_{pv}	derating factor of PV [kW]
$G_{T,STC}$	incident radiation at the standard test conditions [Wm^{-2}]
α_p	temperature coefficient [-]
$T_{c,STC}$	PV cell temperature at the standard test conditions [°C]
$T_{a,NOCT}$	ambient temperature under the NOCT [°C]
$G_{T,NOCT}$	solar radiation under the NOCT [Wm^{-2}]
η_c	electrical conversion efficiency of PV [%]
$\eta_{Kapitza}$	Kapitza cycle efficiency [%]
$\eta_{cryo-pump}$	cryogenic pump efficiency [%]
$\eta_{turbines}$	turbine efficiency [%]
Γ	system operation cost function [$]
$\hat{\alpha}(P, C_{averse})$	robustness function [%]
$\hat{\beta}(P, C_{taking})$	opportunity function [%]

Chapter 4

A	constant in battery degradation model [-]
R	gas constant [J/(mol*K)]
T	environment temperature [K]
$\lambda_{i,j}^{pro,ask}$	$aggregator_i$'s bidding price to $prosumer_j$ [£/kWh]
β	activation energy coefficient [-]
γ	fixed-cost coefficient [£/kWh]
z	power law factor [-]
$x_{i,j}$	volume of electricity that $prosumer_j$ decides to sell to $aggregator_i$ [kWh]
$\lambda_i^{DA,bid}$	$aggregator_i$'s bidding price at the day-ahead market [£/kWh]
$\lambda_{i,j}^{pro,ask}$	$aggregator_i$'s bidding price to $prosumer_j$ [£/kWh]
c	number of battery cycles from the initial state of the battery

μ_x, μ_z	Lagrangian multipliers for inequality constraints [-]
$F_i(x), G_i(z)$	indicator functions [-]
$L_0(x, z, \mu_x, \mu_z, \lambda)$	Lagrangian function [-]
$V^k(\cdot)$	Lyapunov function of the optimisation problem [-]
$\mathbb{1}$	N-dimensional identity vector
χ	closed convex feasible sets of trading electricity matrix
$\mathbf{\Lambda}$	closed convex feasible sets of asking price matrix
C_a, D_b	convex feasibility sets
V	set of nodes on a graph
$\mathcal{E}$	set of the edges on a graph

Chapter 5

$WACC^{norm}$	weighted average cost of capital in normal terms [USD/kg]
$WACC^{real}$	weighted average cost of capital in real terms [USD/kg]
ε	scaling exponent [-]
η	carrier efficiency [%]
r_{ij}	normalised value in TOPSIS [-]
A^+, A^-	ideal and worst solution in TOPSIS [-]
D_i^+, D_i^-	distances in TOPSIS [-]
C_i^*	relative closeness in TOPSIS [-]
S_i	utility value in VIKOR [-]
R_i	regret value in VIKOR [-]
Q_i	final VIKOR value [-]

Chapter 1

1. Introduction

1.1 Research background and energy system shifts

The transition towards sustainable, resilient, and low-carbon energy systems has become one of the most pressing global trends of the 21st century. Climate change mitigation targets and increasing renewable energy integration require transformative changes in how energy systems are planned, operated, and optimised (Čuček et al., 2021). Within this context, multi-energy systems (MES) have emerged as critical infrastructures capable of harmoniously integrating diverse energy vectors, including electricity, heat, liquid air, and hydrogen, thus enhancing energy system efficiency, flexibility, and resilience (Mancarella, 2014; Qi et al., 2022). The transition to a future, sustainable MES is driven by three shifts: in the source of operational complexity, in the architecture of system control, and in the criteria for strategic evaluation. These shifts collectively create the new class of complexities that are critical in the MES transition.

The first shift is in the source of operational uncertainty, driven by the increasing adoption of intermittent renewable energy sources. The computational frameworks of traditional energy systems were built on dispatchable thermal power plants, which can be precisely controlled to meet demand. However, the integration of intermittent renewable energy sources introduces volatility in the energy generation, which is driven by the weather (Bhandari, 2025). Therefore, deep uncertainty poses a challenge for traditional scheduling models, as historical data-derived probabilistic distributions cannot capture the actual state of energy systems.

The second shift is from centralised control to decentralised coordination. The conventional energy system is controlled by a centralised architecture with utility companies delivering energy to passive consumers. This architecture was changed by the penetration of distributed energy resources, such as rooftop photovoltaic panels (Ren et al., 2022). This penetration transformed consumers into prosumers. In addition, decentralised decision-making technologies have matured, allowing autonomous local decisions and dynamic interaction (Pan & McElhannon, 2018). These prosumers now have the computational power to interact dynamically with each other and with a new class of market mediators: aggregators (Burger et al., 2017). This transformation from a centralised architecture to a network of interacting agents requires a different computational framework than the traditional centralised framework.

Finally, the third shift is in the criteria for strategic evaluation. In traditional methods, long-term decisions were primarily driven by frameworks based on single metrics, usually the levelised cost of energy. The global shifts to address climate change indicate that the traditional economic-centric framework no longer applies. An example of this shift is the strategic decision to establish large-scale intercontinental green hydrogen supply chains. Countries with rich renewable energy sources and established port infrastructure have set an ambitious goal for green hydrogen export. (Scholvin et al., 2025). In addition, nations also seek to import green hydrogen to meet net-zero goals; however, choosing the appropriate green hydrogen carrier (GHC) remains a critical challenge (IRENA, 2022). The decision of the GHC pathway extends beyond the traditional single metric decision frameworks. Policymakers and investors face the trade-off between GHC performance, economic performance, environmental footprint, and carrier efficiency.

1.2 Emergent complexities and challenges

The shifts described in the previous section create a nested hierarchy of decision-making complexities across multiple scales of energy systems. The first complexity is

in the operational scale. The challenges of making decisions when future states of key decision variables, particularly market prices, are subject to deep uncertainty, leading to uncertainty complexity. This complexity creates a practical problem for micro-grid operators with new energy storage assets. In a volatile market with intermittent energy sources, the electricity prices could be unpredictable. The operator faces challenges in scheduling the micro-grid operation with appropriate risk levels. Thus, there is a lack of a computational framework to manage the deep uncertainty.

Moving beyond the operational challenges, the shift towards decentralisation in energy generation and decision-making creates the interactional complexity at the transactional scale. This complexity brings challenges to managing a system of autonomous and competing agents with private information and objectives. Especially when multiple aggregators compete by setting attractive prices to incentivise prosumers, this creates a game-theoretic dynamic where the competing agents must achieve market equilibrium while preserving data privacy. This practical challenge for incorporating new market participants (aggregators and prosumers) requires a new computational framework that can coordinate with dynamic market interactions while preserving data privacy.

At the strategic scale, the shift in evaluation criteria creates evaluative complexity. This is the challenge of choosing long-term technology pathways with distinct performance, specifically the strategic decision of selecting a GHC pathway for international hydrogen trade. Policymakers and investors are no longer choosing GHC based on a single criterion, such as economic performance. Instead, their decisions become multi-dimensional, where the trade-offs among different criteria performance should be considered. This requires a computational framework that can handle the multi-criteria evaluation problem.

1.3 Thesis scope and aims

The emergent complexities arising from uncertainty, interaction, and evaluation make the traditional deterministic, centralised, and single-objective computational framework inadequate for managing them. Therefore, this thesis aims to address the framework gap by developing and validating new computational frameworks. Each of the new frameworks is developed to manage a specific layer of complexity, providing decision support for the multi-scale MES transition. Specifically, the new computational frameworks are:

- At the operational scale, this thesis addresses uncertainty complexity by developing a framework that moves beyond probabilistic forecasting to enable risk-aware scheduling for novel energy assets under deep market uncertainty.
- At the transactional scale, this thesis then addresses interactional complexity by formulating a decentralised and game-theoretic framework capable of coordinating a market of multiple competing aggregators to achieve a stable equilibrium, while preserving the prosumers' privacy.
- At the strategic scale, the thesis addresses evaluative complexity by constructing an integrated multi-criteria framework that provides a transparent process for resolving the trade-offs inherent in long-term technology pathway decisions.

By developing methodological innovations for each of these layers, this thesis contributes a coherent set of computational tools designed to navigate the complexities of the modern energy transition.

1.4 Thesis structure

The structure of this thesis is designed to address the overarching research question by navigating the nested hierarchy of complexities outlined in this chapter. As illustrated in Figure 1-1, the thesis is organised into seven chapters. Chapter 1 introduces the real-

world problem context and identifies the three shifts in the energy transition that give rise to emergent complexities. Chapter 2 reviews the existing academic literature through the lens of the complexity taxonomy. It examines current approaches to managing uncertainty, interactional, and evaluative complexities, identifying the specific research gaps that this thesis aims to address.

Chapter 3 formalises the research design. It presents the overarching research question, the taxonomy of decision-making complexity, and the three subsidiary research objectives that guide the three studies of this thesis.

Chapter 4 addresses the first layer of uncertainty complexity. It develops a novel hybrid computational framework combining Information Gap Decision Theory (IGDT) and the State Transition Algorithm (STA). This framework is then applied to the practical challenge of scheduling an LAES-equipped micro-grid, demonstrating its ability to manage deep market uncertainty and accommodate different risk preferences.

Chapter 5 addresses interactional complexity in the transactional scale. It formulates a Multi-Leader Multi-Follower Game (MLMFG) to model the dynamic market interaction between aggregators and prosumers. A decentralised graph-based consensus algorithm is developed to solve this game.

Chapter 6 addresses evaluative complexity at the strategic scale. It contributes an integrated Multi-Criteria Decision-Making (MCDM) framework that synthesises discounted techno-economic analysis, comprehensive life-cycle assessment, and carrier efficiency metrics. The proposed framework's utility is demonstrated by applying it to the strategic evaluation of green hydrogen carriers for the previously unexamined South Africa-UK supply chain.

Finally, Chapter 7 concludes the thesis. It provides a synthesis of the findings of the thesis. In addition, this chapter reflects on the socio-technical and ethical implications

of the proposed frameworks, discusses research limitations, and provides recommendations for future work.

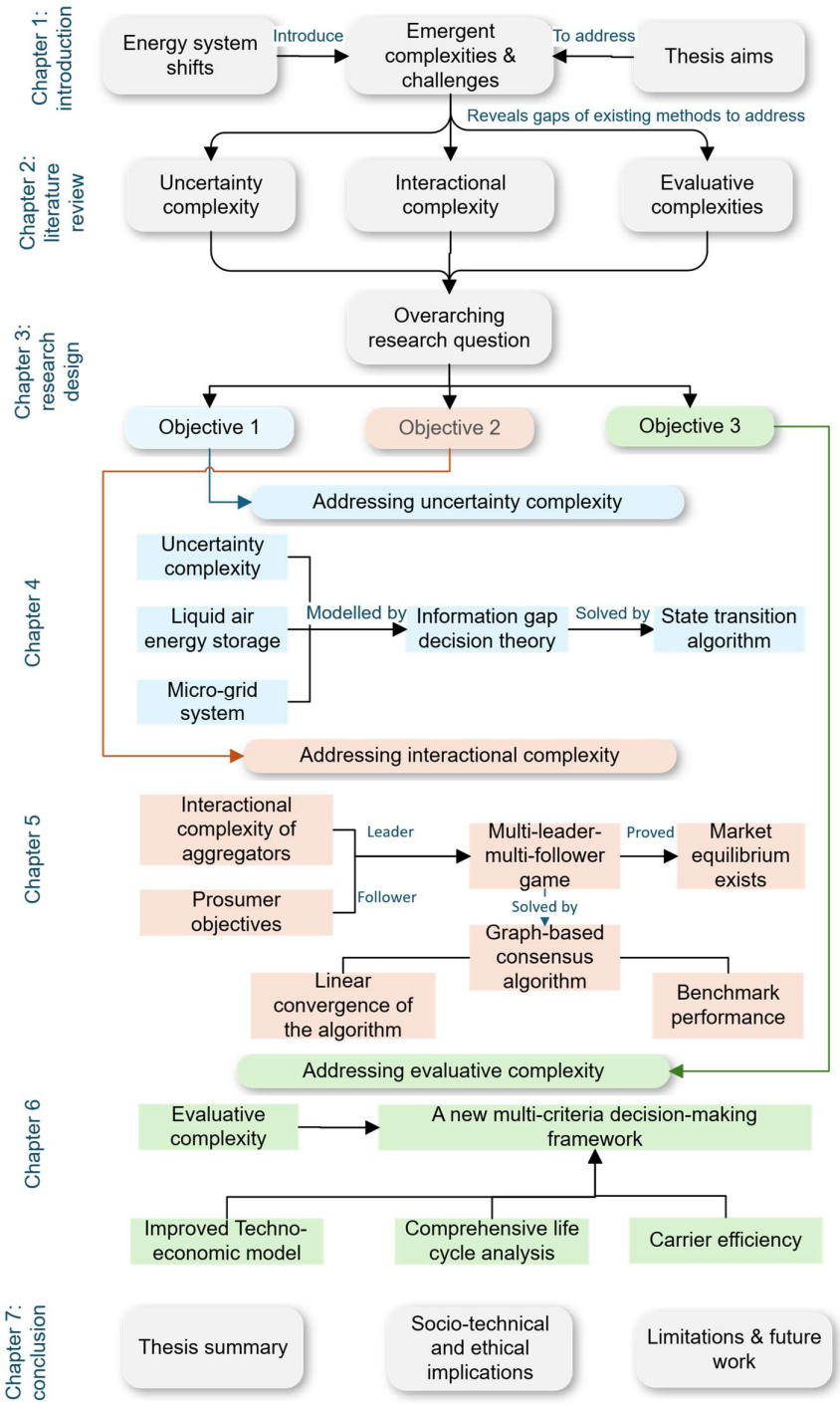

Figure 1-1 Thesis structure

Chapter 2

2. Literature review[1]

2.1 Chapter introduction

Through the lens of nested complexity, this review systematically examines state-of-the-art computational frameworks for managing uncertainty, interactional, and evaluative complexities in energy systems. By assessing the limitations of existing methods in each of these three domains, this chapter identifies the specific research gaps that motivate the overarching research question and subsidiary objectives in Chapter 3. This process provides the academic literature background for the new computational frameworks developed in this thesis.

[1] Part of this chapter is adapted from

Yao, R., Hu, Y., & Varga, L. (2023). Applications of Agent-Based Methods in Multi-Energy Systems—A Systematic Literature Review. *Energies*, 16(5), 2456. https://doi.org/10.3390/en16052456

Yao, R., Xie, H., Wang, C., Xu, X., Du, D., Varga, L., & Hu, Y. (2024). A multi-agent-based micro-grid day-ahead optimal operation framework with liquid air energy storage by hybrid IGDT-STA. *Journal of Energy Storage*, 86, 111318. https://doi.org/10.1016/j.est.2024.111318

Cheng, X.[†], **Yao, R.**[†], Postnikov, A., Hu, Y., & Varga, L. (2024). Decentralized intelligent multi-party competitive aggregation framework for electricity prosumers. *Applied Energy*, 373, 123860. https://doi.org/10.1016/j.apenergy.2024.123860

[†]Authors have equal contributions

Yao, R., Li, Y., Varga, L., & Hu, Y. (2025). A multi-criteria framework for evaluating hydrogen carriers for large-scale intercontinental exports. *Energy Policy*, 210, 115040, https://doi.org/10.1016/j.enpol.2025.115040

2.2 Uncertainty complexity in operations

At the operational scale of multi-energy systems, such as microgrids, a key decision-making challenge is the shift from deterministic scheduling to managing uncertainty and complexity. This form of complexity is caused by the intermittency of renewable generation and the increasing volatility of electricity markets. This section critically reviews existing computational frameworks for addressing this complexity.

2.2.1 Challenges of deep uncertainty

The operation and planning of a micro-grid are affected by uncertainties in wind and photovoltaic power generation, system load, and market electricity prices. To address uncertainties, the existing literature on multi-energy scheduling mainly uses two branches of programming methods: Stochastic Programming (SP) and Robust Optimisation (RO).

SP is a probabilistic method for optimisation under uncertainty, which models uncertainty through probabilistic distribution functions. SP formulates the decision-making process as a two-stage process, where the first stage focuses on making decisions before the uncertainty is realised, and the second stage generates actions after the uncertainty is realised (R. Zhang et al., 2021). SP usually include using Monte Carlo simulation to generate scenario sets representing future states, aiming to optimise system costs across the weighted scenarios.

A study adopted SP with 100 Monte Carlo simulations to optimise a multi-energy micro-grid with hydrogen vehicle fuelling (Mei et al., 2021). The results show that the stochastic approach with forecast updating can save daily operational costs by 18% compared with static baselines. Another study adopted two-stage stochastic programming to size a hybrid energy storage system, including battery and thermal storage (Shen et al., 2021). By generating 200 scenarios to represent wind, load, and temperature uncertainty, the results show that leveraging thermal inertia within a

stochastic approach can reduce total investment cost by 6.7%. Furthermore, a study integrates SP with global sensitivity analysis for the planning of distributed energy sources in high-rise buildings (J. Zhang et al., 2023). The comparative analysis results show that static models consistently underestimate the annual costs, with CO_2 emissions varying by 10% across scenarios.

Despite the quantitative benefits, the three studies collectively mentioned the limitations of adopting SP. First, the accuracy of SP solutions relies on the accuracy of the underlying known and stationary probability distribution of random variables, including solar irradiance (Mei et al., 2021), wind profile (Shen et al., 2021), or feed-in tariff (J. Zhang et al., 2023), where the distributions are usually Gaussian or Normal distributions. The reliance on assumed distributions highlights the limitations of SP in the context of deep uncertainty, where historical data may not accurately predict market volatility. Hence, some researchers use RO as an optimisation method in multi-energy systems.

Instead of assuming specific distribution functions, RO addresses uncertainty by modelling with uncertainty sets (He et al., 2017). Then the RO is used to optimise the multi-energy system under the worst-case realisation of uncertain variables (Martinez-Mares & Fuerte-Esquivel, 2013). However, the results of RO could be overly conservative, sacrificing economic opportunities in multi-energy system scheduling. The traditional RO framework lacks the ability to generate risk-seeking strategies that align with decision-makers' risk profiles. The Information Gap Decision Theory (IGDT) is a viable computational framework for handling deep uncertainty. Specifically, IGDT does not require probabilistic distributions of key decision variables. In addition to maximising the system robustness for risk-averse decision-makers, it can also pursue opportunities for risk-seeking decision-makers to exploit favourable deviations (Nasr et al., 2020).

Some researchers have recently used the IGDT method to model the micro-grid system. The IGDT method can help decision-makers choose the most economical and feasible solutions for the micro-grid system under uncertainty. A robust framework is proposed using the IGDT method to realise the effective operation of island micro-grids, considering the uncertainty of photovoltaic power generation and demand (Nasr et al., 2019). In addition, a short-term power generation dispatch method for grid-connected micro-grids is proposed to obtain the optimal bidding strategy, considering the demand response program based on the IGDT method under uncertain upstream grid prices (Mehdizadeh et al., 2018).

2.2.2 Challenges of novel storage assets

In addition to the uncertainty complexity from prices and renewable energy, the emerging energy storage assets also introduce complexity from physical operation. Liquid air energy storage (LAES) is an emerging energy storage technology that involves complex thermodynamic processes, including compression, liquefaction, and expansion. The complex thermodynamic process introduces additional complexities into the multi-energy system scheduling. Current research on LAES mainly focuses on thermodynamic and economic analysis (Borri et al., 2021; Cui et al., 2021; Su et al., 2023; Y. Zhou et al., 2023). When LAES operation scheduling is considered, studies use a simplified linear model for operation optimisation (B. Lin et al., 2019). To address the combined complexity from uncertainty and physical operation, researchers integrated the IGDT with heuristic algorithms, such as genetic algorithm (GA) and particle swarm optimisation (PSO) (Kennedy & Eberhart, 1995; Tezer et al., 2017).

A study integrates IGDT with modified PSO to construct robust step-wise offer curves for a price-taker generation station in a day-ahead market (Nojavan et al., 2015). Kim and Kim (2021) present an energy management framework for grid-connected micro-grids. The framework constructs staircase bidding strategies for micro-grid operators with incentive demand programmes, which are optimised by a modified PSO algorithm

(H. J. Kim & Kim, 2021). These traditional intelligent optimisation algorithms, such as GA and PSO, are mainly inspired by imitating social phenomena or natural laws. Unlike conventional intelligent optimisation algorithms, the state transition algorithm (STA) is an intelligent optimisation algorithm based on structural learning and shows better performance than conventional algorithms (X. Zhou et al., 2012). The core concept of STA is treating a solution to an optimisation problem as a state. The generation and update process of the solution is treated as a state transition process. The algorithm's solution process is based on the state-space expression in modern control theory, and four state transformation operators are constructed during optimisation.

2.2.3 The need for a hybrid framework

The literature review reveals a gap in the computational frameworks used for uncertainty handling and for complex asset optimisation. As detailed in Section 2.2.1, IGDT is a viable computational framework for handling deep market uncertainty. However, existing applications of IGDT in energy systems predominantly rely on convex optimisation techniques or heuristic algorithms such as PSO (Majidi et al., 2019; Nojavan et al., 2015). Hence, the **Research Gap 1** is identified.

> **Research Gap 1**: There is currently no optimisation framework that couples the risk-averse/risk-seeking logic of IGDT with the structural learning capabilities of STA. Such a hybrid computational framework is necessary to simultaneously address the uncertainty complexity of volatile markets and the physical complexity of assets like LAES.

This thesis addresses this specific gap in Chapter 4 by developing a novel multi-agent IGDT-STA framework that can handle the different risk preferences of decision-makers.

2.3 Interactional complexity in decentralisation

This section critically reviews the computational architectures and market mechanisms proposed to manage the transition of decentralisation. This section begins by examining the role of Multi-Agent Systems (MAS) as the enabling infrastructure for local autonomy in Section 2.3.1. Then, Section 2.3.2 critiques the limitations of cooperative coordination models. Section 2.3.3 analyses the emerging need for competitive, game-theoretic frameworks to capture the strategic interactions between aggregators and prosumers.

2.3.1 Multi-agent system for energy management

To address the interactional complexity of the energy system transition, the first requirement is computational architectures that enable energy assets to make autonomous decisions. Multi-agent systems (MAS) have emerged as a computational framework to provide bottom-up autonomy. Section 2.3.1 reviews the application of MAS architecture across scales in the MES.

2.3.1.1 Enabling local autonomy

The principal objective of the agent is to act as a digital representation of physical assets, abstracting the operational information to make local decisions and communicate with other agents. Studies reviewed in this section demonstrated how diverse local energy assets could be represented as distinct agents to collectively manage the local multi-energy system at the building scale.

The earliest published research on local energy system management was a framework for the cognitive construction of agents in building energy management systems (Conte et al., 2009). Zhao et al. (2013) designed a MAS control strategy with three distinct agents: an electricity agent, a heating agent, and a cooling agent responsible for optimising the three end-demands, respectively. The decision-making of the heating agent and the cooling agent is based on energy cost minimisation with the responding

energy carrier. The decision-making of electricity agents includes two objectives: minimising the peak load and communicating with grids (electricity grid and natural gas grid) for price updating. The CPLEX solver achieves the agents' optimisations (Zhao et al., 2013). The control strategy demonstrates that the decomposition of the central objective is important for scalability. A MAS-based building energy management system was adopted to enhance distribution-grid resilience by leveraging the multi-energy flexibility of smart home appliances (Ahrens et al., 2021).

Cai et al. (2016) proposed a general multi-agent control approach for the HVAC system. This approach consists of an agent definition framework and a control optimisation procedure. The agents are required to define a collection of objective functions and constraints based on the framework guidelines (Cai et al., 2016). The framework then formulates the optimisation problem based on the consensus algorithms, including the sub-gradient method and ADMM. Cai et al. (2016) also pointed out a potential issue in implementing the consensus-based algorithm, in which the algorithm could not reach a consensus point when the decision time had been reached.

In addition, the integration of MAS with Internet of Things (IoT) technologies established a connection between the physical and cyber layers. González-Briones et al. (2018) proposed a multi-agent building temperature management system to increase energy usage efficiency. On the physical side, the authors deployed temperature-monitoring and occupancy-sensing sensors within wireless sensor networks to gather data for system optimisation. On the logic side, the multi-agent system processes collected data and returns an optimised HVAC system's control strategy (González-Briones et al., 2018). The case study demonstrated that this control strategy could achieve an average energy savings of 41%. W. Li et al. (2021) developed a multi-agent control scheme for the HVAC system on an IoT-based wireless sensor network. This scheme balances the performance and power consumption of battery-powered sensors through multi-objective optimisation using ADMM. The power consumption of the

sensors is reduced by using the event-driven control approach rather than the time-driven optimisation approach (W. Li et al., 2021).

Demand response (DR) or demand-side management (DSM) is a popular research field in energy system management at the local scale. DR or DSM is a management strategy to manage the demand load based on the availability of the electricity supply. The selected articles show that an MAS is a valuable approach to implementing the DR or DSM. Devia et al. (2021) adopted distributed co-evolutionary optimisation algorithms with agent-based architectures to reduce consumption profiles. The control strategy is divided into two phases. The first phase is to extract and store energy-use information for every room, along with temperature variance. The second phase is to control every heating device in the house with distributed optimisation. Other than cost reduction, the results also show that the inclusion of thermal storage units could increase the overall system's efficiency (Devia et al., 2021). A MAS control architecture DSM is proposed for thermostatically controlled loads (TCLs), enabling anonymous communication among TCL agents via a network while preserving TCL internal temperature privacy (Franceschelli et al., 2021). The MAS optimisation was based on a dynamic consensus algorithm.

The literature reviewed in this section confirms that MAS provides a foundational architecture for establishing local autonomy and preserving privacy at the local building scale. The coordination of these agents introduces an emergent complexity. If local agents focus solely on individual objectives, aggregate behaviour may affect network-level performance. Therefore, it is essential to review the literature that focuses on the coordination of agents in a connected network. The following section examines how MAS architectures are scaled to manage the system performance at the district level.

2.3.1.2 Enabling district-scale management

Scaling up from the local autonomy at the building level, the next level of interactional complexity occurs when coordinating agents within a shared physical system, such as

a multi-energy district system. The literature addresses the coordination challenge through three research themes: optimal design of the multi-energy district energy system, fully decentralised operational control, multi-energy micro-grid management, and management with district heating system & heating clusters.

- District energy system design

Beyond the operation of a single building, a key challenge is the collective planning and designing of interconnected assets. Kyriakarakos et al. (2013) developed an energy management system for optimal component sizing of poly-generation micro-grids that can meet the needs of consumers in remote areas for potable water, hydrogen, space heating, space cooling, and electricity. A multi-agent-based DSM is embedded in the management system for load shedding when generation capacities cannot meet demand. The MAS is designed in a hierarchical manner. The components in a building, such as lighting and refrigeration, are controlled by the intelligent agents, which are supervised by an upper-level building control agent (Kyriakarakos et al., 2013). The component control agents are responsible for disconnecting the virtual power lines when load shedding is required. Karavas et al. (2015) further developed the agent-based poly-generation micro-grid management system from a hierarchical architecture to a decentralised architecture, which does not require a central agent for optimisation. The component agents communicate with each other to update the system parameters, such as surplus power, consumed power, or remaining capacity (battery agent). The energy management system aims to minimise net present cost (optimal design) and optimise fuzzy cognitive map weights (optimal control). The system optimisation results compared with a centralised management system, showing that the decentralised approach presented a 2% lower net present cost than the centralised approach. Karavas et al. (2017) investigated the multi-agent decentralised management of the poly-generation micro-grid with game theory. The previous decentralised management system is a cooperative case where agents work cooperatively to minimise the global

cost function (Karavas et al., 2017). However, the agents could have conflicting interests, so agents interact with each other in a non-cooperative way. Thus, Karavas et al. (2017) used a non-cooperative game model with a Nash equilibrium to simulate the competitiveness between electrolysis agent and desalination agent as both compete to consume more power. Another cooperative game is modelled with fuel cell and battery agents since these two agents aim to meet the corporation's load demand. Compared with the previous purely cooperative management system, the game-theory-based approach reduced costs by 1.62%.

H. Wang et al. (2021) proposed a game-theory-based optimal component-sizing method for the multi-energy district energy system configuration. The authors used compressed air energy storage (CAES) for electricity and thermal storage instead of using batteries and thermal tanks. Each component agent's utility function is defined by the net present value function in both cooperative games and non-cooperative games (H. Wang et al., 2021). The Shapley value and Nash equilibrium were used to solve the cooperative and non-cooperative game models (Nash, 1950; Shapley, 1971). The results showed that coalition formation results in better economic outcomes for individual agents and the system. S. Jin et al. (2021) proposed a game theory-based component optimisation method for a multi-energy micro-grid. The main contribution of the proposed method is the incorporation of uncertainties in the renewable energy generation with a probability density function (S. Jin et al., 2021). Moreover, the agents' utility function was set to annualised economic profit throughout the life cycle. It has also been noted that future research could focus on incomplete information games when information asymmetry occurs. These studies demonstrate that decentralised agents can successfully negotiate the complex capacity sizing problem (a form of interactional complexity) without sending complete information to the central planner.

- Fully decentralised district energy system control

In terms of control of the district energy system, the literature researches replacing the central controller with a coordination mechanism by direct agent-to-agent communication. Harb et al. (2015) introduced a decentralised day-ahead scheduling strategy for a multi-energy micro-grid for cost minimisation with Mixed-Integer Linear Programming (MILP). The global MILP problem is decomposed into a series of local problems with Dantzig-Wolfe decomposition (Dantzig & Wolfe, 1961). The local problem is the local objective function for each agent, which is solved by the iterative column generation procedure (Nemhauser & Wolsey, 1988). After comparing the decentralised control with a centralised scheduling approach, it has been shown that the centralised approach offers a better solution than the decentralised approach. Nonetheless, the centralised approach to computation time increases exponentially with the increasing number of agents. Thus, the decentralised approach has advantages in terms of system scalability as the decentralisation reduces the computation time required (Harb et al., 2015). Blaauwbroek et al. (2015) proposed a multi-agent-based decentralised algorithm with mixed-integer quadratic programming to balance the distributed energy resources and flexible appliances, such as HP and CHP. Y.-S. Li et al. (2016) proposed a decentralised control method for coupled heat and power systems. This control method involves two first-order consensus protocols for heat supply optimisation and electricity supply optimisation. The optimisation is carried out in an alternating iterative way so that electricity supply and heat supply converge on an optimal solution alternatingly. The decentralised method results in a better solution than the centralised method with Lagrangian relaxation (Henwood, 1996).

Nguyen & Ishihara (2021) proposed decentralised management for household clusters with fuel cells (FCs) and CHP with a peer-to-peer trading architecture. The non-convexity problem in fuel cell operation is addressed by linearising the FC consumption and production. As a result, the peer-to-peer trading problem could be solved with the ADMM algorithm. Alishavandi & Moghaddas-Tafreshi (2019) presented a decentralised operation strategy for multi-energy micro-grids with interactive clearing

energy prices. The clearing price is determined through communication between generation and consumption agents. In each time step, the clearing price is used in calculating each agent's profit function and the system's social welfare. In addition, the gradient projection method was used for profit function and social welfare optimisation (Bertsekas, 1997). The results showed that this decentralised method had slightly better performance in cost reduction than the centralised method, as photovoltaics (PV) agents tended to maximise their own profit. However, social welfare decreased when an individual agent's profit increased. Shabani and Moghaddas-Tafreshi (2020) presented a similar decentralised approach with interactive clearing prices to optimise a multi-energy system micro-grid. The agents were programmed to optimise the social welfare at the first stage, then to optimise their own profit. The results agreed with (Alishavandi & Moghaddas-Tafreshi, 2019) in that the fully decentralised approach had lower social welfare but higher individual profits than the centralised approach. Shabani & Moghaddas-Tafreshi (2019) also observed that the demand response program was able to increase both system social welfare and agent profit. Moreover, an investigation of the peer-to-peer trading scheme in a decentralised model was suggested for future research.

Samadi et al. (2020) proposed a decentralised management strategy with reinforcement learning (RL). The optimal agent behaviour policy was evaluated with the action-value Q function (Bowling & Veloso, 2002; Sutton & Barto, 2018). The agents can find an optimal action policy by interacting competitively with one another. The trade-off between exploration and exploitation is an important consideration for an agent to determine the best action. Thus, Samadi et al. (2020) compared three action selection methods, including soft-max, epsilon-greedy, and upper confidence bound methods. They showed that the soft-max method had the best performance over the other methods. Kumari & Tanwar (2021) extended the Q-leaning-based RL management on micro-grids with blockchain communication. The communication and agreement among the stakeholders are achieved based on blockchain-encrypted smart contracts to ensure

privacy. Instead of using the discrete Q-learning method, Dong et al. (2021) proposed multi-energy micro-grid management with the asynchronous advantage actor-critic algorithm based on deep RL, which was first introduced by (Mnih et al., 2016). The result shows that the asynchronous algorithm could shorten the training time by 30% compared with the deep Q network. The decentralised computational methods reviewed in this section demonstrate that agent architecture can provide privacy and scalability to the multi-energy system. However, effective communication among agents remains a key bottleneck in implementation. Therefore, Section 2.3.3 explores this topic in greater detail.

- Multi-energy micro-grid management

Coupling of multiple energy carriers into agent interaction is another source of interactional complexity. Literature investigated how agents can handle this complexity. Anvari-Moghaddam et al. (2017) proposed an optimal control scheme for a building-integrated micro-grid with distributed generation units and demand response. A mixed objective function was formulated to optimise energy operation costs and convenience levels by building agents. At the micro-grid level, a central grid battery is responsible for compensating for the energy mismatch. The central battery agent was optimised with the Bayesian reinforcement learning (BRL) algorithm (Firouzi et al., 2012). The proposed BRL method was compared with Q learning (Wei et al., 2015) and time-based reinforcement learning (Sheikhi et al., 2016). The results showed that the proposed BRL method leads to faster learning and higher reward than the other methods. Kolen et al. (2017) also proposed a control scheme combining bi-level optimisation of the building and micro-grid. The building-level optimisation aims to minimise the total number of switch events. The operation functions (peak-to-valley distance) on the grid level are optimised with decentralised agent interactions by updating the local energy fluctuation function. The performance of the proposed bi-level scheme is a trade-off between building-level optimisation and grid-level optimisation due to the narrowed search

space. Hutty et al. (2020) investigated the feasibility of reversible solid oxide cells for micro-grid operation using multi-agent simulation in the UK and Texas. The authors suggested that, in future research, simulated battery and reversible solid oxide cells as a hybrid energy storage system could be considered, and how hybrid storage systems perform compared to traditional battery storage systems could be investigated.

Moghaddas-Tafreshi et al. (2019) proposed a multi-energy micro-grid optimal operation scheme considering uncertainties in renewable energy generation and energy demand, as well as a demand response program. The uncertainties in renewable energy generation were modelled with a Weibull distribution of wind speed in wind turbine agents. The load agents simulated uncertainties of the electrical and thermal load with the normal distribution function. Both wind turbines and load agents generate 1000 scenarios in a Monte Carlo simulation each hour to evaluate the micro-grid performance. The demand response program from (Nikmehr et al., 2017) is implemented in the load agent program. Li et al. (2020) established a three-layer control model for micro-grid management with the improved particle swarm optimisation algorithm. The authors combined adaptive weights and chaotic search into the PSO algorithm to avoid local optima. The results showed that the proposed algorithm had a much smaller computation standard deviation than the original PSO and chaotic search PSO. H. Liu et al. (2020) proposed a hierarchical control scheme for a multi-energy micro-grid considering the multi-agent game. In the first layer (decision layer), the generation agents participate in a static cooperative game with complete information to maximise their own profit. The Nash equilibrium point of the cooperative game is solved by the evolutionary game theory combined Q-learning method (J. Hu & Wellman, 2003). Khan et al. (2021) proposed a hierarchical multi-agent control architecture on the multi-energy micro-grid with three layers. In formulating the optimisation problem, harmful gas emissions and multi-energy generation costs were considered in the objective function. Farinis et al (2021) proposed a micro-grid management system with a building system operator that considers plug-in EVs as energy storage components.

Two of the studies investigated the operation strategy of an energy hub. Lin et al. (2018) proposed a multi-agent energy hub operation control considering EV penetration rate and EV behaviour simulation. EV agents simulated the travel patterns and charging patterns, including the uncontrolled, rapid patterns. The behaviour simulation result was then passed to the energy hub control system as electricity demands. The vehicle-to-grid (V2G) technology was considered in operation optimisation by adding the V2G cost function to the global optimisation function. The results showed that the demand brought by increased EV penetration could be met with gas turbines. Moreover, the electricity and cooling prices were lower because of the V2G technology in the reference case. Zeng et al. (2019) proposed an optimal dispatch scheme of an energy hub considering the integrated demand response program. The demand response program is achieved by designing the user agents' objective function, which minimises the cost of electricity, thermal, cooling load, and EV cost. The EV charging and discharging behaviours are considered with a random variable to indicate the charging state of the EV. The optimal dispatch of the energy hub was formulated into a multi-objective optimisation problem, which includes minimisation of user cost, maximisation of generator profit, and maximisation of operating income. Zeng et al. used the NSGA-III to find the Pareto frontier. The optimal solution of each agent in the Pareto frontier was obtained with the technology for order preference, similar to the ideal solution method (Han et al., 2013).

- District energy management with district heating system and heating clusters

Finally, specific coordination protocols have been developed to manage physical network constraints, particularly in district heating networks and clusters of Thermostatically Controlled Loads (TCLs). Haque et al. (2017) proposed a unified multi-agent control strategy to manage congestion and voltage limits in the district electricity distribution network with PVs and HPs. Bünning et al. (2018) proposed a distributed control method for bidirectional low-temperature networks (BLTN). BLTN

is a new district heating and cooling network concept that promises more network efficiency. The temperature set point is optimised using the Nelder-Mead simplex method in Python (Nelder & Mead, 1965). The consumer and producer agents are distributed in the network, tracking the local set point. Based on the difference between the optimised set point and the current set point, the agents calculate local cost functions and submit proposals to the markets. The centralised broker evaluates all the proposals and chooses the most cost-efficient combination to implement. The results showed that the BLTN with the proposed control method could reduce energy consumption by more than 50% in comparison to conventional district heating systems.

Claessens et al. (2018) proposed an optimisation control approach for TCL-connected district heating systems. This approach combined reinforcement learning and a market-based multi-agent system. After aggregating the TCL cluster state information, the TCLs select the optimal action under the action policy with the Fitted Q-Iteration batch reinforcement learning algorithm (Ruiz et al., 2009). Then, the optimised actions were dispatched to the cluster of TCLs with a market-based multi-agent system. Claessens et al. (2018) highlighted a future research direction to investigate autonomous feature extraction techniques. Behboodi (2018) introduced a transactive load control scheme for TCLs in real-time retail market energy prices. Each TCL is aggregated with an agent to bid in the retail market based on temperature and anticipated energy price state information. This scheme requires less accuracy in price forecasting than a demand profile scheme since the proposed scheme only requires the mean and volatility of energy price in a specific time window. Table 2-1 summarises the application MAS architecture at the district scale. These applications have successfully coordinated district-scale multi-energy systems, such as a micro-grid. When a collection of such district-scale energy systems is connected, the regional network's reliability and economic performance need to be considered, as discussed in the next section.

Table 2-1 Summary of agent-based applications at district scale

Reference	Energy Carrier						Storage Type	Focused Topic	Approach	Platform
	Electricity	Heating	Cooling	Gas	Hydrogen	EV				
District level design										
(Kyriakarakos et al., 2013)	✓	✓	✓		✓		Electric storage and hydrogen storage	Optimal design of multi-energy micro-grid with demand-side management	PSO	TRNSYS, MATLAB, and GenOpt
(Karavas et al., 2015)	✓				✓		Electric storage and hydrogen storage	Decentralised energy management and component sizing of multi-energy micro-grid	PSO	TRNSYS, MATLAB and GenOpt
(Karavas et al., 2017)	✓				✓		Electric storage and hydrogen storage	Game theory-based multi-energy micro-grid optimal component sizing	PSO	TRNSYS, MATLAB and GenOpt
(H. Wang et al., 2021)	✓	✓					Electric storage and thermal storage (CAES)	Game theory-based capacity optimisation of multi-energy district system with CAES	PSO	Not mentioned
(S. Jin et al., 2021)	✓			✓			None	Game theory-based component optimisation method for multi-energy micro-grid	PSO	Not mentioned
Decentralised control										
(Blaauwbroek et al., 2015)	✓	✓		✓			Electric storage and thermal storage	Decentralised multi-energy micro-grid control	Mixed-integer quadratic programming	JADE, MATLAB
(Harb et al., 2015)	✓	✓					Thermal storage	Decentralised control of multi-energy micro-grid	Gurobi optimizer	JADE
(Y.-S. Li et al., 2016)	✓	✓					Electric storage and thermal storage	Decentralised control of electricity and heating coupled system	Consensus theory	Not mentioned

(Alishavandi & Moghaddas-Tafreshi, 2019)	✓	✓	✓	✓			Electric storage and thermal storage	Decentralised multi-energy micro-grid management for cost and emission minimisation	Gradient projection	Anylogic
(Shabani & Moghaddas-Tafreshi, 2020)	✓	✓			✓		Electric storage, thermal storage, and hydrogen storage	Fully decentralised multi-energy micro-grid control with an interactive clearing price	Gradient projection algorithm	Anylogic
(Samadi et al., 2020)	✓	✓					Electric storage and thermal storage	The decentralised control of multi-energy micro-grid with reinforcement learning	Q-learning	MATLAB
(Nguyen & Ishihara, 2021)	✓	✓		✓	✓		Hydrogen storage	Distributed P2P trading with fuel cells	ADMM	MATLAB
(Kumari & Tanwar, 2021)	✓	✓	✓	✓			None	Multi-energy micro-grid management with blockchain-based communication	Q-Learning	Not mentioned
(Yu et al., 2021)	✓	✓		✓			Electric storage, thermal storage, and gas storage	Multi-energy micro-grid optimisation	Asynchronous advantage actor-critic algorithm	Open AI
Micro-grid management										
(Anvari-Moghaddam et al., 2017)	✓	✓					Electric storage and thermal storage	Optimal management of building integrated micro-grid	BRL	JADE and MATLAB
(Kolen et al., 2017)	✓	✓		✓			Thermal storage	Decentralised control for clusters of electro-thermal heating devices for switch event and peak-to-valley distance optimisation	CPLEX	MESCOS
(Yang et al., 2018)	✓	✓					Thermal storage	Optimal dispatch of CHP units	Newton-Raphson	MATLAB
(H. Lin et al., 2018)	✓	✓	✓	✓		✓	Electric storage	EV impact on EH management	Taboo search	Anylogic

(Moghaddas-Tafreshi et al., 2019)	✓	✓		✓	✓		Electric storage, thermal storage, and hydrogen storage	Multi-energy micro-grid optimisation	PSO	MATLAB
(Zeng et al., 2019)	✓	✓	✓				Electric storage and thermal storage	Optimal dispatch scheme of an energy hub with integrated demand response	NSGA-III	Not mentioned
(C. Li et al., 2020)	✓	✓					Electric storage and thermal storage	Multi-energy micro-grid optimisation	Chaotic search PSO	JADE and MATLAB
(H. Liu et al., 2020)	✓	✓	✓	✓		✓	Electric storage and thermal storage	Hierarchical control of multi-energy micro-grid with RL	Q-learning	Not mentioned
(Hutty et al., 2020)	✓				✓		Hydrogen storage	Feasibility study with reversible solid oxide cells	Greedy algorithm	Anylogic
(Khan et al., 2021)	✓	✓		✓	✓	✓	Electric Storage	Multi-energy micro-grid optimisation	Generalized pattern search algorithm	JADE and MATLAB
(Farinis & Kanellos, 2021)	✓	✓	✓			✓	Electric storage and EV	Multi-energy micro-grid optimisation	PSO	Not mentioned
With heating network and clusters										
(Haque et al., 2017)	✓	✓					None	Network congestion and voltage control	Active power curtailment mechanism	JADE and MATLAB
(Claessens et al., 2018)	✓	✓					None	Optimal control of TCL and district heating network with RL	Batch reinforcement learning	Not mentioned
(Behboodi et al., 2018)	✓	✓					None	Transactive control of TCL with DR	Market bidding	Not mentioned
(Bünning et al., 2018)	✓	✓	✓				None	Distributed control of bidirectional low-temperature network	Simplex Nelder-Mead method and market bidding	Python and Modelica

2.3.1.3 Enabling regional scale integration

To manage the complexity of the integration of multiple district-scale energy systems, the literature has covered hierarchical MAS architecture and the Energy Hub (EH) concept. In contrast to the horizontal peer-to-peer communication in the district scale, the regional MAS usually adopts a hierarchical architecture to decompose the regional multi-energy system into nested layers. Gao and Ai (2018) proposed a three-layer control scheme for MESs with the integration of micro-grids. In the control scheme, agents include regional system layer agents (top), micro-grid cluster layer agents (middle), and component layer agents (bottom). Top-layer agents are responsible for regional energy network optimisation. Upon receiving top-layer optimisation results, middle-layer agents will check with network limits and coordinate micro-grid clusters. The bottom components agents are responsible for each unit's voltage and frequency control.

Zhang and Yu (2019) introduced a real-time control strategy for multi-area MESs. The control strategy is based on the Stackelberg game, where a global agent behaves as a leader, and the rest of the local MES are followers. The top-layer global MES is responsible for improving the response performance of the entire system, whereas the bottom-layer agent is responsible for cost optimisation. The Stackelberg game is solved with Q-learning. The results showed that the proposed learning methods computed faster than common heuristic algorithms, including genetic algorithms, particle swarm optimisation, and differential evolution.

In 2007, the concept of the energy hub (EH) was introduced to model the multi-energy flow on the regional level energy network (Geidl & Andersson, 2007b, 2007a). The EH concept was soon welcomed by academics. The following selected articles adopted the MAS to manage EHs. Gonzalez De Durana et al. (2014) developed a multi-agent, multi-energy flow calculation framework for the EH network. The other energy carriers' flow, such as natural gas and water, mimics the electricity power flow calculation. The multi-

energy flow problem was solved with the classic Gauss-Seidel algorithm (Bergen & Vittal, 2000). Loose et al. (2020) used a similar concept with unified agents for both district heating and electricity network simulation, while the calculation was done using the Newton-Raphson algorithm. Skarvelis-Kazakos et al. (2016) proposed a hierarchical management framework for networked EHs. Each EH agent is responsible for optimising internally, then participating in the energy market via a centralised commercial agent. The authors also conducted a lab experiment to evaluate the technical feasibility of agent-based control with a micro-CHP. The experiment showed that the agent-based control was technically feasible with cost-efficient equipment, such as a personal laptop. Zhang et al. (2021) proposed a consensus-based control on the EH network with adaptive dual control to ensure operational security and cost minimisation. Farshidian et al. (2021) formulated the multi-EH planning problem as a competitive game between the EHs. Mohamed et al. (2020) provide a distributed energy management scheme for smart islands, consisting of networked multi-energy micro-grids, EHs, and plug-in EVs. The optimisation is achieved with the primal-dual method of multipliers, which showed a better accuracy and convergence time than the ADMM method (Sherson et al., 2017).

Xi et al. (2020) proposed an automated generation control scheme combining a double deep Q network and an action discovery algorithm. The proposed scheme showed a faster convergence rate than the traditional Q-learning method. T. Wang & Zhang (2021) proposed a two-layer multi-EH coordination strategy with micro-grid clusters. Each layer was formulated with the cooperative game. The deep deterministic policy gradient algorithm solved the two-layer optimisation problem. Li et al. (2016) proposed a multi-agent reliability evaluation method for the multi-energy network considering the uncertainties of wind generation. This method adopted the Smart Agent Communication algorithm to achieve system reconstruction automation (Petcu & Faltings, 2005). Kou, Bie et al. (2021) proposed a reliability evaluation model that considers data privacy for each energy subsystem. The reliability evaluation model was

designed in a distributed architecture with agent communication. Kou, Wang, et al. (2021) also proposed a multi-energy network coordination method with a distributed accelerated descent algorithm. One of the selected studies proposed a novel multi-agent simulation framework for the multi-energy economy system. Zhu et al. (2020) introduced a novel energy-economy system simulation approach based on the Java Agent Development Framework. This simulation framework enables the modeller to define the simulation time step based on the demand, considering the compatibility of different simulation time steps. The summary of regional-level energy system management is shown in Table 2-2.

Table 2-2 Summary of agent-based application at regional scale

Source	Energy Carrier						Storage Type	Focused Topic	Approach	Platform
	Electricity	Heating	Cooling	Gas	Hydrogen	EV				
(Gonzalez De Durana et al., 2014)	✓	✓		✓			None	Multi-energy flow calculation	Gauss-Seidel algorithm	Anylogic
(G. Li et al., 2016)	✓	✓	✓	✓			Electricity storage	IES reliability evaluation with agent-based modelling	K-1 algorithm to evaluate fault occurrence	Anylogic
(Skarvelis-Kazakos et al., 2016)	✓	✓		✓	✓		Electric storage	Energy hub network optimisation	Java optimisation modeler	JADE and JOM
(Gao & Ai, 2018)	✓	✓		✓			Electricity storage and thermal storage	Multi-level hierarchical control of IES with multiple micro-grids	Multi-energy network control	PSCAD and EMTDC
(X. Zhang & Yu, 2019)	✓	✓		✓			Gas storage	Real-time coordinated control of multi-area IES	Solve fast Stackelberg equilibrium with Q-learning	MATLAB
(Zhu et al., 2020)	✓	✓		✓			None	Novel simulation framework with multi-energy economy coupled system	Linear programming	JADE
(Loose et al., 2020)	✓	✓					None	Unified multi-energy network simulation	Newton-Raphson	Agent Workbench and JADE
(Mohamed et al., 2020)	✓	✓		✓		✓	Electric storage	Smart island management	PDMM	Not mentioned
(Xi et al., 2020)	✓	✓		✓		✓	Fly wheel storage	Multi-energy network automatic generation control	DDQN-AD	Not mentioned
(N. Zhang et al., 2021)	✓	✓		✓			None	Multi-energy network control	Adaptive dual and consensus algorithm	Not mentioned
(Farshidian et al., 2021)	✓	✓		✓			Electric storage	Multi-EH planning	GAMS	GAMS
(Kou, Bie, et al., 2021)	✓	✓		✓			Electric storage and gas storage	Reliability evaluation of multi-energy network	ADMM	MATLAB and MOSEK
(Kou, Wang, et al., 2021)	✓	✓		✓			None	Multi-energy network coordination	Distributed accelerated descent	MATLAB
(T. Wang & Zhang, 2021)	✓	✓		✓			Electric storage	Multi-EH coordination	DDPG	Python

2.3.2 Market interaction with game theory in aggregation

As reviewed in Section 2.3.1, two shifts coincide in the multi-energy system. The first shift is the decentralisation of energy generation in the building to district scale, turning consumers into prosumers. The second shift is the decentralisation of decision-making, with local autonomy for agents. Thus, the decentralisation of both electricity generation and decision-making spawned novel approaches for prosumers to participate in electricity markets. There are two pathways for prosumers to trade surplus electricity: 1) selling excess electricity to local consumers, in the form of peer-to-peer trading. 2) selling aggregated excess electricity to the upstream grid, with a centralised agent control architecture, which is also referred to as virtual power plants (VPP). VPP is a framework to coordinate and export excess local electricity from prosumers beyond local communities to a list of regional electricity markets, including futures and forward markets, day-ahead markets, ancillary markets, intraday markets, and real-time balancing markets (Jafari & Akbari Foroud, 2020; Rahimiyan & Baringo, 2016; Shabanzadeh et al., 2016).

VPP frameworks are usually hierarchical aggregation management processes that coordinate clusters of DER units to profit from participating in the electricity market. As a result, DER owners need to grant aggregation operators access to their assets. The centralised decision-making architecture requires a central computing unit to collect operational statuses from DERs and provide operational instructions based on optimisation results (Kardakos et al., 2016; Zamani et al., 2016).

Recent work, therefore, investigates decentralised electricity service aggregation through virtual intermediaries, namely aggregators. Obi et al. (2020) provided a detailed review of the viable grid services that aggregators can provide. The grid services include asset aggregation, dispatch, standby generation, and ancillary services (Obi et al., 2020). Iria et al. (2020) proposed a privacy-preserving bidding strategy for an aggregator to bid in the day-ahead market. The bidding strategy is designed to ensure the security of the distribution network. The bidding strategy is obtained by ADMM

(Iria et al., 2022). A bi-level convex formulation approach was also explored for the optimal bidding of an aggregator in the day-ahead market (Shomalzadeh et al., 2022). Nevertheless, the formulations assume a single aggregator and do not explore the competition among the aggregators.

In addition, the hierarchy of the market interaction leads to a bi-level market structure, which is often modelled as a Stackelberg game in the literature (X. Zhang & Yu, 2019). In the Stackelberg game formulation, the market is led by a single leader and participated in by many followers. However, the modern energy markets involve multiple competing leaders, such as multiple aggregators, to compete for electricity aggregation, which leads to significant interactional complexity. This requires a multi-leader-multi-follower game (MLMFG), considering both the horizontal competition among leaders and vertical reaction by followers. The game theory formulation, particularly the MLMFG models, is suited to capture the dynamic market interaction in energy markets (M. Hu & Fukushima, 2015). MLMFG is a game theory model to compromise among multiple interacting decision units and competition among decision-makers of multiple hierarchical systems. A collection of players at the upper level compete in a Nash game constrained by the equilibrium conditions of another Nash game at the lower level. The players in the upper- and lower-levels are called leaders and followers, respectively. The optimal strategies of the leaders are determined based on the conjectured reactions of the followers.

Xiao et al. (2020) used the MLMFG model to propose a privacy-preserving aggregation framework to participate in the day-ahead market, where aggregated prosumers are the leaders and end-users are followers. The game model is solved by mixed integer linear programming (Xiao et al., 2020). Hong et al. (2023) adopted the MLMFG model to optimise aggregation across both the day-ahead market and the local electricity market. The diagonalisation algorithm is used to solve the MLMFG model (Hong et al., 2023).

The literature reviewed in Section 2.3 reveals a disconnection between the agent-based computation infrastructure and IoT technologies, and the complex market interactions

in prosumer aggregation. The computation infrastructure, such as edge computing, is a viable technological pathway to solve the complex market model. However, there is no computational framework to address the interactional complexity from the integration of both horizontal and vertical market interactions. Consequently, this section identifies the disconnection as **Research Gap 2**.

> **Research Gap 2**: There is no computational framework that can accommodate the bi-level interactional complexity among aggregators and prosumers with an algorithm that can solve the MLMFG in a fully decentralised manner.

Chapter 5 addresses this gap by proposing a novel computational framework for intelligent aggregation, in which competing aggregators (leaders) and prosumers (followers) iteratively reach equilibrium through a novel graph-based consensus algorithm with proven linear convergence.

2.4 Evaluative complexity in strategic decisions

Unlike operational and transactional challenges, strategic decisions involve selecting long-term technology pathways from among alternatives with distinct attributes. Hence, the energy systems are no longer optimised solely for cost minimisation with a single technology pathway; economic viability, environmental sustainability, and energy efficiency are also vital inputs for decision-making. As a result, the evaluative complexity emerges.

A prime example of this complexity is the development of international green hydrogen supply chains. As nations commit to net-zero targets, policymakers and practitioners face a critical strategic choice: selecting the right hydrogen carrier. This Section reviews how existing approaches address evaluative complexity through techno-economic and environmental models. Section 2.4.1 examines the policy contexts that drive the development of the green hydrogen economy. Section 2.4.2 assesses the existing evaluative frameworks and highlights a knowledge gap within them.

2.4.1 Green hydrogen policy and evaluative complexity

The shift to low-carbon energy supply with green hydrogen is supported by the green hydrogen policies at the state level. The shifts introduce a form of evaluative complexity, where selecting a GHC pathway that satisfies divergent requirements across the international green hydrogen supply chain.

On the demand side, major industrial economies have established ambitious hydrogen targets that require the development of international green hydrogen supply chains. The European Union's hydrogen policy sets out a domestic production target of 10 million tons by 2030 (Erbach & Jensen, 2021). The hydrogen review by IRENA also highlights that the domestic production in the EU may not meet the growing demand, hence importing green hydrogen is an important strategy to fill the demand gap (IRENA, 2019).

Japan has positioned itself as a pioneer of the green hydrogen industry, where Japan sets a target of 3-million-ton hydrogen supply chain by 2030 and 20 million tons by 2050. In addition to hydrogen, Japan's hydrogen policy highlights the critical role of hydrogen carriers, such as ammonia, in decarbonising the energy sector (Green Hydrogen Organisation, 2025). The United Kingdom's hydrogen strategy supports both electrolytic and carbon capture-enabled hydrogen. More specifically, the UK Hydrogen Strategy sets out an ambitious plan to deliver 5 GW of green hydrogen by 2030, exploring the import of GHCs to close the supply gap (DESNZ, 2024).

On the supply side, countries with rich renewable resources could seize this opportunity for economic development and industrialisation. South Africa has great potential to be a key player in green hydrogen export, due to its abundance of renewable energy resources (Rehman et al., 2022). Hence, South Africa has established a strategic plan to become a major green hydrogen exporter, to capture 4% of the global green hydrogen market by 2050 (CSIS, 2022). To meet hydrogen demand, evaluating and selecting appropriate GHCs is crucial. The choice of GHC will affect costs of supply, environmental footprint, and supply chain efficiency, ultimately determining whether national strategies can translate into real-world projects. Current literature often evaluates these metrics in isolation, as the following sub-sections review the existing evaluation framework for international green hydrogen trade.

2.4.2 Limitations of existing evaluation frameworks

The existing literature evaluates the performance of GHC pathways with techno-economic, environmental, and combined assessment frameworks. For research adopting a techno-economic analysis framework, a key finding in the literature is the dominance of renewable energy costs. As shown in Table 2-3, studies by Kenny et al. (2024) and Heuser et al. (2019) both conclude that the availability and cost of renewable resources in the exporting country are the most significant drivers of the final Levelised Cost of Hydrogen (LCOH). In addition, the choice of carrier introduces substantial variations in the upfront investments. Specifically, Raab et al. (2021) analysed the large-

scale hydrogen export system from Australia to Japan with a comparative cost analysis of three green hydrogen carriers: LH_2, DBT and TOL. The significant capital expenditure (CAPEX) required for liquefaction plants and cryogenic infrastructure made LOHCs, such as DBT and TOL, more economical than LH_2. This highlights a key difference between carriers that require high upfront investment and those that are compatible with existing energy infrastructure. The analysis by Niermann et al. (2021) provides additional insights into LHOC operations, where the cost competitiveness of LOHCs depends on the cost of dehydrogenation heat supply. Using hydrogen to supply heat will increase overall system costs and reduce system efficiency.

The second stream of research focuses on the comparative international study of GHCs' supply chains, particularly in terms of environmental aspects, using life cycle assessment (LCA). A consistent finding from the literature is the importance of the electricity used for electrolysis. Noh et al. (2023) conducted the LCA and energy efficiency analysis on hydrogen imports to Korea. The results show that the carbon intensity of the grid in the exporting country is a critical factor determining the final environmental footprint. Abeynaike and Barbenel (2024) conducted a cradle-to-grave LCA on exporting NH_3 and LH_2 from New Zealand to Japan, using the partially decarbonised grid of New Zealand. The results show that there is no net environmental benefit compared with Japan's existing grid, even though New Zealand's grid supply is more than 80% renewable. Beyond electricity supply, Cho et al. (2024) assessed the life cycle impact of different LOHC production methods. The results indicate that utilising biomass-derived TOL and DBT can result in a lower environmental impact compared to their fossil-based counterparts.

Table 2-3 Literature review on the international hydrogen carriers

Reference	Carriers considered	Export Country	Import Country	Assessment Method
Studies on techno-economic analysis of hydrogen carriers				
(Kenny et al., 2024)	LH_2 and NH_3	Chile, Namibia, and Morocco	Germany	Levelised cost
(Song et al., 2021)	LH_2, NH_3, and TOL	China	Japan	Levelised cost
(Niermann et al., 2021)	LH_2, DBT, MeOH, NEC, CGH_2	Algeria	Germany	System efficiency and levelised cost
(Heuser et al., 2019)	LH_2	Patagonia	Japan	Levelised cost
(Restelli et al., 2024)	LH_2	North Africa	North Italy	Levelised cost and process simulation
(Raab et al., 2021)	LH_2, TOL, and DBT	Australia	Japan	levelised cost
Studies on the environmental impact analysis of hydrogen carriers				
(Abeynaike & Barbenel, 2024)	LH_2 and NH_3	New Zealand	Japan	Global warming potential
(Noh et al., 2023a)	LH_2, CGH_2, TOL, NH_3	Australia	South Korea	Global warming, acidification and eutrophication potential
(Cho et al., 2024)	TOL and DBT	Australia	Netherland, South Korea, and Japan	ReCiPe Midpoint and Endpoint
Studies combined techno-economic and environmental impact analysis				
(Lee et al., 2022)	LH_2, NH_3, MeOH, TOL, and DBT	Australia	South Korea	levelised costs and carbon intensity
(Godinho et al., 2023)	TOL, DBT	Portugal	Netherland	levelised cost and global warming
(Dickson et al., 2022)	LH_2, NH_3, MeOH, synthetic natural gas, TOL, DBT	Does not specify	Does not specify	Levelised cost and CML-IA life cycle impact assessment

Recent studies also combine the techno-economic and carbon footprint calculations, which consistently highlight the trade-off between economic and environmental performance. No single GHC optimises all criteria simultaneously. Dickson et al. (2022) analysed the levelised costs and environmental impact of liquid hydrogen, ammonia, methanol, synthetic natural gas, TOL, and DBT. The results show that ammonia and methanol are the most promising hydrogen carriers in terms of economic performance, while LH_2 has the lowest overall environmental impact. Similar findings were reported by Lee et al. (2022), who investigated the techno-economic and carbon intensity performance of five hydrogen carriers, including LH_2, NH_3, MeOH, TOL, and DBT. For the target export from Australia to South Korea, TOL is the most cost-effective hydrogen carrier, while ammonia is recommended for the lowest carbon emissions in a fully renewable energy-supplied scenario.

The literature review above highlights that the intrinsic trade-off creates evaluative complexity. One hydrogen carrier will excel in one policy-relevant criterion but not in another. For example, LH_2 tends to have low environmental impacts (Dickson et al., 2022), but high-levelised costs (Song et al., 2021). Such distinct performance makes carrier selection a source of evaluative complexity. This recurring conflict highlights the need for a framework to resolve these trade-offs. Although Multi-Criteria Decision-Making (MCDM) has been applied to solve the conflict, two gaps remain within existing frameworks.

First, the economic criterion is oversimplified. The MCDM framework by Oner & Khalilpur (2022) uses a simplified LCOH model that does not account for the time value of cash flows or inflation, both of which are essential for evaluating long-term, capital-intensive hydrogen projects. Second, environmental criteria often focus only on carbon emissions. The majority of existing LCA literature on the international trade of hydrogen carriers, as shown in Table 2-3, focuses almost exclusively on Global Warming Potential (GWP) or its variants as the sole environmental criterion. This narrow focus omits environmental impact from other damage pathways, such as fine particulate matter formation. Thus, this thesis has identified the **Research Gap 3**:

> **Research Gap 3**: There is currently no integrated MCDM framework that simultaneously evaluates hydrogen carriers based on discounted techno-economic performance, comprehensive life-cycle environmental impacts, and

carrier-specific energy efficiency. Furthermore, the strategic potential of the South Africa–UK green hydrogen corridor has not been analysed in existing literature.

Chapter 6 closes this gap with a novel MCDM framework that quantitatively evaluates GHCs with discounted technical-economic analysis and comprehensive environmental assessment. The evaluation framework is applied to five leading carriers (LH_2, NH_3, methanol, TOL and DBT) for the South Africa-UK supply chain, thereby providing the first holistic ranking of GHC options for this corridor.

2.5 Chapter summary

This chapter has reviewed existing computational frameworks through the lens of nested complexity. The analysis of uncertainty complexity revealed a gap in a non-probabilistic, risk-aware optimisation framework. The review of interactional complexity highlighted the need for a decentralised, competitive multi-party aggregation model. Finally, the assessment of evaluative complexity identified the lack of an integrated framework combining discounted economics with comprehensive environmental metrics. These identified gaps collectively provide a foundation for the overarching research question and methodological design presented in the subsequent chapter.

Chapter 3

3. Research methodology

3.1 Introduction

Fundamental shifts in decision-making are driving the transition to a multi-energy system. The first shift is the nature of operational uncertainty, caused by the increasing adoption of intermittent renewable energy sources. The second shift involves a structural shift from centralised control to distributed coordination, transforming the conventional top-down architecture of the electricity grid into a bottom-up construction of autonomous agents. The third shift relates to the criteria used for strategic evaluation, moving away from a sole focus on cost with multi-criteria decision-making. As a result, traditional computational frameworks that are deterministic, centralised, and focused on a single objective cannot effectively address the complexities introduced by these three shifts.

Section 3.2 explains how these three shifts create a nested complexity that motivates the overarching research question of this thesis. Section 3.3 outlines the selection of methods to address the research question and explains why they are appropriate. Section 3.4 outlines the main data sources and assumptions used in the following chapters.

3.2 Research question

The three shifts outlined in Section 3.1 create a nested hierarchy of decision-making complexities that develop as the energy system expands from operational to strategic levels. At each level of this hierarchy, a dominant form of complexity makes the traditional computational frameworks inadequate. At the lowest operational scale, traditional computational frameworks are designed to solve deterministic scheduling problems, where demands are predictable, and electricity generation is dispatchable. However, the rising integration of intermittent wind and solar power introduces uncertainty into energy scheduling, making the deterministic computational framework unsuitable for systems with significant renewable resources. Furthermore, probabilistic

distributions based on historical data may not accurately predict market volatility, resulting in an information gap regarding future market prices. This operational uncertainty is a critical source of complexity, which can be regarded as uncertainty complexity. It presents a major challenge for micro-grid operators who face unpredictable electricity market price volatility (Nojavan et al., 2015). The ability of agents to manage this complexity and formulate operational strategies that align with the risk preferences of micro-grid operators underpins collective action within the broader energy system.

Building on the operational scale, the shift from centralised control to distributed coordination gives rise to interactional complexity. This next layer of complexity arises because the system comprises many diverse agents, each with its own operational strategies. The adoption of distributed energy resources makes the system difficult to manage with a single controller, where each distributed energy asset aims to maximise its own utilities. At the transactional scale, the interactions among agents introduce a game-theoretic dynamic where an agent's decision depends on others'. The existing centralised computational framework faces challenges in addressing such distributed dynamic interactions among agents. Therefore, interactional complexity remains at the transactional level.

At the top of the hierarchy, shifts in strategic evaluation lead decision-makers to choose among different technology pathways with unique characteristics. Traditionally, the strategic decision-makers were guided by the conventional single objective of minimising the levelised cost of energy. However, strategic decisions, such as choosing the appropriate green hydrogen pathways for international trade, are multidimensional. Policymakers and investors must choose a hydrogen carrier based on multiple evaluation metrics, subject to lower-level complexities. For example, the economic criteria can represent the aggregated financial performance under market volatilities (uncertainty complexity) and market transactions (interactional complexity). The decision-making at the strategic scale, hence, should be based on multi-criteria evaluation, which can be regarded as evaluative complexity.

The nested hierarchy of complexities reveals gaps between the future multi-energy systems and the traditional computational frameworks. New computational frameworks

are required to address the emerging complexities. This revelation motivates the **overarching research question** of this thesis:

> **Overarching research question**: What new computational frameworks are required to manage the nested hierarchy of uncertainty, interactional, and evaluative complexities that emerged at different scales of multi-energy system transition?

To provide a comprehensive answer to this question, this thesis adopts a multi-scale research methodology. The literature review in Chapter 2 identified three research gaps in existing computational frameworks, which informed the research objectives of this thesis. Each objective aims to address a specific layer of the hierarchy of complexity where the identified gaps exist. From the operational to the transactional, and finally to the strategic scale, the three research objectives collectively address the overarching research question.

The first research objective focuses on the foundational layer of the hierarchy, uncertainty complexity. This objective addresses research gap 1: the need for a risk-adjusted computational framework for novel assessments under severe market uncertainty.

> **Objective 1**: To establish a computational framework that is able to guide decision-makers with different risk preferences for energy assets under severe uncertainty.

This objective targets the operation of the energy systems. It requires developing a framework that does not rely on assumptions about the probabilistic distributions of key decision variables. The second objective builds on the operational scale to address the interactional complexity, responding to the research gap 2 in the lack of a decentralised multi-party competition market framework.

> **Objective 2:** To formulate a computational framework that is capable of coordinating the decentralised agents with game-theoretic interactions.

This objective aims to address the limitations of existing single-aggregator or centralised aggregation frameworks. The final objective is at the strategic scale of

hierarchy to address the evaluative complexity, responding to the gap in a multi-criteria strategic assessment framework.

> **Objective 3**: To construct a computational framework that moves beyond single-metric decision-making to resolve the strategic trade-offs inherent in multi-criteria decision-making.

Collectively, the three objectives form a coherent response to the overarching research question. By developing new computational frameworks, this thesis informs the future decision-making tools for the multi-scale energy system transition. The following section explains the justification and rationale for why the methods are suitable for fulfilling the research objectives.

3.3 Methodological framework

The research objectives outlined in Section 3.2 reveal the need for new computational frameworks to manage the complexities in multi-energy transition. This section provides a justification and rationale for the research methods adopted to construct the new computational frameworks. As illustrated in Figure 3-1, each research objective is achieved with a specific methodological innovation, which collectively answers the overarching research question.

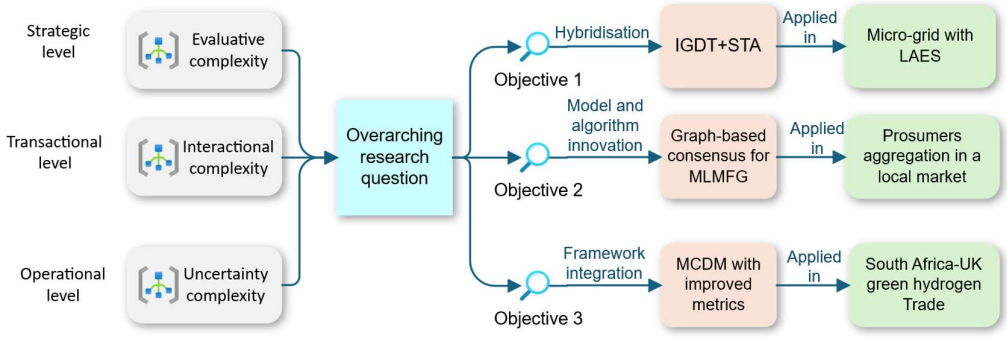

Figure 3-1 Schematic of the methodological framework.

To achieve **Objective 1**, this thesis proposes a new computational framework by hybridising the risk management principles of IGDT with the structured optimisation from STA. The core challenge to achieving this objective is making decisions under deep, non-probabilistic distributions. Existing uncertainty-handling methods, such as stochastic programming, rely on known, stationary probability distributions. IGDT is a non-probabilistic framework explicitly designed for decision-making under severe uncertainty, especially the deep uncertainty of electricity market prices.

As reviewed in Chapter 2, most of the existing literature on IGDT application in energy system scheduling uses convex optimisation. The novel energy assets, such as LAES, require optimisation using a non-convex method. Hence, the risk-based logic of IGDT was hybridised with the STA, which is a powerful heuristic search algorithm. Compared with traditional heuristic algorithms such as GA and PSO, STA has structure-learning capabilities and demonstrates better performance. This novel hybrid IGDT-STA framework can schedule microgrids based on decision-makers' risk preferences, thereby addressing **Objective 1**.

To achieve **Objective 2**, both game-theoretical models and algorithmic innovations for optimisation were required. The key challenge is that the transactional scale is to model and solve a decentralised market with a hierarchical structure with competing agents. The existing literature often adopts Stackelberg game models with a single leader structure. This structure cannot capture horizontal competition among multiple aggregators, a key transition in future energy markets. Therefore, this thesis adopts the MLMFG formulation, as it can capture the horizontal competition among leaders (aggregators) and the hierarchical response of followers (prosumers).

Existing methods for solving game-theoretic models are usually centralised and require global information from all market participants. The centralised algorithm could not fulfil the privacy requirements of the distributed energy asset owners. This gap motivates the development of a novel graph-based consensus algorithm. This algorithm provides a decentralised method for solving the MLMFG model via peer-to-peer information exchange via edge computing. As a result, the innovation in game theoretic models and optimisation algorithms fulfils **Objective 2** by providing a computational framework for future multi-party aggregation.

Finally, this thesis achieves **Objective 3** by methodological innovation in framework integration and enhancement. The strategic challenges of choosing technology pathways with distinct performance in key indicators, such as levelised costs and environmental footprint, make single-metric analysis insufficient. This leads to selecting MCDM as the appropriate class of methods. This thesis adopts the Analytic Hierarchy Process (AHP) with TOPSIS and VIKOR. The AHP provides a transparent method for capturing stakeholder priorities and weighting the decision criteria. The subsequent use of both TOPSIS and VIKOR provides a quantitative ranking of potential candidates. TOPSIS identifies the ideal solution that excels on key metrics, while VIKOR identifies the best compromised solution that minimises regret.

The key methodological innovation in MCDM is the enhancement of the decision inputs. The literature review revealed that existing MCDM applications in green hydrogen trade often use simplified criteria inputs, such as an undiscounted levelised cost model or a focus solely on global warming potential. This thesis proposed an integrated framework that considers the time value of money and production, and a comprehensive life cycle assessment using the ReCiPe Endpoint method. This integration of enhanced criteria fulfils **Objective 3** by providing a transparent computational framework to navigate strategic trade-offs.

3.4 Data sources, assumptions, case study design

To validate the proposed computational framework, each framework is applied to a specific case study that represents the complexities of operational, transactional, and strategic scales. This section details the data sources, modelling assumptions, and case study design employed to validate the research objectives.

To validate the IGDT-STA framework for managing the uncertainty complexity at the operational scale, the case study design focuses on a grid-connected micro-grid in Northwest China. Several critical assumptions were made during the operational optimisation. First, the thermodynamic processes in the LAES system, such as compression, liquefaction, and expansion, are modelled as a steady-state system. Second, the micro-grid is assumed to be a price taker in the day-ahead market, meaning its operations do not affect the market prices. This assumption allows the study to focus solely on the impact of price uncertainty on the micro-grid.

The case study design at the operational scale compares a standard GA representing heuristic optimisation, a stochastic programming approach representing probabilistic risk management, and a Monte Carlo simulation representing a baseline of random scenarios. The case study includes running numerical models under various risk preference levels to generate robustness and opportunity curves. This design allows for a direct quantitative comparison of methods.

Moving to addressing the interactional complexity, the validation of the graph-based algorithm for MLMFG is conducted with the SimBench dataset (Meinecke et al., 2020). Specifically, an urban low-voltage distribution topology is combined with 57 synthetic prosumers to create the competitive environment. There are two critical assumptions in the case study design. First, all agents, including aggregators and prosumers, are assumed to follow the utility-maximising rationale, meaning the utility of the actions determines their actions. Second, the battery degradation for V2G participants is assumed to follow a power-law distribution, which is important for prosumers' utility functions to remain convex.

The case study design of transactional scale combines numerical and complexity analysis. The numerical results of market interactions show that the system converges to a market equilibrium. In addition, the proposed graph-based algorithm is also benchmarked with other decentralised optimisation methods, which are detailed in Chapter 5.

Finally, to validate the new MCDM framework for managing evaluative complexity at the strategic scale, the case study is focused on the previously unexamined hydrogen corridor. The data sources of this case study include the techno-economic model and the environmental analysis model. The details of the data sources and assumptions are presented in Chapter 6 and Appendix A1 and A2.

The key assumptions for the strategic scale case study are twofold. First, this case study assumes the project lifetime of 20 years, which is an input for the techno-economic model for calculating LCOH and internal rate of return. The choice of a 20-year project life is to align the project with the key technological component, the proton exchange membrane. Second, the supply chain is assumed to be a steady-state system delivering a fixed annual volume of hydrogen.

In addition to the base-case analysis, this case study includes a scenario-based sensitivity analysis. These sensitivity cases are constructed with systematic changes in critical parameters, such as the renewable capacity factor in South Africa. Furthermore, a criteria-weighting analysis is performed to determine the different stakeholder priorities.

3.5 Chapter Summary

This chapter builds the methodological foundation for the thesis. The shifts in operational uncertainty, decentralised coordination, and strategic evaluation create a nested hierarchy of decision-making complexities. How to address these complexities in computational frameworks is the overarching research question of this thesis.

Accordingly, the research design is structured to address the research gap at a specific level of complexity. First, a new computational framework for risk-inclusive operations is required to manage the uncertainty complexity at the operational scale. Second, a new computational framework for decentralised coordination is needed for management interactional complexity at the transactional scale. Lastly, a new computational framework is required for multi-criteria decision-making for managing evaluative complexity at the strategic scale. This chapter also details the high-level data sources, assumptions, and case study designs. Chapters 4, 5, and 6 will demonstrate how these new computational frameworks can effectively facilitate the multi-scale transition towards a sustainable energy future.

Chapter 4

4. Addressing complexity in LAES micro-grids operation under severe market uncertainty[2]

4.1 Chapter introduction

The emergence of novel physical energy storage technologies, such as compressed air energy storage (CAES) and liquid air energy storage (LAES), introduces additional complexity to the conventional energy systems. Physical air-based storage technologies, such as CAES and LAES, combine high safety with low environmental impacts (Yan et al., 2021). CAES converts electrical energy into potential energy of compressed air molecules, which are stored in underground caverns or other suitable locations. CAES has a high safety level, but its deployment is constrained by suitable geological formations, e.g. caves or abandoned mines (Damak et al., 2020; Heo et al., 2022). On the other hand, LAES is a novel large-scale physical energy storage technology that compresses and condenses air into a liquid state in the cryogenic storage tank, as shown in Figure 4-1. It should be noted that the round-trip efficiency of LAES ranges from 50% to 60%, depending on the system design (She et al., 2017). Although LAES tends to have lower round-trip efficiency than other storage methods, it has the advantages of high energy storage density, accessible storage, and is less restricted by geographical conditions compared with CAES.

[2] This chapter is adapted from **Yao, R.**, Xie, H., Wang, C., Xu, X., Du, D., Varga, L., & Hu, Y. (2024). A multi-agent-based micro-grid day-ahead optimal operation framework with liquid air energy storage by hybrid IGDT-STA. *Journal of Energy Storage*, 86, 111318. https://doi.org/10.1016/j.est.2024.111318

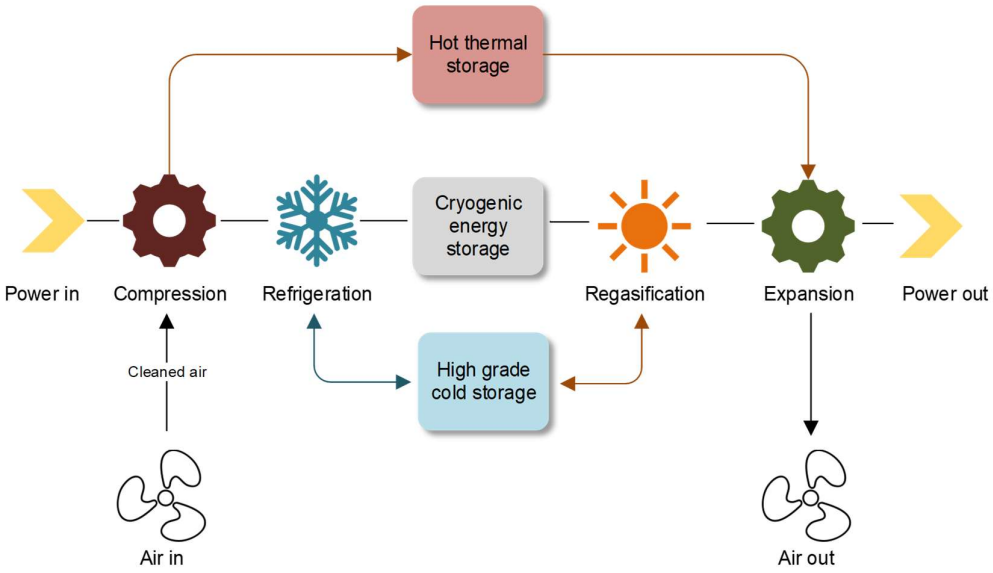

Figure 4-1 Schematic diagram of LAES system operation.

In addition, the operation strategy should be able to suit the risk preferences of decision-makers. Thus, this chapter addresses **Objective 1** on the need to establish a computational framework that can consider different risk profiles of decision-makers with new energy assets. This chapter achieves this objective through three contributions:

- The IGDT method is implemented on a micro-grid with LAES for the first time to solve the optimal operation problem with uncertainty in market electricity prices.
- This chapter proposed a novel operational framework of the IGDT-STA hybrid method with a multi-agent system to optimise the robustness function and opportunity function to suit the risk preferences of decision-makers.
- This chapter compared the proposed IGDT-STA method with genetic algorithm optimisation techniques, stochastic method, and Monte Carlo method in a case study. The results showed the effectiveness of IGDT-STA.

The remainder of the chapter is organised as follows. Section 4.2 details the hybrid IGDT-STA method. Section 4.3 describes its implementation in a multi-agent LAES micro-grid. Section 4.4 presents the case study and comparative results. Section 4.5 summarises key findings.

4.2 Uncertainty decision-making with IGDT-STA

This section explains the mathematical formulation of the IGDT-STA method. Section 4.2.1 describes the IGDT mathematical models, and Section 4.2.2 includes the mathematical formulation of STA.

4.2.1 IGDT mathematical models

The IGDT effectively manages system uncertainties by focusing on the information gap. Rather than relying on probability distributions, it specifically addresses the divergence between anticipated and actual values within an uncertainty parameter. As a result, IGDT is able to model uncertainties with a severe lack of information (Majidi et al., 2019). The following section explains the details of the system model, the uncertainty model, and performance requirements in IGDT.

4.2.1.1 IGDT system model

The decision variables and uncertainty parameters in the decision space and uncertainty space are P and λ, respectively. The system model can be expressed as the optimisation problem (4.1) to minimise the system cost.

$$\begin{aligned} &Minimise \quad C(P,\lambda) \\ &s.t. G_i(P,\lambda) \geq 0, \qquad i = 1, \dots, m \\ &\quad H_j(P,\lambda) = 0, \qquad j = 1, \dots, n \end{aligned} \tag{4.1}$$

where $C(P,\lambda)$ is the system cost function which takes decision variable P and uncertainty parameter λ as function input. $G_i(P,\lambda) \geq 0$ and $H_j(P,\lambda) = 0$ are inequality and equality constraints, respectively.

4.2.1.2 Uncertainty model

The uncertainty model of IGDT aims to describe the information gap between the predicted value of the uncertainty parameter and its true value (Ben-Haim, 2006). The uncertainty model can be expressed as Eq. (4.2):

$$U\left(\alpha, \hat{\lambda}_t\right) = \left\{\lambda_t : \frac{\left|\lambda_t - \hat{\lambda}_t\right|}{\hat{\lambda}_t} \leq \alpha\right\}, \alpha \geq 0 \tag{4.2}$$

where λ_t denotes the actual value of the uncertain parameter. $\hat{\lambda}_t$ denotes the predicted value of the uncertainty parameter. α is the bound for system uncertainty levels. In essence, the uncertainty model ensures that the deviation of the uncertainty parameter λ_t with respect to $\hat{\lambda}_t$ will not exceed $\alpha\hat{\lambda}_t$.

4.2.1.3 Performance requirements

The IGDT performance requirements are the quantitative evaluations of objective function performance with respect to system robustness and opportunity values. The performance requirements consist of the robustness function Eq. (4.3), and the opportunity function Eq. (4.4).

$$\hat{\alpha}(P, C_{averse}) = \max_{\alpha}\{\alpha: \max(C(P,\lambda)) \leq C_{averse}\} \tag{4.3}$$

where C_{averse} is the target system cost that risk-averse decision-makers are willing to pay. The function value $\hat{\alpha}(P, C_{averse})$ indicates the maximum possible system uncertainty with a given cost target C_{averse}. In other words, Eq. (4.3) returns the maximum fluctuation bound for uncertainty parameter λ. The greater value of $\hat{\alpha}(P, C_{averse})$ means the system is more robust and less susceptible to uncertainties. Therefore, the risk-averse decision-makers are able to make robust decisions, ensuring the system is immune to uncertainties.

$$\hat{\beta}(P, C_{taking}) = \min_{\alpha}\{\alpha: \min(C(P,\lambda)) \leq C_{taking}\} \tag{4.4}$$

where C_{taking} is the target system cost that risk-taking decision-makers are willing to pay. The opportunity function Eq. (4.4) returns the minimum fluctuation range of uncertain variables that risk-taking decision-makers usually allow. This function mainly evaluates the positive aspects of uncertainty and finds the minimum uncertainty level that the system can tolerate by reducing costs.

4.2.2 STA implementation

STA uses the state space representation in modern control theory as a framework to solve optimisation problems (X. Zhou et al., 2012).

With state space representation, the unified form of STA is (X. Zhou et al., 2012):

$$\begin{cases} x_{k+1} = A_k x_k + B_k u_k \\ y_{k+1} = f(x_{k+1}) \end{cases} \tag{4.5}$$

where $f(\cdot)$ denotes the objective function. x_k is the current state which corresponds to a solution to the optimisation problem. x_{k+1} is the next state and y_{k+1} is the fitness value at next state. A_k and B_k denote the state transition matrices, which can also be regarded as state transformation operators. u_k denotes the function of x_k and the historical state. With state space representation, the STA method defines four state transformation operators to solve optimisation problems.

- Rotation transformation:

$$x_{k+1} = x_k + \omega \frac{1}{n\|x_k\|_2} R_r x_k \tag{4.6}$$

where $\omega \in \mathbb{R} > 0$ denotes a rotation factor. $R_r \in \mathbb{R}^{n\times n}$denotes a random matrix whose entries are uniformly distributed random variables between $[-1,1]$. $\|\cdot\|_2$ denotes Euclidean norm (or L2 norm) of a vector. n is the dimension of the state x_k. The rotation operator has the functionality to search in a hypersphere with the maximum radius ω, which has been proven in (X. Zhou et al., 2012).

- Translation transformation:

$$x_{k+1} = x_k + \beta R_t \frac{x_k - x_{k-1}}{\|x_k - x_{k-1}\|_2} \tag{4.7}$$

where $\beta \in \mathbb{R} > 0$ denotes a translation factor. $R_t \in \mathbb{R}$ denotes a uniformly distributed random variable on interval [0,1]. The translation transformation aims to line search for a possible better candidate solution, which can be regarded as a heuristic operator.

- Expansion transformation:

$$x_{k+1} = x_k + \gamma R_e x_k \tag{4.8}$$

where $\gamma \in \mathbb{R} > 0$ denotes an expansion factor. $R_e \in \mathbb{R}^{n\times n}$ denotes a random diagonal matrix under normal distribution. The expansion transformation is designed for global search with probabilities to search the whole space.

- Axesion transformation:

$$x_{k+1} = x_k + \delta R_a x_k \tag{4.9}$$

where $\delta \in \mathbb{R} > 0$ denotes an axesion operator. $R_a \in \mathbb{R}^{n \times n}$ denotes a sparse random diagonal matrix under the normal distribution, with only one random entry being non-zero. The axesion transformation has the functionality to strengthen single-dimensional search (X. Zhou et al., 2019).

In addition to the state space representation and transformation operators, STA method also incorporated sampling in the optimisation process. A representative sampling technique is used to avoid enumerating all potential candidate states (X. Zhou et al., 2019). The STA performs a transformation operation with multiple times, parameterised by a positive integer Ψ_{SE}, representing search enforcement constant. After explaining the four transformation operations and sampling techniques, the STA can be described with the following pseudocode:

State ← initialisation(Ψ_{SE})
Best ← fitness(funfcn, State)
Repeat
  if $\omega < \omega_{min}$ **do**
    $\omega \leftarrow \omega_{max}$
  end if
  Best ← expansion (funfcn, Best, Ψ_{SE}, β, γ)
  Best ← rotation (funfcn, Best, Ψ_{SE}, β, ω)
  Best ← axesion (funfcn, Best, Ψ_{SE}, β, δ)
  $\omega \leftarrow \frac{\omega}{fc}$
until the termination criterion is met

The initialisation (·) in the above pseudocode initialise a candidate solution in the feasible set. The fitness (·) selects the best solution with state vector after evaluation with the objective function. During the optimisation process, the rotation operator ω decrease periodically from maximum value ω_{max} to minimum value ω_{min} with lessening coefficient fc. Noticeably, the translation operation is implemented in the other three operations once a better candidate solution is found. Thus, the translation operator β is passed to the other three operations: expansion (·), rotation (·), and axesion (·).

4.2.3 IGDT-STA hybrid optimisation algorithm

The proposed IGDT-STA decision-making strategy integrates the STA algorithm into the IGDT's optimisation process. The IGDT-STA involves two distinct stages. During the first stage, STA is utilised to optimise a risk-neutral strategy using prediction data. In the second stage, STA optimises the performance requirement functions of the IGDT, which encompasses both the robustness function and the opportunity function, based on the risk-neutral strategy obtained in the first stage. The micro-grid's optimal operation strategy with LAES is developed, accounting for uncertain market electricity prices. Figure 4-2 depicts the IGDT-STA method flowchart, and the solution process is summarised as follows:

(1) Input the necessary data of the micro-grid system, such as the parameters of wind power generation, photovoltaic power generation, micro gas turbine, LAES, and the predicted value of the market electricity price.

(2) The base optimisation model of the micro-grid with LAES is formulated. This model aims to minimise the operation cost of micro-grids with LAES and considers various constraints from LAES, micro gas turbine, and tie-line transmission power.

(3) The STA method is used to solve the basic optimisation model of the micro-grid with LAES and further obtain the risk-neutral strategy, which is the minimum operating cost strategy of the system based on the predicted market price. The minimum operating cost under this strategy is also called the risk-neutral cost.

(4) Different cost targets are set according to the minimum operating cost corresponding to the obtained risk-neutral strategy. The cost targets can be divided into two categories: the cost target greater than the risk-neutral cost and the cost target less than the risk-neutral cost.

(5) Judge the category of the cost target. When the target cost is greater than the risk-neutral cost corresponds to the robustness optimisation model, the model aims to maximise the robustness function in the IGDT method. When the target cost is less than the risk-neutral cost corresponds to the opportunity optimisation model, the model aims to minimise the opportunity function in the IGDT method. The above two models both consider the constraints of the system.

(6) The STA method is applied to solve the micro-grid's robust and opportunity optimisation models with LAES, respectively. As a result, it obtains the risk-averse strategy and the risk-taker strategy.

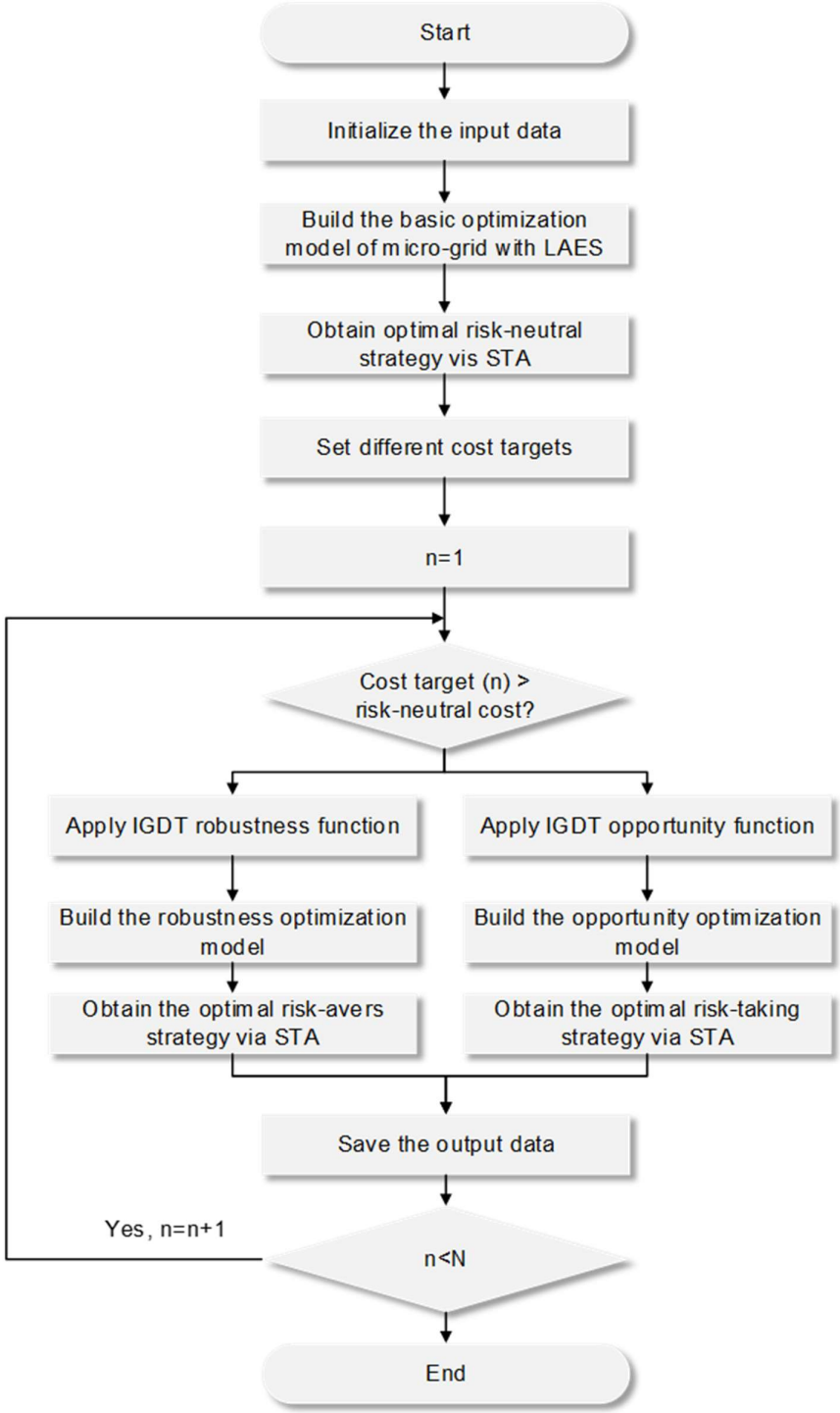

Figure 4-2 The flow chart of IGDT-STA

4.3 MAS-Based micro-grid coordination model

This section describes the details of the MAS-based micro-grid coordination model, where the agents solve for optimal operation strategy cooperatively. Section 4.3.1 explains the structure of the coordination model, and Section 4.3.2 describes the details of agent tasks.

4.3.1 Micro-grid environment

The micro-grid environment, as shown in Figure 4-3, includes a power grid agent, load agent, photovoltaic agent, wind turbine agent, micro-turbine agent, LAES agent, and micro-grid coordination agent. The power grid agent is responsible for retrieving the day-ahead price information, and the load agent is accountable for forecasting the day-ahead load curves. The details of the remaining agents will be explained in Section 4.3.2.

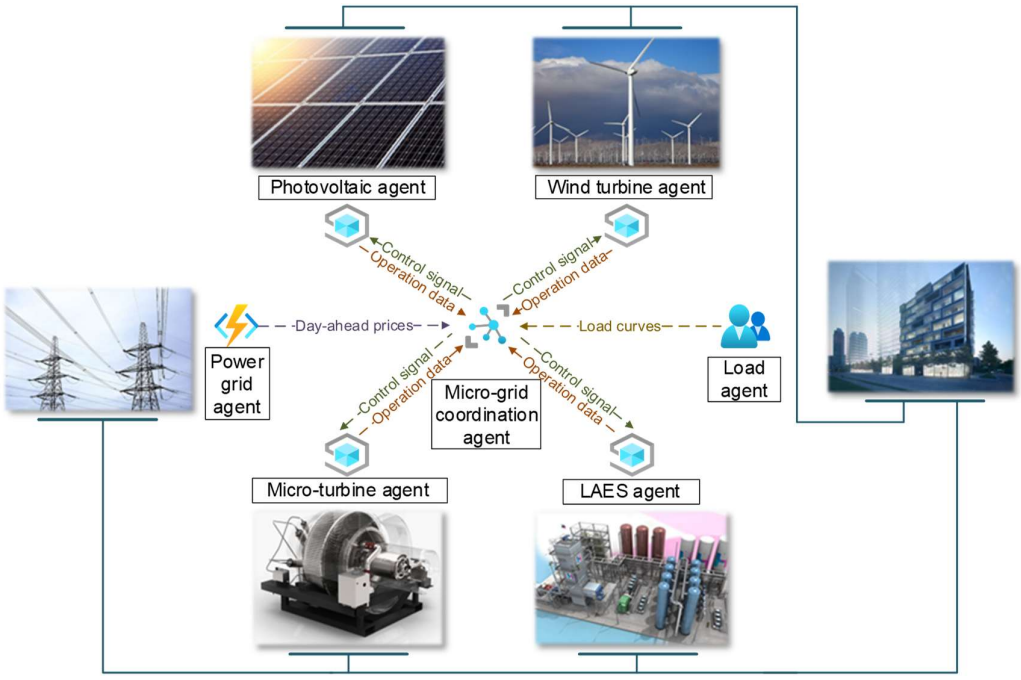

Figure 4-3 Schematic diagram of the micro-grid with multi-agent system.

4.3.2 Agent task description

The section explains the task details of the wind turbine agent, the photovoltaic agent, the LAES agent, the micro-turbine agent, and the micro-grid coordination agent.

4.3.2.1 Wind turbine (WT) agent

The WT agent is responsible for supervising the active operation status of wind turbine generator, sending cost coefficient signal and WT output power P_{WT}^{t} to micro-grid coordination agent at each time period. The WT output power is formulated according to (Soroudi et al., 2012):

$$P_{WT}^{t}(\omega_t) = \begin{cases} 0, & if\ \omega_t \le \omega_{in}^{cut}\ or\ \omega_t \ge \omega_{out}^{cut} \\ \frac{\omega_t - \omega_{in}^{cut}}{\omega_{rated} - \omega_{in}^{cut}} P_{WT}^{rated}, & if\ \omega_{in}^{cut} \le \omega_t \le \omega_{rated} \\ P_{WT}^{rated}, & if\ \omega_{rated} \le \omega_t \le \omega_{out}^{cu} \end{cases} \tag{4.10}$$

where ω_{in}^{cut} and ω_{out}^{cut} are the cut-in and cut-out wind speed respectively. ω_{rated} and P_{WT}^{rated} are the rate speed and power of WT units respectively. ω_t is the wind speed at time t, whose probability distribution can be modelled with Weibull probability density function (Aghbalou et al., 2018):

$$PDF(\omega_t) = \frac{k}{c}\left(\frac{\omega_t}{c}\right)^{k-1} e^{-\left(\frac{\omega_t}{c}\right)^{k}} \tag{4.11}$$

where $k \in (0, \infty)$ and $c \in (0, \infty)$ are the shape and scale parameters respectively for Weibull distribution.

4.3.2.2 Photovoltaic (PV) agent

The PV agent directly supervises the active operation status of PV arrays and reports the operation cost coefficient and PV array output power P_{PV}^{t} to the micro-grid coordinated agent. PV array output power is formulated with Eq. (4.12) (Homer Energy, 2016):

$$P_{PV}^{out} = P_{PV}^{rated} f_{pv} \left(\frac{G_T}{G_{T,STC}}\right)\left[1 + \alpha_p\left(T_c - T_{c,STC}\right)\right] \tag{4.12}$$

where P_{PV}^{rated} and f_{pv} are the rated power and derating factor of the PV array units respectively. G_T is the solar radiation incident on the PV array units, and $G_{T,STC}$ is the

incident radiation at the standard test conditions. α_p is the temperature coefficient of PV power. $T_{c,STC}$ is the PV cell temperature at the standard test conditions. T_c is the PV cell temperature, which can be calculated with Eq. (4.13) (Duffie & Beckman, 2013; Homer Energy, 2016):

$$T_c = T_a(t) + G_T\left(\frac{T_{c,NOCT} - T_{a,NOCT}}{G_{T,NOCT}}\right)\left(1 - \frac{\eta_c}{\tau\alpha_{absorb}}\right) \tag{4.13}$$

where $T_a(t)$ is the ambient temperature. $T_{c,NOCT}$ is the nominal operating cell temperature (NOCT). $T_{a,NOCT}$ and $G_{T,NOCT}$ are the ambient temperature and solar radiation under the NOCT respectively. η_c is the conversion efficiency of PV array units. τ is the solar transmittance of the cover of PV array units. α_{absorb} is the solar absorptance of the PV array. The final PV output at time t is calculated with an efficient coefficient η_{inv} to P_{PV}^{out}:

$$P_{PV}^{t} = \eta_{inv} P_{PV}^{out} \tag{4.14}$$

The solar radiation incident is modelled with the Beta distribution (Monteiro et al., 2018):

$$PDF(G_T) = \frac{\Gamma(\alpha + \beta)}{\Gamma(\alpha) + \Gamma(\beta)}(G_T)^{\alpha-1}(1 - G_T)^{\beta-1} \tag{4.15}$$

where $\Gamma(\cdot)$ is the Gamma function (Wahbah et al., 2022), $\alpha, \beta \in [0, \infty]$ are shape parameters for Beta distribution.

4.3.2.3 LAES agent

The LAES agent is responsible for supervising the active operation status of the LAES plant and reporting the operation information to the micro-grid coordination agent. The operation information includes charging phase, storage phase, and discharging phase information. During the charging phase, Kapitza cycle acts as a recuperative process to liquefy air and charge the cryogenic energy storage with compressors and cryo-turbines (Tafone et al., 2019). The efficiency of charging process is specified in Eq. (4.16). During the storage phase, the level of cryogenic energy storage is measured by state-of-charge (SOC) balance Eq. (4.17), considering the energy loss in the storage phase with Eq. (4.18). During the discharge phase, the liquid air from the tank is pumped out

by a cryogenic pump and regasified to ambient temperature. The high-pressure air is further heated up by the thermal storage to drive power turbines (Morgan et al., 2015). The final discharge power is calculated by Eq. (4.19) and Eq. (4.20) with consideration of the efficiencies of cryogenic pumps and power turbines.

$$P_{ch-final}(t) = \eta_{Kapitza} \cdot P_{ch}(t) \tag{4.16}$$

$$SOC_{LAES}(t) = SOC_{LAES}(t-1) + P_{ch-final}(t) - P_{dis-final}(t) - SOC_{LAES}^{loss}(t) \tag{4.17}$$

$$SOC_{LAES}^{loss}(t) = \gamma_{loss} \cdot SOC_{LAES}(t) \tag{4.18}$$

$$P_{pump}(t) = \eta_{cryo-pump} \cdot P_{dis}(t) \tag{4.19}$$

$$P_{dis-final}(t) = \eta_{turbine} \cdot P_{pump}(t) \tag{4.20}$$

In addition to the charge, storage, and discharge information listed above, the LAES agent also sends the operational constraints to the micro-grid coordination agent. Constraint (4.C.1) and (4.C.2) specify the range of charging and discharging ranges of LAES unit, where $x(t), y(t) \in \{0,1\}$. Constraint (4.C.3) prevents the LAES plant charges and discharges at the same time at the cryogenic tank. Constraint (4.C.4) indicates the minimum and maximum range of SOC at each time step t.

$$0 \leq P_{ch}(t) \leq P_{ch}^{max} \cdot x(t) \tag{4.C.1}$$

$$0 \leq P_{dis}(t) \leq P_{dis}^{max} \cdot y(t) \tag{4.C.2}$$

$$x(t) + y(t) \leq 1 \tag{4.C.3}$$

$$SOC_{LAES}^{min} \leq SOC_{LAES}(t) \leq SOC_{LAES}^{max} \tag{4.C.4}$$

4.3.2.4 Micro-turbine (MT) agent

The MT agent is responsible for sending the cost coefficient of MT generation unit and micro-turbine specifications, including Constraints (4.C.5) and (4.C.6), to the micro-grid coordination agent. Constraint (4.C.5) and Constraint (4.C.6) indicate operational limits and ramping limits of micro-turbine units respectively.

$$P_{MT}^{min} \leq P_{MT}^{t} \leq P_{MT}^{max} \tag{4.C.5}$$

$$\Delta P_{MT}^{min} \leq P_{MT}^{t} - P_{MT}^{t-1} \leq \Delta P_{MT}^{max} \tag{4.C.6}$$

where P_{MT}^{min} and P_{MT}^{max} are the minimum and maximum generation output limits. ΔP_{MT}^{min} and ΔP_{MT}^{max} are the minimum and maximum ramping limits.

4.3.2.5 Micro-grid coordination agent

The micro-grid coordination agent is responsible for optimising objective function Eq. (4.21) with operational information from other agents.

$$\Gamma = \sum_{t=1}^{24} (\xi_{MT} \cdot P_{MT}^{t} + \xi_{WT} \cdot P_{WT}^{t} + \xi_{PV} \cdot P_{PV}^{t} + \xi_{LAES} \cdot |P_{LAES}^{t}| + \lambda_t \cdot P_{grid}^{t}) \tag{4.21}$$

where Γ denotes the system operation cost; ξ_{MT} denotes the operating cost coefficient of micro-turbines; P_{MT}^{t} denotes the output power of micro-turbine at time t; ξ_{WT} denotes the operating cost coefficient of wind power generation; P_{WT}^{t} denotes the output power of wind power generation at time t; ξ_{PV} denotes the operating cost coefficient of photovoltaic power generation; P_{PV}^{t} denotes the output power of photovoltaic power generation at time t; ξ_{LAES} denotes the operating cost coefficient of LAES; P_{LAES}^{t} denotes the charge and discharge power of LAES at time t, when $P_{LAES}^{t} \geq 0$, it is considered that the LAES is in the discharging mode, when $P_{LAES}^{t} < 0$, the LAES is in a charging state; λ_t denotes the market price of electricity at time t; P_{gird}^{t} denotes the tie line transition power at time t, when $P_{gird}^{t} \geq 0$ the micro-grid purchases power from the upper grid.

Once the objective function Eq. (4.21) is established, the micro-grid coordination agent considers decision-makers' risk preferences, including risk-averse and risk-taking options. Risk-averse decision-makers are concerned with the system robustness that can be quantified with the robustness function of IGDT. The robustness function value $\hat{\alpha}(P, C_{averse})$ represents the maximum uncertainty level corresponding to the risk-averse cost target C_{averse}. On the other hand, risk-taking decision-makers aim to spend as little cost as possible to keep the system running smoothly. The decision is based on

opportunity function, where the opportunity function value $\hat{\beta}(P, C_{taking})$ represents the minimum level of uncertainty under the risk-taking cost target C_{taking}.

- Problem formulation with risk-averse decision-makers

For risk-averse decision-makers, the micro-grid coordination agent considers the uncertainty of electricity prices to establish a robustness function for the micro-grid system. According to the uncertainty model Eq. (4.2), the high market electricity price can be expressed as:

$$\lambda_t = (1+\alpha)\hat{\lambda}_t \tag{4.22}$$

Substituting Eq. (4.22) into the operating cost function Eq. (4.21):

$$\Gamma_{averse} = \sum_{t=1}^{24}\left(\xi_{MT}(P_{MT}^t) + \xi_{WT}(P_{WT}^t) + \xi_{PV}(P_{PV}^t) + \xi_{LAES}(P_{LAES}^t) + (1+\alpha)\hat{\lambda}_t \cdot P_{grid}^t\right) \tag{4.23}$$

Substitute the given maximum cost target C_{averse} into Eq. (4.23):

$$\alpha(P, C_{averse}) = \frac{\sum_{t=1}^{24}\left(\xi_{MT}(P_{MT}^t) + \xi_{WT}(P_{WT}^t) + \xi_{PV}(P_{PV}^t) + \xi_{LAES}(P_{LAES}^t) + \hat{\lambda}_t P_{grid}^t\right) - C_{averse}}{-\sum_{t=1}^{24}\hat{\lambda}_t P_{grid}^t} \tag{4.24}$$

C_{averse} is the target system cost that risk-averse decision-makers are willing to pay. As explained in Section 4.2.1, the principle of risk-averse strategy is to obtain the maximum robustness function value $\hat{\alpha}(P, C_{averse})$ under the cost target C_{averse}. the micro-grid coordination agent optimises the following optimisation problem (4.25):

$$\text{Maximise}\left\{\frac{\sum_{t=1}^{24}\left(\xi_{MT}(P_{MT}^t)+\xi_{WT}(P_{WT}^t)+\xi_{PV}(P_{PV}^t)+\xi_{LAES}(P_{LAES}^t)+\hat{\lambda}_t P_{grid}^t\right)-C_{averse}}{-\sum_{t=1}^{24}\hat{\lambda}_t P_{grid}^t}\right\} \tag{4.25}$$

The optimisation is subject to Constraints (4.C.1) to (4.C.6), as well as (4.C.7) and (4.C.8):

$$P_{MT}^t + P_{WT}^t + P_{PV}^t + P_{LAES}^t + P_{grid}^t = P_{load}^t \tag{4.C.7}$$

$$P_{grid}^{min} \le P_{grid}^t \le P_{grid}^{max} \tag{4.C.8}$$

- Problem formulation with risk-taking decision-makers

For risk-taking decision-makers, the micro-gird coordination agent aims to minimise the opportunity function value $\hat{\beta}(P, C_{taking})$, which solves the minimum fluctuation range of electricity market price. According to uncertain model of IGDT, the expression of low market electricity price can be expressed as:

$$\lambda_t = (1-\alpha)\hat{\lambda}_t \tag{4.26}$$

Substituting Eq. (4.26) into operating cost function Eq. (4.21):

$$\begin{aligned}\Gamma_{taking} = \sum_{t=1}^{24}\big(&\xi_{MT}(P_{MT}^t) + \xi_{WT}(P_{WT}^t) + \xi_{PV}(P_{PV}^t) + \xi_{LAES}(P_{LAES}^t) \\ &+ (1-\alpha)\hat{\lambda}_t \cdot P_{grid}^t\big)\end{aligned} \tag{4.27}$$

Substitute the given minimum cost target C_{taking} into the Eq. (4.27):

$$\alpha(P, C_{taking}) = \frac{\sum_{t=1}^{24}\left(\xi_{MT}(P_{MT}^t)+\xi_{WT}(P_{WT}^t)+\xi_{PV}(P_{PV}^t)+\xi_{LAES}(P_{LAES}^t)+\hat{\lambda}_t P_{grid}^t\right)-C_{taking}}{\sum_{t=1}^{24}\hat{\lambda}_t P_{grid}^t} \tag{4.28}$$

Then, the micro-grid coordination agent solves the optimisation problem (4.24):

$$\text{Minimise}\left\{\frac{\sum_{t=1}^{24}\left(\xi_{MT}(P_{MT}^t)+\xi_{WT}(P_{WT}^t)+\xi_{PV}(P_{PV}^t)+\xi_{LAES}(P_{LAES}^t)+\hat{\lambda}_t P_{grid}^t\right)-C_{taking}}{\sum_{t=1}^{24}\hat{\lambda}_t P_{grid}^t}\right\} \tag{4.29}$$

Subject to Constraints (4.C.1) to (4.C.8)

Subsequently, the micro-grid coordination agent uses STA to optimise the optimisation problem (4.25) or (4.29), based on the risk preference of decision-makers.

4.4 Case study

In this chapter, the optimisation of micro-grid operation strategy with LAES is formulated under different target costs while considering the uncertainty of market electricity prices. The micro-grid system analysed in this case study is a grid-connected one. It comprises a photovoltaic system, a wind power system, a micro gas turbine system and a LAES system. In the case of the LAES system, it is assumed that the pressure ratio of the compressor and expander in each stage remains constant.

4.4.1 Data preparation

The predicted market price of electricity is shown in Figure 4-4. This chapter assumes that the electricity price sold to the grid is equal to the electricity price purchased from the grid. The system parameters are presented in Table 4-1.

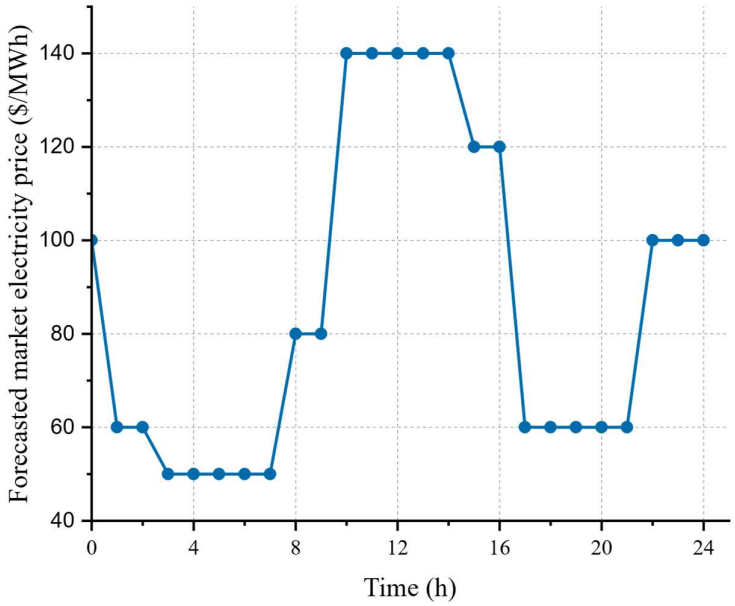

Figure 4-4 Forecast market electricity price for IGDT-STA case study

Table 4-1 System specifications of the micro-gird system

Parameter	Value	Parameter	Value
WT system		LAES system	
P_{WT}^{rated}	3000 kW	P_{LAES}^{max}	5 MW
ω_{in}^{cut}	3 ms^{-1}	P_{LAES}^{min}	-5 MW
ω_{out}^{cut}	25 ms^{-1}	SOC_{LAES}^{max}	20 MW
ω_{rated}	13 ms^{-1}	SOC_{LAES}^{min}	0.5 MW
ξ_{WT}	0.029 \$/kWh	$\eta_{Kapitza}$	85 %
PV system		$\eta_{cryo-pump}$	80 %
P_{PV}^{rated}	3000 kW	$\eta_{turbines}$	80 %
f_{pv}	80 %	γ_{loss}	2 %
α_p	-0.5	ξ_{LAES}	0.025 \$/kWh
$T_{c,NOCT}$	47 ℃	MT system	
$T_{c,STC}$	25 ℃	P_{MT}^{max}	3000 kW
η_c	13 %	P_{MT}^{min}	500 kW

τ	0.0148 MW $m^{-2}K^{-1}$	ξ_{MT}	0.044 \$/kWh
α_{absorb}	30 %	Other parameters	
η_{inv}	90 %	P_{grid}^{max}	3000 kW
ξ_{PV}	0.026 \$/kWh	P_{grid}^{min}	-3000 kW
⋮	⋮		

The efficiencies of LAES plant are obtained from LAES performance research (Borri et al., 2017; Tafone et al., 2019). The load power data comes from a micro-grid in Northwest China, as shown in Figure 4-5. The results of wind power and photovoltaic power generation are shown in Figure 4-6.

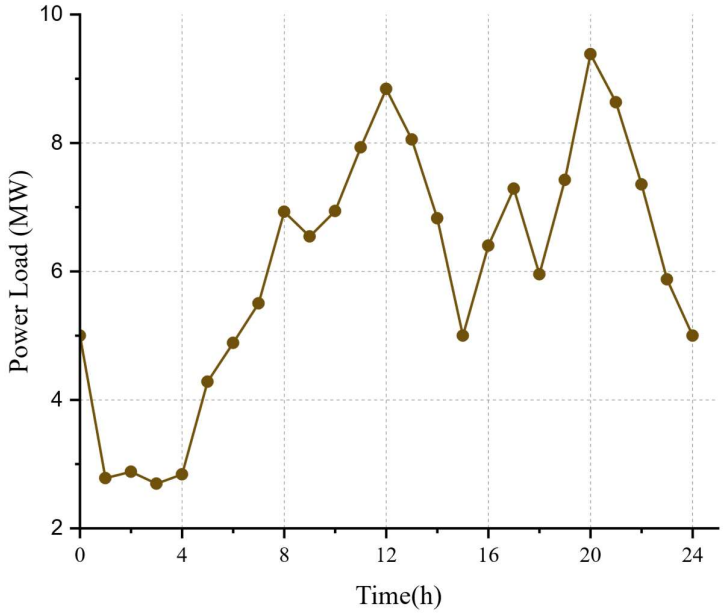

Figure 4-5 Power load in IGDT-STA case study

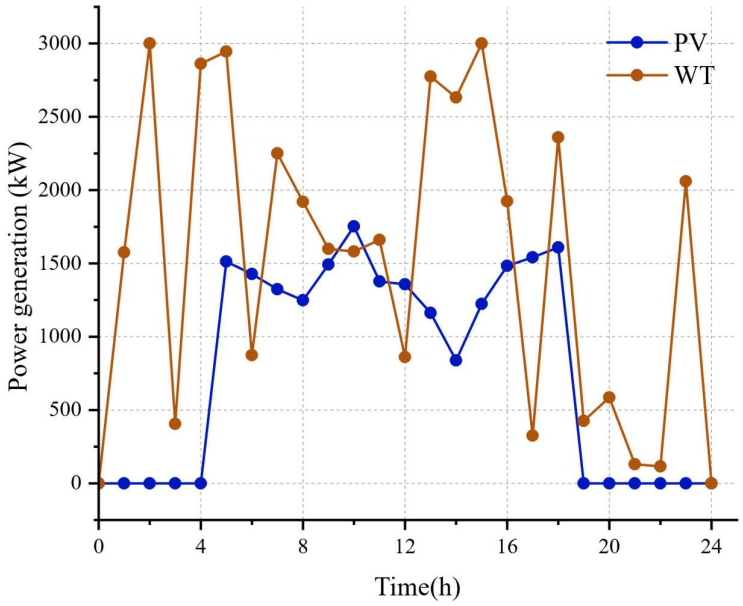

Figure 4-6 The output power of PV and WT in IGDT-STA case study

4.4.2 Risk-neutral results

As illustrated in Section 4.2.3, the first stage of IGDT-STA method is to obtain the risk-neutral strategy. In other words, the robustness and opportunity function values are 0 ($\hat{\alpha} = \hat{\beta} = 0$). This risk-neutral strategy result is shown in Table 4-2, which is obtained by assuming the realised electricity prices are equal to the predicted electricity prices. To demonstrate the effectiveness of the proposed IGDT-STA method, this case study uses the Genetic Algorithm (GA) as a reference optimisation technique. In addition, this case study also compares the risk-neutral strategy with the stochastic method and Monte Carlo method, as demonstrated in (Mirzaei et al., 2021; Powell & Meisel, 2016; Yan et al., 2021)

Table 4-2 Expected operation cost comparison under risk-neutral strategy

	IGDT-STA method	IGDT-GA method	Stochastic method	Monte Carlo method
Expected operation cost ($)	7848.0	9386.6	8748.7	8740.3

The hourly expected operating costs based on the four methods are shown in Figure 4-7. It can be seen from the figures that the expected operating costs of the IGDT-STA method are mainly reduced during the 13th and 15th hour of the day compared with the remaining three methods.

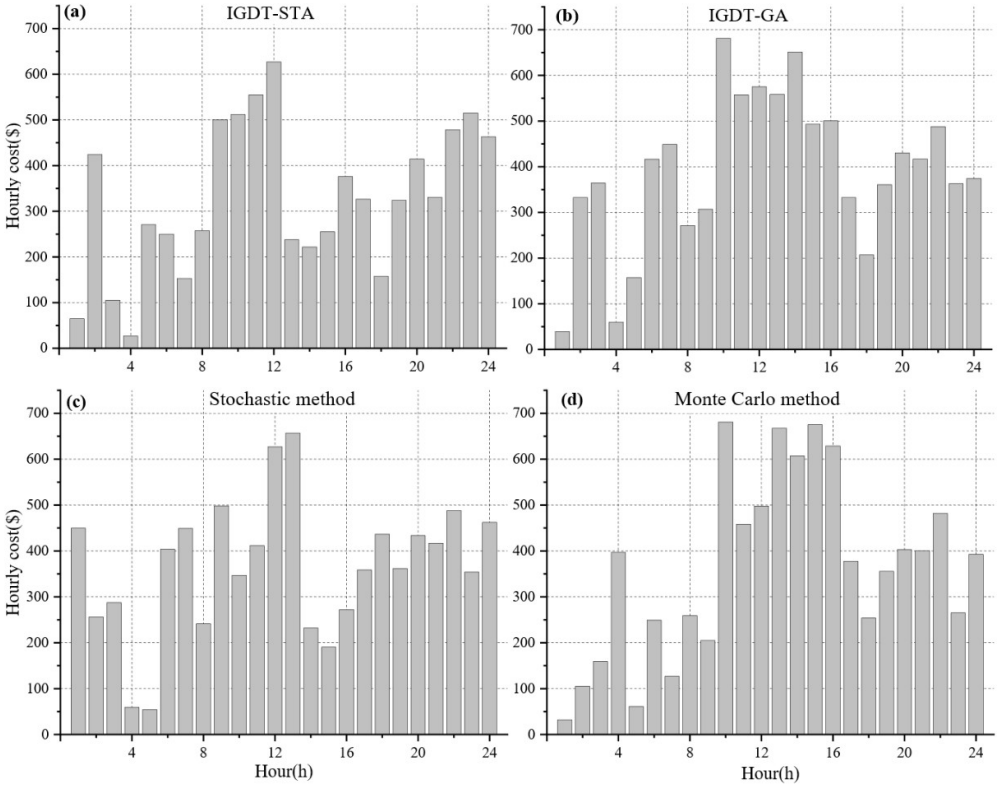

Figure 4-7 Hourly cost of (a) IGDT-STA ; (b) IGDT-GA; (c) Stochastic method; (d) Monte Carlo method.

The micro-grid operation strategies corresponding to the four methods are shown in Figure 4-8 (a) to (d) respectively. With respect to the utilisation of LAES plant, all four operation strategies actively use the storage facility throughout the day. It can be seen from Figure 4-8 (a) that IGDT-STA operation strategy changes LAES in the morning and discharge the stored power during the peak load noon and evening time. In addition, compared with the IGDT-GA method, the operation strategy based on the IGDT-STA method has more output of the micro gas turbine, thereby reducing the purchase of electricity from the main grid.

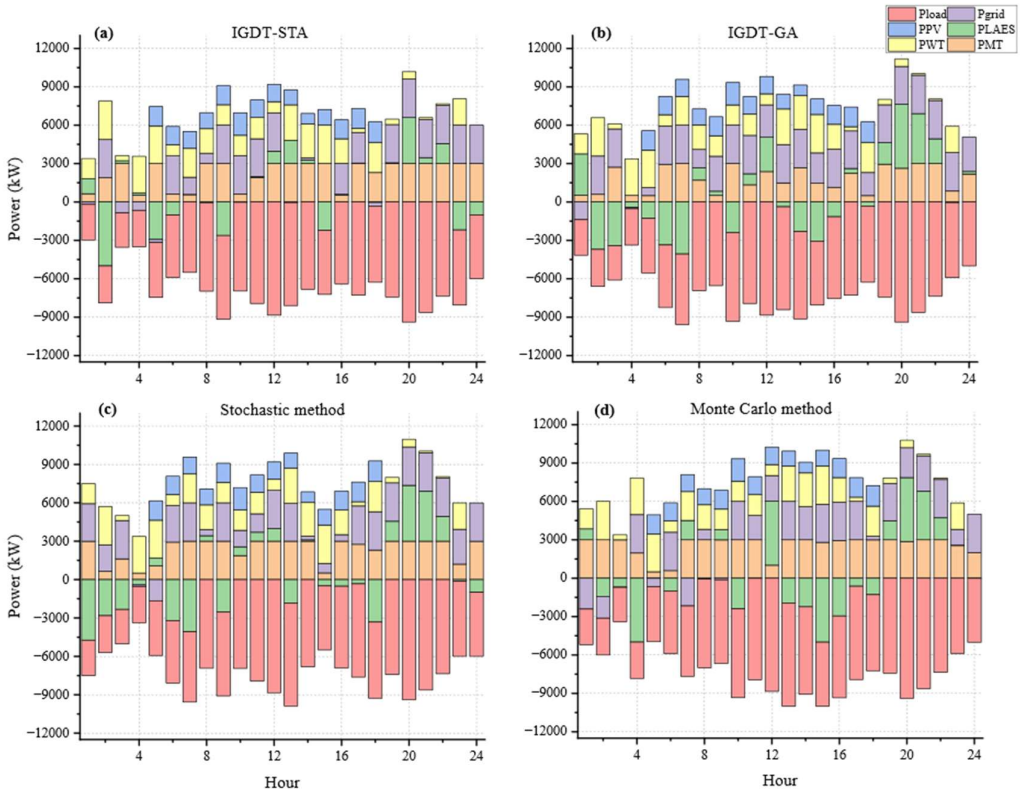

Figure 4-8 Micro-grid operation strategy based on (a) IGDT-STA; (b) IGDT-GA; (c) Stochastic method; (d) Monte Carlo Method.

4.4.3 Risk-based results

The robustness $\hat{\alpha}(\cdot)$ and opportunity $\hat{\beta}(\cdot)$ function explained in Section 4.2.1 were employed to form the risk-averse strategy and risk-taking strategy. The results of risk-averse strategy and risk-taking strategy with different target cost is shown in Figure 4-9. A risk-taking decision maker aims to maximise the opportunity function with a smaller target cost than the risk-neutral cost. The trend of $\hat{\beta}(C_{taking})$ with respect to C_{taking} is plotted in Figure 4-8 (a). In this case study, the cost step is set to 3% of the risk-neutral operating cost, i.e. \$281.60 for the IGDT-GA method and \$235.44 for the IGDT-STA method.

It is evident that $\hat{\beta}(C_{taking})$ increases with risk-taking targe cost C_{taking} decreases for both IGDT-STA and IGDT-GA. Upon comparing the results of IGDT-STA and IGDT-GA, the IGDT-STA method yields a lower $\hat{\beta}(C_{taking})$ than IGDT-STA. For instance, at an opportunity cost of \$7612.0, the IGDT-STA method boasts an opportunity coefficient

of 0.1399, while the IGDT-GA method has an opportunity coefficient of 0.3744. These results show that IGDT-STA could obtain a risk-taking strategy with less uncertainty compared to the IGDT-GA method.

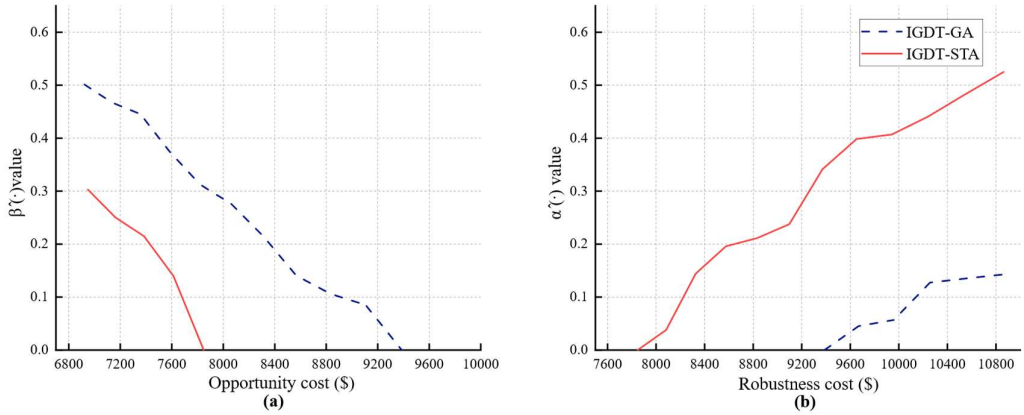

Figure 4-9 Opportunity curve and robustness curve with IGDT-STA and IGDT-GA (a) Opportunity cost curve; (b) Robustness cost curve.

Figure 4-8 (b) shows the relationship curve between the robustness cost and the robustness coefficient $\hat{\alpha}(C_{averse})$, which can be obtained based on optimisation problem (3.20). In this case study, the cost step is set to 3% of the risk-neutral operating cost. It is evident that the robustness coefficient rises $\hat{\alpha}(C_{averse})$ as the robustness cost increases, regardless of the methodology employed. This suggests that the robustness of the system is enhanced with increased operation costs. Notably, the proposed IGDT-STA approach displays greater robustness than IGDT-GA. For example, at a robustness cost of $10089.0, the IGDT-STA method has a robustness coefficient of 0.3741, while the IGDT-GA method only has a coefficient of 0.0567. Thus, if the decision-maker favours risk aversion, they can make resilient choices by accepting higher operating costs.

4.5 Chapter summary

LAES systems are promising energy storage solutions, as they are not limited by geographical conditions and have low environmental impacts. This chapter researches the optimal operation strategy of a micro-grid with LAES. When formulating the optimal operation strategy to reduce the operation cost of the system and considering the impact of the uncertainty of the market electricity price, a day-ahead optimal operation method of micro-grid with LAES based on IGDT-STA is proposed. The

method is mainly divided into two stages. Firstly, the STA method is used to optimise the risk-neutral strategy. Then, based on the obtained operation strategy, the STA method is used to optimise the robustness and opportunity function in the IGDT method.

The case study results show that compared with the IGDT-GA method, the stochastic method, and Monte Carlo method, the IGDT-STA method obtains a lower system operation cost of $7848. In the second stage, the IGDT-STA method shows a higher robustness coefficient and lower opportunity coefficient than IGDT-GA, offering stronger robustness and better opportunity. Future research could further investigate the following two directions: 1) The information gap decision theory is only used for the uncertainties in the market electricity price in this study. Future studies could investigate the potential applications of IGDT on the coupled uncertainties from renewable energy generation and market electricity price. 2) This chapter treats liquid air energy storage as a steady system. Future research could treat the LAES system as a dynamic system to investigate the dynamic performance of compressors and expanders between different dispatch strategies.

Chapter 4

5. Addressing interactional complexity in decentralised prosumer aggregation market[3]

5.1 Chapter introduction

The widespread adoption of distributed energy resources (DER) has led to increased applications of decentralised decision-making in MES. Major forms of DER include solar PV, wind turbines, and EVs when V2G technologies are considered (Jain et al., 2017; Pan & McElhannon, 2018). Such DER technologies enable users to produce electricity for self-consumption and sell the excess electricity to peers or upstream electric companies, i.e., becoming so-called prosumers. As a result, the electricity flow is no longer unidirectional but bidirectional. As shown in Figure 5-1, the increasing penetration of DER units on low and medium-voltage networks transformed how electricity is generated, transmitted, and consumed (Guerrero et al., 2020).

[3] This chapter is adapted from Cheng, X.[†], **Yao, R.**[†], Postnikov, A., Hu, Y., & Varga, L. (2024). Decentralized intelligent multi-party competitive aggregation framework for electricity prosumers. *Applied Energy*, 373, 123860. https://doi.org/10.1016/j.apenergy.2024.123860

[†]Authors have equal contributions

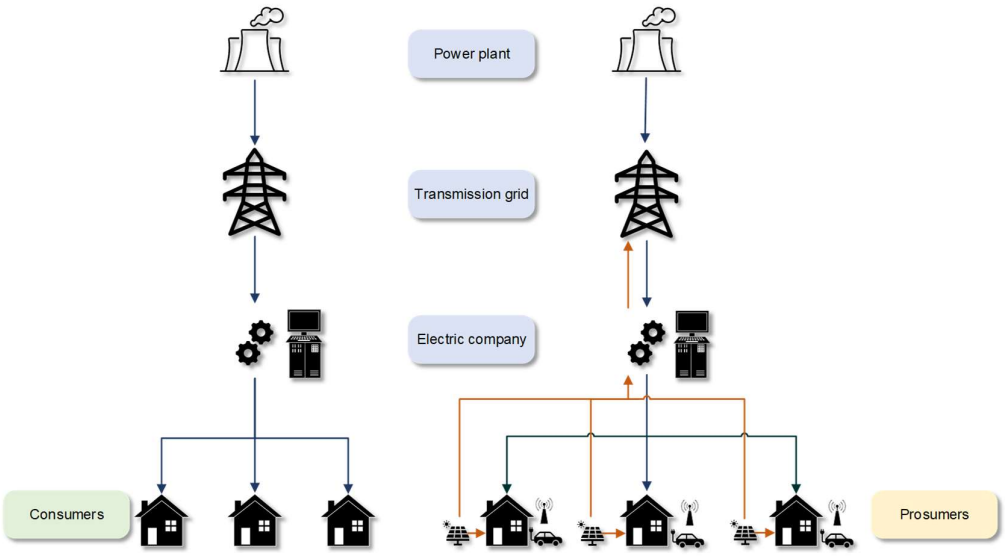

Figure 5-1 Power system transitions. (a) schematic drawing of the unidirectional power flow with consumers under the current power system structure; (b) schematic drawing of bidirectional power flow with prosumers for future power system structure.

The physical decentralisation is paralleled by a digital one. The growing popularity of Internet-of-Things (IoT) technologies enables entities in the power system to communicate with each other through bidirectional information flow (J. Jin et al., 2014). For example, prosumers not only can communicate with electric companies, but also communicate with peers via the Internet. More importantly, IoT technologies provide computation resources to users, enabling local data processing and storage. The computational ability provided by IoT technologies makes edge computing an emerging computation technique in the energy system (Pan & McElhannon, 2018). Edge computing can provide low-latency communication, which is crucial for decentralised decision-making (Xiong et al., 2020).

With these two fundamental transitions, multiple electricity aggregators can compete to maximise profit while prosumers form coalitions to maximise their utilities. The resulting interactions can be naturally modelled as a multi-leader-multi-follower game (MLMFG), where each aggregator is a leader and each prosumer is a follower. Chapter 5 achieves **Objective 2** by employing the MLMFG theory and demonstrating that its equilibrium can still be solved in a decentralised manner through a novel graph-based

consensus algorithm executed on edge devices. The contributions of Chapter 5 are summarised as follows:

- Proposed an intelligent aggregation framework with a multi-aggregator MLMFG model, which can be solved by a novel graph-based consensus algorithm. The multi-aggregator MLMFG model has been proven with the existence and uniqueness of the solution to the model. The novel graph-based consensus algorithm has been proven to converge with a linear convergence rate.
- Demonstrated the applicability of the proposed intelligent aggregation framework in a case study. The proposed algorithm is also compared with state-of-the-art algorithms using benchmark analysis. The proposed algorithm has less communication complexity than the state-of-the-art algorithms.

The rest of this chapter is organised as follows: Section 5.2 explains the mathematical formulation of the intelligent aggregation framework. Section 5.3 provides the simulation results of the proposed framework and algorithm. Section 5.4 concludes this chapter.

5.2 Intelligent aggregation framework

The proposed decentralised intelligent aggregation framework is shown in Figure 5-2. In the proposed framework, a prosumer is regarded as a household with ownership of the DER units. Each prosumer is assumed to have the computational ability in a standalone decision-making module, such as edge computing embedded smart meters (Sirojan et al., 2019). The prosumers and aggregators are able to send bidding and asking signals to each other through internet protocols. The Distribution System Operator (DSO) also broadcasts the network constraints to the aggregators as well as prosumers.

During market interactions, a prosumer cooperates with other prosumers to maximise the joint welfare of the prosumers. In the meantime, an aggregator competes with other aggregators to maximise the expected utility by changing to the asking price (also referred to as the offer price). Thus, such optimisation problems are a bi-level optimisation problem of an MLMFG. The MLMFG model can be subsequently solved by the proposed graph-based consensus algorithm. The optimised result implies the fact that both levels of the market reach equilibrium at the same time. Hence, the system

reaches a co-equilibrium state. It should be noted that aggregators are responsible for two stages of actions, where aggregators first accumulate electricity from prosumers and then sell it to the wholesale market.

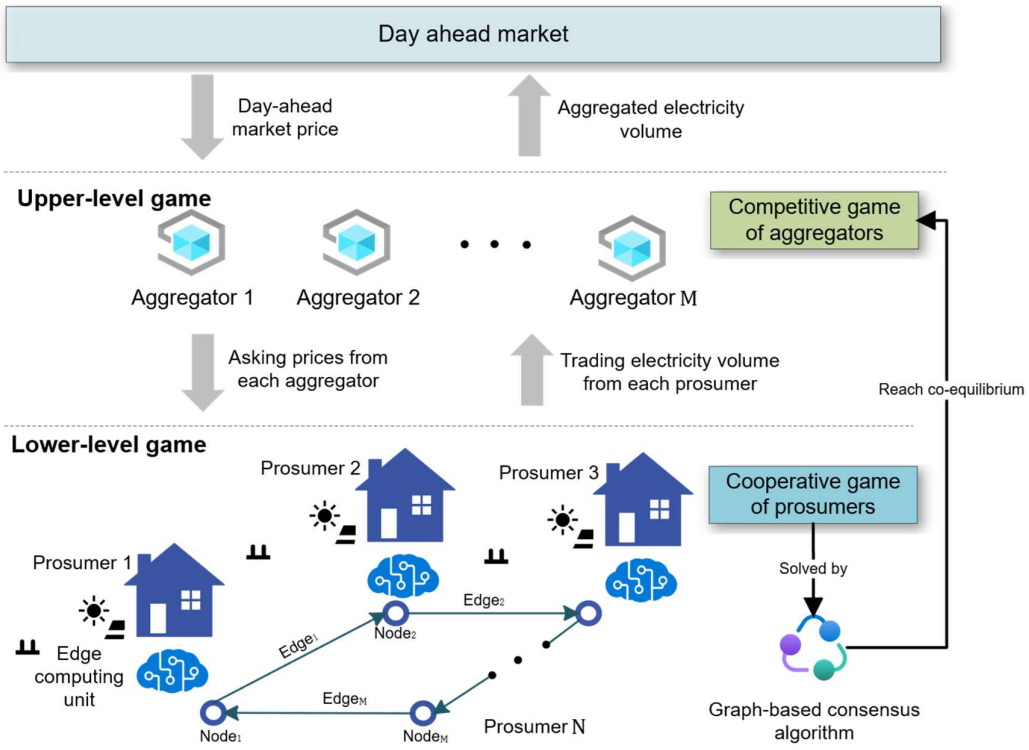

Figure 5-2 Intelligent aggregation architecture.

5.2.1 Bi-level market equilibrium model

This chapter proposes a unified bi-level market co-equilibrium model for decentralised intelligent multi-party aggregation with DER-enabled prosumers. The co-equilibrium model is proposed for a distribution network with M aggregators and N prosumers. The volume of electricity that $prosumer_j$ decides to sell to $aggregator_i$ is denoted as $x_{i,j}$. The volume of electricity $x_{i,j}$ can be expressed as a set $\{x_{i,j}|x \in \mathbb{R}, i = 1,2,\dots,M;\ j = 1,2\dots,N\}$. This trading volume of electricity in the distribution network forms a real-valued matrix of $\boldsymbol{X} \in \mathbb{R}^{M\times N}$. The volume of electricity that $aggregator_i$ receives is denoted $x_{i,*} = [x_{i,1}, x_{i,2}, \dots x_{i,N}]$, which is the i^{th} row vector of matrix $\boldsymbol{X}$. The volume of electricity that $prosumer_j$ decides to sell is denoted as $x_{*,j} = [x_{1,j}, x_{2,j}, \dots x_{M,j}]^T$, which is the j^{th} column vector of $\boldsymbol{X}$.

The business model of aggregators is important because it reflects the motivations behind aggregators' desire to facilitate electricity aggregation. In the proposed market model, aggregators' revenue accrues when they sell aggregated electricity in the day-ahead market at the current day-ahead price. It is also important to consider the cost of aggregation. This chapter assumes that the aggregators are the price-takers of the day-ahead market, which means that the aggregators' decisions do not affect the day-ahead market price. More specifically, the day-ahead prices for input parameter for the aggregation framework. The aggregation cost should consider two components: variable cost and fixed cost (Burger et al., 2017). As a result, the utility function of aggregators is formulated as Eq. (5.1) and Eq. (5.1.a):

$$\arg\max_{\lambda_{i,j}^{pro}} \sum_{j=1}^{N} (\lambda_i^{DA,bid} - \lambda_{i,j}^{pro,ask} - \gamma)\, x_{i,j}, \qquad i = 1,2,\dots M \tag{5.1}$$

$$s.t. \quad \underline{\lambda}_{i,j}^{pro,ask} \leq \lambda_{i,j}^{pro,ask} \leq \overline{\lambda}_{i,j}^{pro,ask} \tag{5.1.a}$$

where $\lambda_i^{DA,bid}$ is the aggregators' bidding price at the day-ahead market, making $\lambda_i^{DA,bid} x_{i,j}$ the revenue for aggregate $x_{i,j}$ amount of electricity. As aggregators are price takers in the day-ahead market, the $\lambda_i^{DA,bid}$ is fixed in the bi-level market model. The decision variable $\lambda_{i,j}^{pro,ask}$ is the asking price of $aggregator_i$ promise to pay $prosumer_j$, which makes $\lambda_{i,j}^{pro,ask} x_{i,j}$ the variable cost of aggregators. The fixed cost component is parameterised by a fixed-cost coefficient γ. In Eq. (5.1), $aggregator_i$ aim to maximise the utility, which is the total profit $aggregator_i$ can make for providing the aggregation services.

Apart from the utility function, the optimisation problem of aggregators also includes the constraint (5.1.a). $\underline{\lambda}_{i,j}^{pro,ask}$ and $\overline{\lambda}_{i,j}^{pro,ask}$ are the lower and upper bounds for the asking price at the prosumer-aggregator market. The lower bound $\underline{\lambda}_{i,j}^{pro,ask}$ is set to ensure the profitability of aggregators and the upper bound $\overline{\lambda}_{i,j}^{pro,ask}$ is to prevent excess profits of aggregators. The price bounds are pre-determined by the regulatory body to ensure the competitiveness of the market.

Eq. (5.2) indicates the utility function of the prosumer, which consists of three terms. The first term $\lambda_{i,j}^{pro} x_{*,j}$ represents the payments received from aggregators, which is the

revenue for prosumers. On the other hand, this chapter treats battery degradation as utility loss for prosumers to participate the aggregations. The battery degradation model is based on the power law model in (C. Liu et al., 2019).

$$\arg\max_{x_{*,j}} \sum_{i=1}^{M} \lambda_{i,j}^{pro} x_{*,j} - \mathbb{I}^T A e^{\left(\frac{\beta x_{*,j}}{RT}\right)^{c^z}} + x_{*,j}^T \frac{\partial A e^{\left(\frac{\beta x_{*,j}}{RT}\right)^{c^z}}}{\partial \mathrm{x_{i,j}}}, \tag{5.2}$$

$$j = 1,2, \dots N$$

$$s.t. \quad x_{*,j} \leq \bar{x}_{*,j} \tag{5.2.a}$$

$$\underline{x}_{i,*}^{DA} \leq x_{i,*} \leq \overline{x}_{i,*}^{network} \tag{5.2.b}$$

where A is a constant. R and T are the gas constant and temperature, respectively. β is the activation energy coefficient. c is the number of battery cycles from the initial state of the battery. z is the power law factor. The third term is a first-order utility derivative term to ensure the convergence of the bi-level game. The optimisation problem of prosumers also includes the constraint (5.2.a) and (5.2.b). Constraint (5.2.a) is constrained by battery discharge rate, and it indicates the upper bound of $x_{*,j}$. Constraint (5.2.a) can be treated as the column-wise constraint on the trading electricity matrix $\boldsymbol{X}$. In addition, the trading electricity matrix $\boldsymbol{X}$ is bounded column-wise by the $\underline{x}_{i,*}^{DA}$, the minimum bidding size at the DA market, and $\overline{x}_{i,*}^{network}$, the network constraint is informed by the distribution system operator. The proof of the market co-equilibrium model is demonstrated in the rest of this sub-section.

The existence and uniqueness of the optimal solution ensure that the aggregation process will reach a co-equilibrium state where the utility values of both aggregators and prosumers are optimal. $\boldsymbol{\chi}$ and $\boldsymbol{\Lambda}$ are defined as the closed convex feasible sets of the aggregate volume matrix $\boldsymbol{X} \in \mathbb{R}^{M \times N}$ and ask price matrix $\boldsymbol{\Lambda} \in \mathbb{R}^{M \times N}$, respectively. A point $(\mathbf{X}^*, \boldsymbol{\Lambda}^*) \in (\boldsymbol{\chi}, \boldsymbol{\Lambda})$ is the bi-level optimum solution if it can meet the two inequality requirements (5.3) and (5.4) simultaneously:

$$\sum_{j=1}^{N} (\lambda_i^{DA,bid} - \lambda_{i,j}^{pro,ask^*}) x_{i,j} > \sum_{j=1}^{N} (\lambda_i^{DA,bid} - \lambda_{i,j}^{pro,ask}) x_{i,j} \tag{5.3}$$

$$\sum_{i=1}^{M} \lambda_{i,j}^{pro} x_{*,j}^{*} - \mathbb{I}^T A e^{\left(\frac{\beta x_{*,j}^{*}}{RT}\right)^{c^z}} + \mathbb{I}^T \frac{\partial A e^{\left(\frac{\beta x_{*,j}^{*}}{RT}\right)^{c^z}}}{\partial \mathrm{x_{i,j}}} > \sum_{i=1}^{M} \lambda_{i,j}^{pro} x_{*,j} - \mathbb{I}^T A e^{\left(\frac{\beta x_{*,j}}{RT}\right)^{c^z}} + \mathbb{I}^T \frac{\partial A e^{\left(\frac{\beta x_{*,j}}{RT}\right)^{c^z}}}{\partial \mathrm{x_{i,j}}} \tag{5.4}$$

Before proving the optimal point exists in MLMFG, the following notation is introduced to enhance the readability of the proof. Eq. (5.5) and (5.6) represent the second and third term of the prosumers' utility functions. $L_j\left(x_{*,j}\right)$ is close and convex with a minimum feasible solution. $\theta_j\left(x_{*,j}\right)$ can be regarded as the first-order derivative of Eq. (5.5): $\theta_j\left(x_{*,j}\right) = \frac{\partial L_j(x_{*,j})}{\partial \mathrm{x_{i,j}}}$.

$$L_j\left(x_{*,j}\right) = Ae^{\left(\frac{\beta x_{*,j}}{RT}\right)^{c^z}} \tag{5.5}$$

$$\theta_j\left(x_{*,j}\right) = \frac{\partial x_{*,j} A e^{\left(\frac{\beta x_{*,j}}{RT}\right)^{c^z}}}{\partial \mathrm{x_{i,j}}} \tag{5.6}$$

Assumption 1. The utility function of each prosumer should satisfy the Lipschitz gradient continuity. There exists an upper bound value k satisfying that:

$$\nabla_{x_{*,j}} \left\{ \sum_{i=1}^{M} \lambda_{i,j}^{pro} x_{*,j}^{k+1} - \mathbb{I}^T L_j\left(x_{*,j}^{k+1}\right) \right\} - \nabla_{x_{*,j}} \left\{ \sum_{i=1}^{M} \lambda_{i,j}^{pro} x_{*,j}^{k} - \mathbb{I}^T L_j\left(x_{*,j}^{k}\right) \right\} \preccurlyeq k\left(x_{*,j}^{k+1} - x_{*,j}^{k}\right) \tag{5.7}$$

where $\nabla_{x_{*,j}}$ is the first-order differential operator. $A \preccurlyeq B$ means $A - B$ is at least a positive semi-definite matrix.

Proof

Converting the concave function of the optimisation problem represented by (5.1) and (5.2) in MLMFG to a convex function can respectively obtain the upper-level optimisation problem represented by (5.8) and the lower-level optimisation problem represented by (5.9). (5.8.a) is a general representation of the constraints of aggregators (5.1.a). Similarly, (5.9.a) represents the constraints of prosumers (5.2.a) and (5.2.b).

Aggregators' optimisation problem:

$$\underset{\lambda_{i,*}^{pro}}{\arg\min} -\sum_{j=1}^{N}(\lambda_i^{DA,bid} - \lambda_{i,j}^{pro,ask})\, x_{i,j}, \qquad i = 1,2,\dots M \tag{5.8}$$

$$s.t. \quad c_a\left(\lambda_{i,*}^{pro}\right) \in C_a, \;\; a = 1,2,\dots A \tag{5.8.a}$$

Prosumer's optimisation problem:

$$\underset{x_{*,j}}{\arg\min} -\sum_{i=1}^{M}\lambda_{i,j}^{pro}x_{i,j} + \mathbb{I}^T L_j\left(x_{*,j}\right) - \mathbb{I}^T\theta_j\left(x_{*,j}\right), \qquad j = 1,2,\dots N \tag{5.9}$$

$$s.t. \quad d_b\left(x_{*,j}\right) \in D_b, \;\; b = 1,2,\dots B \tag{5.9.a}$$

The inner loop in MLMFG can be regarded as an optimisation problem with a Gauss-Seidel ADMM. It should be noted that the $aggregator_i'$s payment to $prosumer_j$, $\lambda_{i,j}^{pro}$ are fixed during the inner loop.

$$\underset{\boldsymbol{x}_{*,j}}{\arg\min} -\sum_{i=1}^{M}\lambda_{i,j}^{pro}x_{i,j} + \mathbb{I}^T L_j\left(x_{*,j}\right) - \mathbb{I}^T\theta_j\left(x_{*,j}\right), \qquad j = 1,2,\dots N \tag{5.10}$$

$$s.t. \quad \mathbb{I}_{C_a}\left(\lambda_{i,*}^{pro}\right), \;\; a = 1,2,\dots A \tag{5.10.a}$$

$$s.t. \quad \mathbb{I}_{D_b}\left(x_{*,j}\right), \;\; b = 1,2,\dots B \tag{5.10.b}$$

The lower-level optimisation problem (5.9) can then be transferred to the augmented Lagrangian function with $\mu_x = [\mu_1^x, \mu_2^x, \dots, \mu_p^x]$ and $\mu_z = [\mu_1^y, \mu_2^y, \dots, \mu_q^y]$ as Lagrangian multipliers for inequality constraints:

$$x_{*,j}^{k+1} = \underset{x_{*,j}}{\arg\min}\, L_0\left(x_{*,j}, \mu_x^*, \mu_z^*, \lambda^*\right) \tag{5.11}$$

Based on the **Assumption 1**, the utility function reaches the optimal value when $\frac{\partial L_o\left(x_{*,j},\mu_x^*,\mu_z^*,\lambda^*\right)}{\partial x_{i,j}} = 0$. Thus, for any index pair i and j at the $k+1$ step, Equation (5.12) is obtained:

$$-\frac{\partial \lambda_{i,j}^{pro} x_{*,j}^{k+1}}{\partial x_{i,j}} + \frac{\partial L_j\left(x_{*,j}^{k+1}\right)}{\partial x_{i,j}} - \frac{\partial L_j\left(x_{*,j}^{k}\right)}{\partial x_{i,j}} + \frac{\partial \mu_{x,j}^{k+1}\left(\mathbb{I}_{D_b}\left(x_{*,j}^{k+1}\right)\right)}{\partial x_{i,j}} + \frac{\partial \frac{\rho}{2}\left\|\mathbb{I}_{D_b}\left(x_{*,j}^{k+1}\right)\right\|}{\partial x_{i,j}} = 0 \tag{5.12}$$

It has been proved that the inequality-constrained ADMM can restrict the solution projected into the feasible domain of the indicator function. When k is sufficiently large, the gradient of the indicator functions can be zero. When the gradients of the indicator function vanish, then we can obtain the Eq. (5.13):

$$\frac{\partial \lambda_{i,j}^{pro} x_{*,j}^{k+1}}{\partial x_{i,j}} = \frac{\partial L_j\left(x_{*,j}^{k+1}\right)}{\partial x_{i,j}} - \frac{\partial L_j\left(x_{*,j}^{k}\right)}{\partial x_{i,j}} \tag{5.13}$$

$\left(x_{i,j}^{k+1} - x_{i,j}^{k}\right)$ can be multiplied by both sides of Equation (5.13) to obtain the Equation (5.14):

$$\frac{\partial \lambda_{i,j}^{pro} x_{*,j}^{k+1}}{\partial x_{i,j}}\left(x_{i,j}^{k+1} - x_{i,j}^{k}\right) = \left(\frac{\partial L_j\left(x_{i,j}^{k+1}\right)}{\partial x_{i,j}} - \frac{\partial L_j\left(x_{i,j}^{k}\right)}{\partial x_{i,j}}\right)\left(x_{i,j}^{k+1} - x_{i,j}^{k}\right) \tag{5.14}$$

Based on the variational inequality in (M. Hu & Fukushima, 2011), Eq. (5.15) can be inferred.

$$\left(\frac{\partial L_j\left(x_{i,j}^{k+1}\right)}{\partial x_{i,j}} - \frac{\partial L_j\left(x_{i,j}^{k}\right)}{\partial x_{i,j}}\right)\left(x_{i,j}^{k+1} - x_{i,j}^{k}\right) \geq 0 \tag{5.15}$$

Then

$$\frac{\partial \lambda_{i,j}^{pro} x_{i,j}^{k+1}}{\partial x_{i,j}}\left(x_{i,j}^{k+1} - x_{i,j}^{k}\right) \geq 0 \tag{5.16}$$

Therefore

$$\sum_{i=1}^{M}\sum_{j=1}^{N} \frac{\partial \lambda_{i,j}^{pro} x_{i,j}^{k+1}}{\partial x_{i,j}}\left(x_{i,j}^{k+1} - x_{i,j}^{k}\right) \geq 0 \tag{5.17}$$

Recall first-order Taylor series of convexity of functions with **Assumption 1**:

$$f(x+p) \approx f(x) + \partial f(x) p \tag{5.18}$$

where $p \to 0$, expand the function $\sum_{i=1}^{M}\sum_{j=1}^{N} f\left(x_{i,j}^{k+1}\right)$ into the optimisation problem when $x_{i,j}^{k+1} \to x_{i,j}^{k}$:

$$\sum_{i=1}^{M}\sum_{j=1}^{N} \lambda_{i,j}^{pro} x_{i,j}^{k+1} = \sum_{i=1}^{M}\sum_{j=1}^{N} \lambda_{i,j}^{pro} x_{i,j}^{k} + \sum_{i=1}^{M}\sum_{j=1}^{N} \frac{\partial \lambda_{i,j}^{pro} x_{i,j}^{k+1}}{\partial x_{i,j}} \left(x_{i,j}^{k+1} - x_{i,j}^{k}\right) \tag{5.19}$$

It can be concluded that:

$$\sum_{i=1}^{M}\sum_{j=1}^{N} \lambda_{i,j}^{pro} x_{i,j}^{k+1} \geq \sum_{i=1}^{M}\sum_{j=1}^{N} \lambda_{i,j}^{pro} x_{i,j}^{k} \tag{5.20}$$

Eq. (5.20) means the revenue of prosumers increases along the vector field. Since the lower-level game is convex and bounded, the optimum of the lower-level game can be achieved. In addition, the upper-level game is linear and bounded, and it can also reach the optimum when the lower-level optimum is achieved. In other words, leader's and follower's game can reach the global optimum if taking sufficient iteration steps. More precisely, from the variational inequality Proposition 2.6 in (Hori et al., 2023), convergence will reach the equilibrium point with:

$$\left\langle \begin{pmatrix} \nabla_{x_{*,1}} \sum_{j=1}^{N} \lambda_{i,j}^{pro} x_{i,j}^{k} \\ \vdots \\ \nabla_{x_{*,N-1}} \sum_{j=1}^{N} \lambda_{i,j}^{pro} x_{i,j}^{k} \\ \nabla_{x_{*,N}} \sum_{j=1}^{N} \lambda_{i,j}^{pro} x_{i,j}^{k} \end{pmatrix}, \begin{pmatrix} x_{*,1}^{k+1} - x_{*,1}^{k} \\ \vdots \\ x_{*,N-1}^{k+1} - x_{*,N-1}^{k} \\ x_{*,N}^{k+1} - x_{*,N}^{k} \end{pmatrix} \right\rangle \leq 0 \tag{5.21}$$

Eq. (5.21) can be set as a stopping criterion of bi-level market convergence.

5.2.2 Solving the bi-level model with a graph-based consensus algorithm

In this section, we propose a novel graph-based consensus algorithm to solve the intelligent aggregation problem with inequality constraints. Section 5.2.2.1 explains how the proposed algorithm considers inequality constraints. Section 5.2.2.2 describes how the proposed algorithm operates on a graph.

5.2.2.1 Considering inequality constraints

Since the standard version of ADMM is only suitable for decomposable convex problems with equality constraints, in order to deal with optimisation problems with inequality constraints, the ADMM algorithm is modified so that it can solve distributed optimisation problems with both equality and inequality constraints.

$$\begin{aligned} &\min f(x) + g(z) \\ &s.t.\ \ Ax + Bz = c \\ &\qquad F_i(x) \le 0 \ \ i = 1, 2, \dots, p \\ &\qquad G_i(z) \le 0 \ \ i = 1, 2, \dots, q \end{aligned} \tag{5.22}$$

Modified optimisation problem (5.22) has variables $x \in \mathbb{R}^n$ and $z \in \mathbb{R}^m$, where $A \in \mathbb{R}^{p\times n}$, $x \in \mathbb{R}^{p\times m}$, and $c \in \mathbb{R}^p$. Note that there are countable convex inequalities that constrain the feasible set of decision vectors x and z. The $F_i(x)$ and $G_i(z)$ are extended-value indicator functions, which are equivalent to:

$$F_i^{'}(x) = \begin{cases} 0, & F_i \le 0 \\ \infty, & F_i > 0 \end{cases}, \qquad i = 1, 2, \dots, p \tag{5.23}$$

$$G_i^{'}(z) = \begin{cases} 0, & G_i \le 0 \\ \infty, & G_i > 0 \end{cases}, \qquad i = 1, 2, \dots, q \tag{5.24}$$

where $F_i' \colon \mathbb{R}^n \to \mathbb{R} \cup \infty$ and $G_i' \colon \mathbb{R}^n \to \mathbb{R} \cup \infty$ are closed, proper and convex. The Lagrangian function of the reconstructed form is:

$$\begin{aligned} &L_0(x, z, \mu_x, \mu_z, \lambda) \\ &\qquad = f(x) + g(z) + \rho/2(\|F_1'(x)\|^2 + \|F_2'(x)\|^2 + \cdots \\ &\qquad + \left\|F_p'(x)\right\|^2 + \langle \mu_x, F'(x)\rangle + \rho/2(\|G_1'(z)\|^2 + \|G_2'(z)\|^2 \\ &\qquad + \cdots + \left\|G_q'(z)\right\|^2) + \langle \mu_z, G'(z)\rangle + \rho/2(\|Ax + Bz - c\|^2 \\ &\qquad + \langle \lambda, Ax + Bz - c\rangle \end{aligned} \tag{5.25}$$

For Eq. (5.25), $F'(\cdot) = [F_1'(\cdot), F_2'(\cdot), \dots, F_p'(\cdot)]$ and $G'(\cdot) = [G_1'(\cdot), G_2'(\cdot), \dots, G_q'(\cdot)]$ are the gradient of extended-value indicator functions $F_i(x)$ and $G_i(z)$. $\mu_x = [\mu_1^x, \mu_2^x, \dots, \mu_p^x]$ and $\mu_z = [\mu_1^y, \mu_2^y, \dots, \mu_q^y]$ are Lagrangian multipliers for inequality constraints. λ is the Lagrangian multiplier for equality constraint. Then, the iterative body of ADMM is shown as below:

$$x^{k+1} = argmin(x, z^k, \mu_x^k, \mu_z^k, \lambda^k) \quad (5.26.a)$$

$$z^{k+1} = argmin(x^{k+1}, z, \mu_x^k, \mu_z^k, \lambda^k) \quad (5.26.b)$$

$$\mu_x^{k+1} = \mu_x^k + \rho F'(x^{k+1}) \quad (5.26.c)$$

$$\mu_z^{k+1} = \mu_z^k + \rho G'(z^{k+1}) \quad (5.26.d)$$

$$\lambda^{k+1} = \lambda^k + \rho(Ax + Bz - c) \quad (5.26.e)$$

However, there is a problem about the gradient of indicator functions of $||F_i'(x)||^2$ and $||G_i'(z)||^2$. Due to the property of a normal cone, it is not possible to get sets of subdifferentials of the group of indicator functions. The extended-value indicator functions can be approximated to obtain gradients:

$$F_i^{'}(x) = \max(0, F_i(x)^m), i = 1, 2, \dots, p \quad (5.27)$$

$$G_i^{'}(x) = \max(0, G_i(x)^m), i = 1, 2, \dots, q \quad (5.28)$$

Then the difference of the function is solvable, the desired solution of the ADMM functions can be solved in the following sub-sections.

5.2.2.2 Convergence analysis

On the analysis that ADMM can be equivalent to the Lyapunov function in analytical optimisation (Boyd et al., 2010) with a similar approach as (Giesen & Laue, 2016):

$$V^k = \frac{1}{\rho}\|\mu_x^* - \mu_x^k\|^2 + \frac{1}{\rho}\|\mu_z^* - \mu_z^k\|^2 + \frac{1}{\rho}\|\lambda^* - \lambda^k\|^2 + \rho\|Bz^{k+1} - Bz\|^2, \quad (5.29)$$

where k is the iteration time. When $k \to \infty$, the parameter $(\mu_x^k, \mu_z^k, \lambda^k,)$ shows incrementally stable behaviour.

Theorem 1. The duality theory claims that the relationship between primal solutions is the solution to dual problems:

$$L_0(x, z, \mu_x^*, \mu_z^*, \lambda^*) \geq L_0(x^*, z^*, \mu_x^*, \mu_z^*, \lambda^*) \quad (5.30)$$

where L_0 is the Lagrangian function and x^*, z^* is the solution of primal.

Theorem 2. The theorem 2 states primal feasibility and convergence of the primal objective function value:

$$\lim_{k \to \infty} r_g^k = 0, \tag{5.31. a}$$

$$\lim_{k \to \infty} r_h^k = 0, \tag{5.31. b}$$

$$\lim_{k \to \infty} f^k = f^*, \tag{5.31. c}$$

$$\lim_{k \to \infty} g^k = g^*, \tag{5.31. d}$$

where $r_g \coloneqq F_i'(x)$ and $r_h \coloneqq Ax + Bz - c$. The convergence of ADMM needs to be identified when inequality constraints are involved, the proof can be obtained through some lemmas. The proof is sketched as below, while similar lemmas without inequality constrains can be found in the appendix of (Boyd et al., 2010).

Lemma 1. The dual variables μ_x^k, μ_z^k are non-negative for all iterations, i.e., it holds that $\mu_x^k \geq 0 \; and \; \mu_z^k \geq 0 \; for \; all \; k \in \mathbb{N}$

Lemma 2. The difference between the optimal objective function value and its value at the $(k+1)^{th}$iterate can be bounded as:

$$\begin{aligned} f(x^*) + g(z^*) - f(x^{k+1}) + g(z^{k+1}) \\ \leq \langle \mu_x^*, r_g^k \rangle + \langle \lambda^*, Ax^{k+1} + Bz^{k+1} - c \rangle \end{aligned} \tag{5.32}$$

Lemma 3. The difference between the value of the objective function at the $(k+1)^{th}$ iterate and its optimal value can be bounded by linear form of $\mu, \; \lambda, \; \rho$.

Lemma 4. The absolute convergence of Lyapunov function Eq. (5.29):

$$\begin{aligned} \left\{ \sum_{k=0}^{\infty} (\|\mu_x^* - \mu_x^k\|^2 + \|\mu_z^* - \mu_x^k\|^2 + \|\lambda^* - \lambda^k\|^2 + \rho \|Bz^{k+1} - Bz\|^2) \right\} \\ \leq \sum_{k=0}^{\infty} (V^k - V^{k+1}) \leq V^0 \end{aligned} \tag{5.33}$$

The hold of **Lemma 4** can be obtained from the first three lemmas. The convergence of value ensures the convergence of ADMM with inequalities.

5.2.2.3 The graph-based ADMM consensus algorithm

The communication networks can be understood as an undirected graph $g(V, \mathcal{E})$, where $V = \{1, 2, \dots, P\}$ is the set of nodes and $\mathcal{E} \in V \times V$ is the set of edges. The cardinality of this set is represented by P and E. An edge is defined as $(i, j) \in \mathcal{E}$, indicating that nodes i and j can share information. The cardinality of P is denoted as $|P|$. To construct the desired graph, each prosumer is assumed only to be connected with their neighbouring prosumers within a certain distance because long-distance communication can be energy-consuming. The system optimisation efficiency can be improved by following a Hamiltonian path, which is a path that visits each vertex exactly once (Rahman & Kaykobad, 2005). The existence of a Hamiltonian path in a graph can be checked with a polynomial time, which is also known as the Non-deterministic Polynomial complete problem (Oltean, 2008). In a prosumer-aggregator network, the graph-based consensus algorithm searches this path on the constructed graph, and the shortest Hamiltonian is employed to update the agents' utility functions to minimise energy consumption.

Once finding the shortest Hamiltonian path in the path, each node with its neighbours can be constructed as a subgraph, and then there will be $|P|$ subgraphs in the system. Two adjacent nodes in a subgraph can share information. When prosumers are equipped with a local computing unit, the solution of the matrix $\boldsymbol{X}$ will be stored locally. Previous researchers have proved that the optimisation in a subgraph can reach a global equilibrium (Mota et al., 2013; Ye et al., 2020). In the optimisation process, a node with updated information will share information with its neighbours, and then using the graph-based ADMM algorithm can completely decentralise the process. The starting point of the traversal can be any node in the Hamiltonian path. The co-equilibria point of the lower-level game in the graph-based method can be defined as follows (Makhdoumi & Ozdaglar, 2017; Mao et al., 2018; Mota et al., 2013):

$$\begin{aligned} &\min_{x_{i,*}} \ \textstyle\sum_{p\in[n]} f_j\left(x_{*,j}^{p}, x_{*,-j}^{p}\right), \\ &s.t. \quad \mathbb{I} \otimes X = Y, \\ &s.t. \quad \left[x_{*,j}^{j}, x_{*,-j}^{j}\right] = Y_j, \end{aligned} \tag{5.34}$$

where $\otimes$ is the Kronecker product. $\mathbb{I}$ indicated the connection of subgraphs. In each iteration of the lower-level game, the optimisation step $x_{*,j}^{(p+1)} =$

$\arg\min_{x_{*,j}} L_0\left(x_{*,j}, \mu_x^{(p)}, \mu_z^{(p)}, \lambda^{(p)}\right)$ is conducted, and updated results will be shared with the connected nodes. After each cyclic iteration in the Hamiltonian path, the matrix X will be delivered to the aggregators. The aggregator will compete to maximise its own utility in Eq. (5.1). The optimisation iteration will continue until the game achieves an equilibrium point. The details of the graph-based ADMM algorithm are demonstrated with the pseudocode shown in Algorithm 5-1.

Algorithm 5-1. Graph-based consensus ADMM

Input: the amount of electricity of each prosumer $j = 1, \dots N$
Output: the matrix $\boldsymbol{X}$, and the prices λ^{pro} offered by each aggregator
Initialize: the randomised first-order utility derivative term, $i = 1, \dots M, j = 1, \dots, N; p \leftarrow 0$
While $\sum_i d(G_i(x_{i,*}^{p+1}) - G_i(x_{i,*}^{p})) < \epsilon$:

{Update the lower-level game}

For j from 1 to N:
L1. Search the followers' game solution by graph-based consensus ADMM, updating the primal and dual variables for the augmented Lagrangian function in $\sum_i d(G_i(x_{i,*}^{p+1}) - G_i(x_{i,*}^{p}))$
L2. Sharing the local graph by connection matrix in the Hamiltonian path
L3. Update the incentive rewards

$$p \leftarrow p + 1$$

{Update the upper-level game}

For i from 1 to M:
U1. Update the transaction prices $\lambda_{i,*}^{pro}$ for each aggregator

End

Figure 5-3 shows a schematic drawing of the proposed graph-based consensus algorithm. Once the Hamiltonian path is constructed, a node with two adjacent nodes can form a sub-graph to share the trading volume information through the private communication link (yellow dash line). For example, node 5, with neighbouring node 4 and node 6, constructs a subgraph. Figure 5-4 shows prosumers sequentially updating the $x_{*,j}$ along the Hamiltonian path (from left to right) with the progression of iteration steps (from top to bottom).

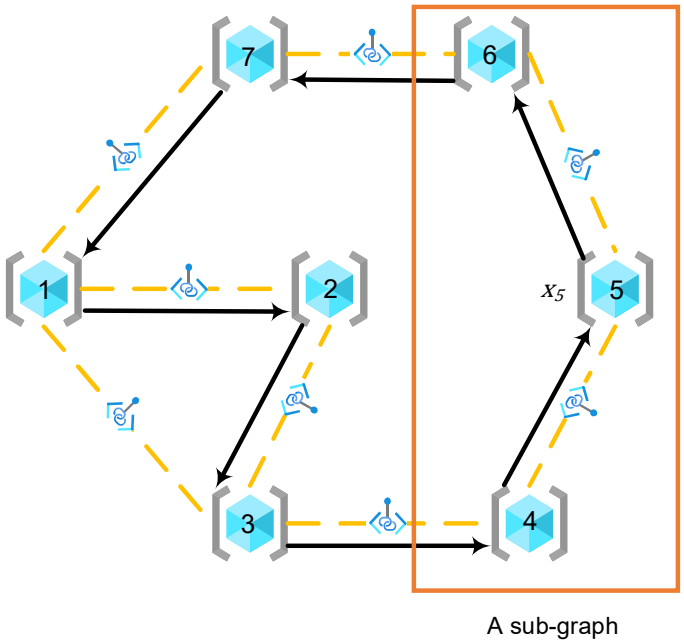

Figure 5-3 Schematic diagram of the graph-based consensus algorithm.

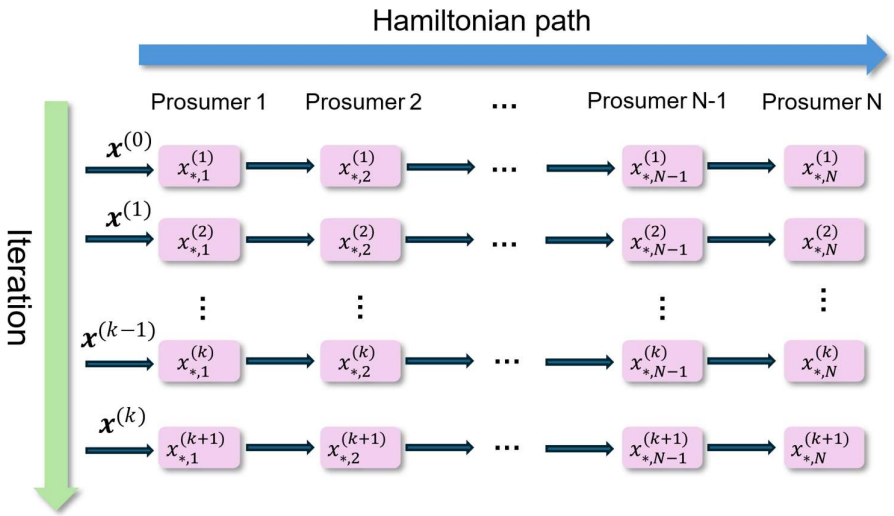

Figure 5-4 Iteration details of the graph-based consensus algorithm.

5.2.2.4 Convergence rate analysis

This section proves that the convergence rate of the proposed algorithm is linear.

Proof.

When step k is sufficiently large:

$$\frac{\partial \mu_{x,j}^{k}\left(\mathbb{I}_{D_b}\left(x_{*,j}^{k}\right)\right)}{\partial x_{i,j}}+\frac{\partial \frac{\rho}{2}\left\|\mathbb{I}_{D_b}\left(x_{*,j}^{k}\right)\right\|}{\partial x_{i,j}}+\frac{\partial \mu_{z,i}^{k+1}\left(\mathbb{I}_{C_a}\left(x_{i,*}^{k}\right)\right)}{\partial x_{i,j}}=0$$
$$\mathbb{I}_{C_a}\left(x_{i,*}^{k}\right),\ \ a=1,2,\dots A \tag{5.35}$$
$$\mathbb{I}_{D_b}\left(x_{*,j}^{k}\right),\ \ b=1,2,\dots$$

Eq. (5.35) indicates the constraints for both levels can be satisfied when the step k is sufficiently large. By applying convexity of $-f\left(\boldsymbol{x}_{i,j}^{*}\right)$ and Equation (5.19), it can be obtained that:

$$\begin{aligned}\sum_{i=1}^{M}\sum_{j=1}^{N} f\left(x_{i,j}^{*}\right) \geq \Bigg\{ & \sum_{i=1}^{M}\sum_{j=1}^{N} f\left(x_{i,j}^{k}\right) \\ & +\sum_{i=1}^{M}\sum_{j=1}^{N}\frac{\partial f_{i,j}\left(x_{i,j}^{k}\right)}{\partial x_{i,j}}\left(x_{i,j}^{*}-x_{i,j}^{k}\right) \\ & +\frac{1}{2}\sum_{i=1}^{M}\sum_{j=1}^{N}\gamma\left(x_{i,j}^{*}-x_{i,j}^{k}\right)^{2}\Bigg\}\end{aligned} \tag{5.36}$$

where γ is a positive constant. The corresponding feasible constraints of both sides can be added to both sides, which yields Augmented Lagrange functions. The Augmented Lagrange function is the sum of all prosumers. By applying the Augmented Lagrange function in Eq. (5.19), it can be obtained that:

$$\begin{aligned}L\left(x_{*,j}^{*},\mu_x^{*},\mu_z^{*},\lambda^{*}\right) & \\ \geq\ & L\left(x_{*,j}^{k},\mu_x^{k},\mu_z^{k},\lambda^{k}\right)+\frac{1}{2}\gamma\|x^{*}-x^{k}\|^{2} \\ & +\mathbb{I}^{T}\nabla_x L\left(x_{*,j}^{k},\mu_x^{k},\mu_z^{k},\lambda^{k}\right)\left(x_{i,j}^{*}-x_{i,j}^{k}\right)\mathbb{I}\end{aligned} \tag{5.37}$$

With

$$L(x,z,\mu_x^{*},\mu_z^{*},\lambda^{*}) \geq L(x^{*},z^{*},\mu_x^{*},\mu_z^{*},\lambda^{*}) \tag{5.38}$$

Then it can be derived to get:

$$\begin{aligned}L(x^{*},\mu_x^{*},\mu_z^{*},\lambda^{*}) & \\ \geq\ & argmin_x\left\{L(x,\mu_x^{k},\mu_z^{k},\lambda^{k})+\frac{1}{2}\gamma\|x-x^{k}\|^{2}\right. \\ & \left.+\mathbb{I}^{T}\nabla_x L(x^{k},\mu_x^{k},\mu_z^{k},\lambda^{k})(x-x^{k})\mathbb{I}\right.\end{aligned} \tag{5.39}$$

Then taking the derivative on the right gives:

$$\|\nabla_x L(x^k, \mu_x^k, \mu_z^k, \lambda^k)\|_2^2 \geq 2\gamma(L(x^k, \mu_x^k, \mu_z^k, \lambda^k) - L(x^*, \mu_x^*, \mu_z^*, \lambda^*)) \tag{5.40}$$

According to the convexity of Lagrangian Eq. (5.40), after substituting the convexity of prosumers' utility function, Eq. (5.41) can be derived:

$$\begin{aligned} & L(x^k, \mu_x^k, \mu_z^k, \lambda^k) \\ & \quad \geq L(x^{k+1}, \mu_x^{k+1}, \mu_z^{k+1}, \lambda^{k+1}) \\ & \quad + \mathbb{I}^T \nabla_x L(x^{k+1}, \mu_x^{k+1}, \mu_z^{k+1}, \lambda^{k+1})^T (x^k - x^{k+1}) \mathbb{I} \\ & \quad \geq L(x^{k+1}, \mu_x^{k+1}, \mu_z^{k+1}, \lambda^{k+1}) \\ & \quad + \sum_{i=1}^{M} \sum_{j=1}^{N} \left(\frac{\partial L\left((x^{k+1}, \mu_x^{k+1}, \mu_z^{k+1}, \lambda^{k+1})\right)}{\partial_{x_{ij}}} \right) \times \frac{1}{k} \left(\frac{\partial L_j\left(x_{i,j}^k\right)}{\partial x_{i,j}} \right. \\ & \quad \left. - \frac{\partial L_j\left(x_{i,j}^{k+1}\right)}{\partial x_{i,j}} \right) \end{aligned} \tag{5.41}$$

When k is sufficiently large, Eq. (5.35) and the Karush-Kuhn-Tucker conditions can be applied such that:

$$\frac{\partial L(x^{k+1}, \mu_x^{k+1}, \mu_z^{k+1}, \lambda^{k+1})}{\partial_{x_{ij}}} + \frac{\partial L_j\left(x_{i,j}^k\right)}{\partial x_{i,j}} - \frac{\partial L_j\left(x_{i,j}^{k+1}\right)}{\partial x_{i,j}} = 0 \tag{5.42}$$

Combining Eq. (5.41) and (5.42) into Eq. (5.40) yields:

$$\begin{aligned} & L(x^k, \mu_x^k, \mu_z^k, \lambda^k) \\ & \quad \geq L(x^{k+1}, \mu_x^{k+1}, \mu_z^{k+1}, \lambda^{k+1}) + 2\frac{\gamma}{k}(L(x^k, \mu_x^k, \mu_z^k, \lambda^k) \\ & \quad - L(x^*, \mu_x^*, \mu_z^*, \lambda^*)) \end{aligned} \tag{5.43}$$

Then reformulating Eq. (5.43) yields:

$$\frac{L(x^{k+1}, \mu_x^{k+1}, \mu_z^{k+1}, \lambda^{k+1}) - L(x^*, \mu_x^*, \mu_z^*, \lambda^*)}{L\left(x^k, \mu_x^k, \mu_z^k, \lambda^k\right) - L(x^*, \mu_x^*, \mu_z^*, \lambda^*)} = \frac{1}{1 + 2\frac{\gamma}{k}} < 1 \tag{5.44}$$

This allows the assertion that the proposed algorithm has a linear convergence rate.

5.3 Intelligent aggregation application and discussion

In this section, the intelligent aggregation architecture is applied with an example of a low voltage (LV) to medium voltage (MV) distribution network with synthetic prosumer data.

5.3.1 Experiment setup

This case study is based on the open-source electric network benchmark database named Simbench (Meinecke et al., 2020). The Simbench data is generated by clustering the publicly available electric network data in Germany. We chose an urban LV distribution network benchmark data from the Simbench database. The benchmark LV distribution network consists of 59 buses, and we modified the bus data to incorporate 57 hypothetical prosumers with 5 PV units with a 5 kW power rating and 57 EVs. The modified distribution network is shown in Figure 5-5. All EVs are assumed to be able to have V2G capabilities. In this example, both PV and EV units are modelled as static generators.

The day-ahead prices used in this case study are obtained from the Nord Pool UK day-ahead price (Nord Pool, 2024), shown in Table 5-1. This chapter selects the 2nd, 8th, 14th and 20th hour for the day-ahead market price. Table 5-2 shows the parameters used in the market co-equilibrium model, and Table 5-3 shows the detailed case study data for the 57 synthetic prosumers.

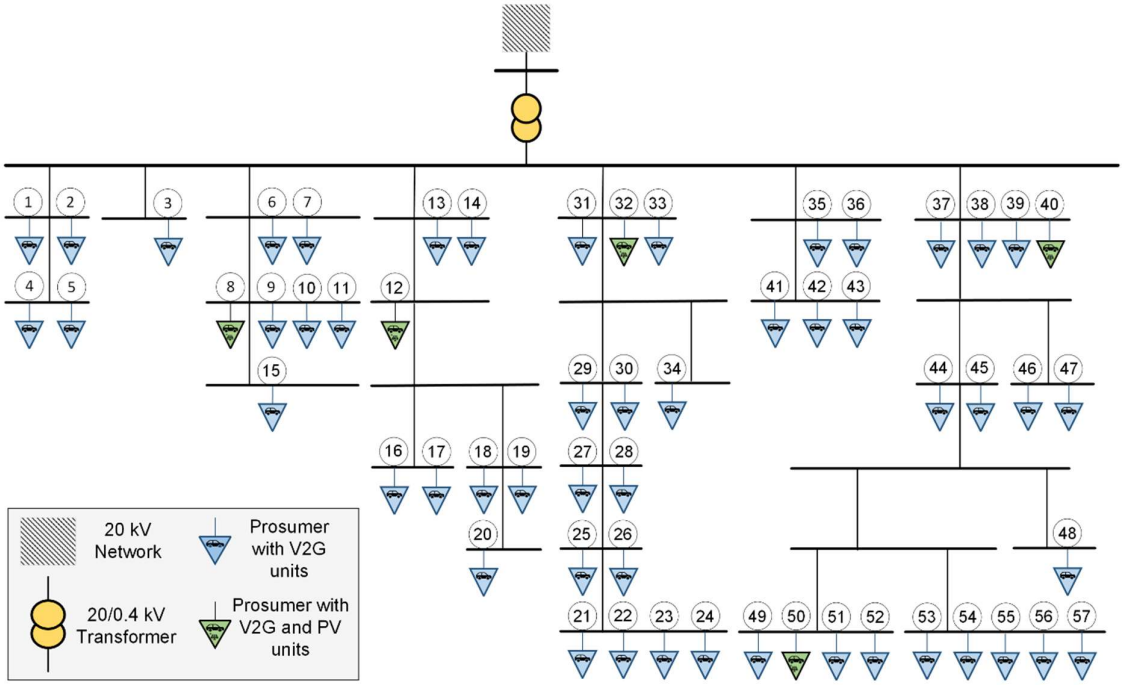

Figure 5-5 LV electric distribution network.

Table 5-1 Day-ahead price in the intelligent aggregation case study

Time	1	2	3	4	5	6	7	8	9	10	11	12
Price (£/kWh)	0.070	0.064	0.067	0.070	0.065	0.060	0.084	0.100	0.103	0.080	0.074	0.072
Time	13	14	15	16	17	18	19	20	21	22	23	24
Price (£/kWh)	0.071	0.070	0.064	0.063	0.060	0.077	0.084	0.100	0.095	0.089	0.077	0.07

Table 5-2 Parameter setup in the intelligent aggregation case study

Parameter	$\underline{\lambda}_{i,j}^{pro,ask}$	$\overline{\lambda}_{i,j}^{pro,ask}$	$\underline{x}_{i,*}^{DA}$	$\overline{x}_{i,*}^{network}$	R	T	β	γ
Value	0.04 (£/kWh)	0.06 (£/kWh)	10 kW	200 kW	8.314 (J/mol K)	300.15K	0.05 (-)	0.1 (-)

Table 5-3 Prosumers information in the intelligent aggregation case study

Prosumer id	A (-)	z (-)	c (-)	$\bar{x}_{*,j}$ (kWh)	**Prosumer id**	A (-)	z (-)	c (-)	$\bar{x}_{*,j}$ (kWh)
1	0.305	0.705	110	7	**30**	0.193	0.593	590	3.6
2	0.18	0.58	90	3.6	**31**	0.323	0.723	250	3.6

3	0.157	0.557	80	3.6	**32**	0.102	0.502	630	7
4	0.311	0.711	330	3.6	**33**	0.28	0.68	90	3.6
5	0.24	0.64	450	7	**34**	0.111	0.511	560	7
6	0.182	0.582	240	3.6	**35**	0.108	0.508	640	7
7	0.266	0.666	130	3.6	**36**	0.262	0.662	340	7
8	0.221	0.621	440	7	**37**	0.203	0.603	530	3.6
9	0.258	0.658	370	7	**38**	0.243	0.643	590	3.6
10	0.137	0.537	380	3.6	**39**	0.117	0.517	260	3.6
11	0.109	0.509	460	3.6	**40**	0.135	0.535	490	7
12	0.333	0.733	540	7	**41**	0.253	0.653	540	3.6
13	0.231	0.631	560	3.6	**42**	0.191	0.591	100	7
14	0.334	0.734	150	7	**43**	0.234	0.634	570	7
15	0.259	0.659	420	7	**44**	0.321	0.721	240	3.6
16	0.167	0.567	70	7	**45**	0.13	0.53	490	7
17	0.209	0.609	370	3.6	**46**	0.197	0.597	520	7
18	0.259	0.659	630	7	**47**	0.201	0.601	60	7
19	0.289	0.689	570	3.6	**48**	0.194	0.594	400	3.6
20	0.207	0.607	360	7	**49**	0.15	0.55	320	7
21	0.33	0.73	190	7	**50**	0.181	0.581	340	7
22	0.139	0.539	190	3.6	**51**	0.193	0.593	500	3.6
23	0.142	0.542	490	7	**52**	0.266	0.666	600	7
24	0.259	0.659	290	7	**53**	0.188	0.588	600	3.6
25	0.249	0.649	560	3.6	**54**	0.346	0.746	170	7
26	0.31	0.71	590	3.6	**55**	0.237	0.637	460	3.6
27	0.225	0.625	100	7	**56**	0.182	0.582	140	3.6
28	0.273	0.673	560	7	**57**	0.335	0.735	630	7
29	0.155	0.555	150	7					

5.3.2 Results and discussion

The shortest Hamiltonian communication path was constructed for communicating between neighbouring prosumers. For demonstration, a front-end web[4] was developed

[4] https://tinyurl.com/3vv8ptzh

to show the Hamiltonian communication path of 57 prosumers, which can be extended to monitor real-time optimisation and information flow sharing. Each prosumer can share their information with their neighbours in the network graph to reach a consensus state. Figure 5-6 demonstrates how the information is shared in the network graph. The network graph is plotted with the geo-tag data provided by Simbench. (a), information flow during the optimisation process is demonstrated, where the nodes in the network construct a Hamiltonian path. (b), subgraphs of node 21 and node 30 were highlighted to indicate the information flow. For subgraph x_{21}, the trading volume information is passed from node 28. Once node 21 optimises the local objective function, the trading volume information is passed to node 24. Similar information flow can also be observed in the subgraph x_{30}, where node 30 optimised the information provided by node 31. Then, node 30 sends the optimised results to node 27.

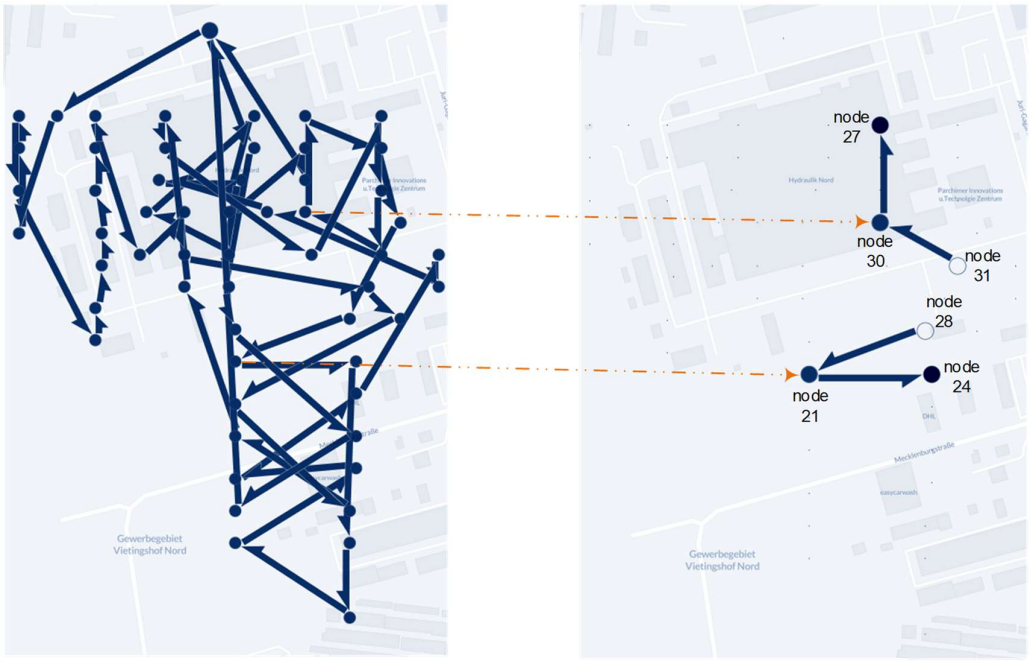

(a) (b)

Figure 5-6 Visualisation of information flow in the network graph.

The result of the aggregation volume of 57 prosumers is shown in Figure 5-7, which is the optimised result of the trading volume matrix $\boldsymbol{X}$ for the lower-level game. There is

a considerable trading volume variance among prosumers due to the differences in their energy assets. The differences include the maximum discharge rating of batteries, as well as the health of the batteries. For example, prosumer 37 has an aged battery ($c = 530$) and a low battery discharge bound ($\bar{x}_{*,37}$=3.6kWh). It is worth noting that the trading volume at night is less than that during the day, which reflects a reasonable game result, i.e., prosumers tend to sell their surplus electricity during the day and charge it at nighttime, because electricity prices are usually higher in the daytime.

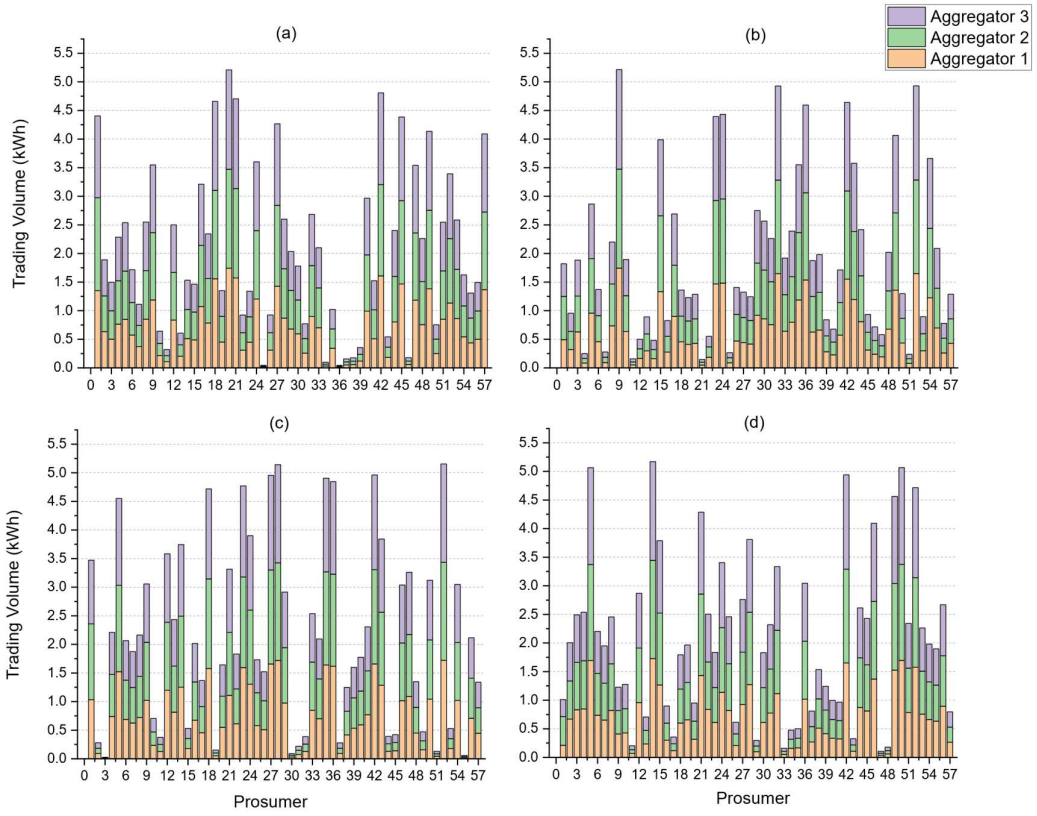

Figure 5-7 Trading volume visualisation (a) the trading volumes at 2 am; (b) the trading volumes at 8 am; (c) the trading volumes at 2 pm; (d) the trading volumes at 8 pm.

In addition to the trading volume, Figure 5-8 shows the game result for upper-level game, where each aggregator competes with each other by determining the aggregation offer price $\lambda_{i,j}^{pro,ask}$. It can be seen from the figure that the price offered to prosumers varied considerably among aggregators. For instance, aggregator 1, aggregator 2, and

aggregator 3 offer to pay 0.044, 0.055, 0.043 £/kWh, respectively, to prosumer 52 at 8 am to aggregate the electricity. As a result, prosumer 52 receive £0.217 from three aggregators. Subsequently, aggregators make £0.092, £0.0914, and £0.0919, respectively, to facilitate the aggregation. Thus, aggregators are able to profit by providing aggregation facilitation services. In addition, the profits of aggregators will increase with more prosumers participating in the aggregation process. The following section will conduct a benchmark analysis to prove the effectiveness of our proposed algorithm.

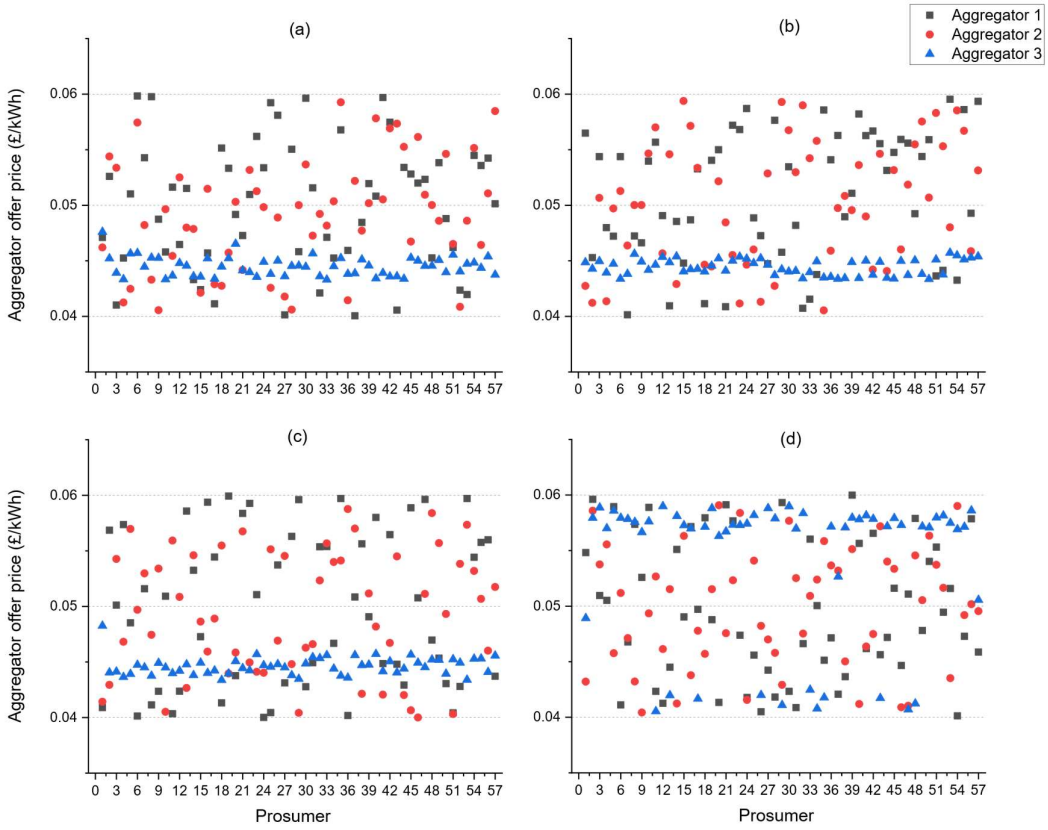

Figure 5-8 Aggregator offer price visualisation (a) the offer price at 2 am; (b) the offer price at 8 am; (c) the offer price at 2 pm; (d) the offer price at 8 pm.

5.3.3 Benchmark analysis

Table 5-4 shows the comparison of the proposed algorithm with the Classical ADMM (Boyd et al., 2010), Walkman ADMM (Mao et al., 2018), and RW-ADMM (Shah & Avrachenkov, 2018). Following the same notation in Section 5.2.2.3, P, E are represented as the total nodes and edges in a graph, where E is an integer in the range

of $[\mathrm{P}, \mathrm{P}(\mathrm{P}-1)]$. Q is denoted as the edge connection matrix, and $\rho_{\max}(\mathrm{Q})$ is the largest eigenvalue of the connection matrix. According to the proof (Deng et al., 2017), the multi-block ADMM can achieve a linear convergence rate in convex problems. Therefore, basic ADMM and its variants can achieve a linear convergence rate. If the bounded error of an optimisation method with a linear convergence rate is expected to be within $(0, \epsilon)$, the iteration time is to $O(\ln\left(\frac{1}{\epsilon}\right))$ (Nocedal & Wright, 2006). The convergence rate analysis of the proposed algorithm and benchmarks is shown in Figure 5-9. The proposed algorithm demonstrates a linear convergence rate consistent with the benchmarks.

Table 5-4 Benchmark comparison of proposed algorithm with other ADMM algorithms

Name	Communication Complexity	Convergence Rate	Privacy Preserving	Graph Structure
Classical ADMM (Boyd et al., 2010)	$O(\ln\left(\frac{1}{\epsilon}\right).\mathrm{P}^3)$	Linear	No	Complete
Walkman ADMM (Mao et al., 2018)	$O(\ln(\frac{1}{\epsilon}).\frac{\mathrm{P}\ln^3(\mathrm{P})}{\left(1-\rho_{\max}(\mathrm{Q})\right)^2})$	Linear	Yes	Random
RW-ADMM ADMM (Shah & Avrachenkov, 2018)	$O(\ln(\frac{1}{\epsilon}).\frac{\mathrm{E}^2}{\mathrm{P}\sqrt{1-\rho_{\max}(\mathrm{Q})}})$	Linear	Yes	Fixed subgraph
Proposed algorithm	$O(\ln\left(\frac{1}{\epsilon}\right).\mathrm{P}^2)$	Linear	Yes	Cycle

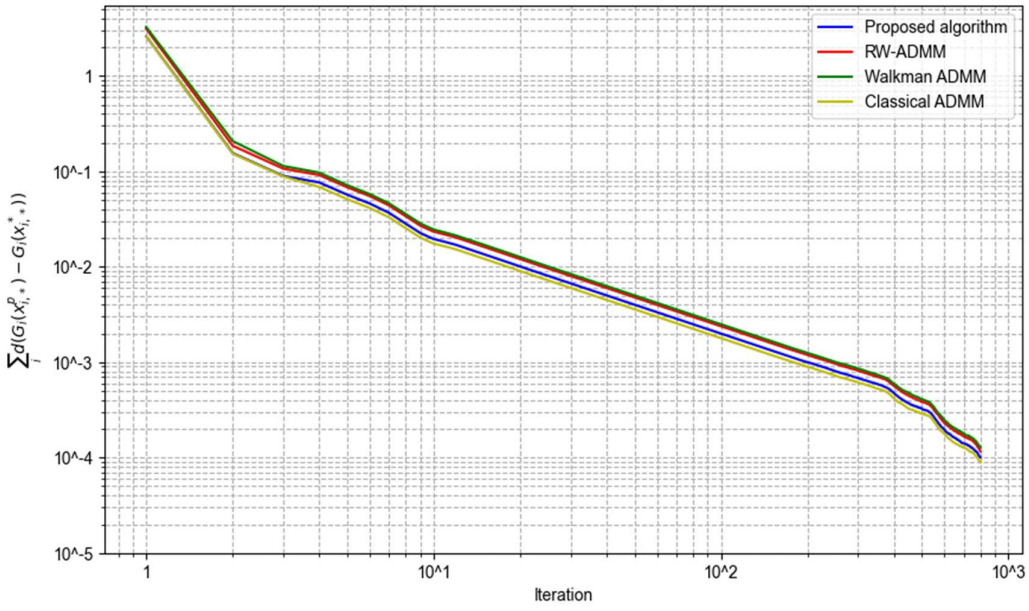

Figure 5-9 Convergence rate analysis of proposed algorithm and benchmarks.

Since all convergence rates are linear, merely measuring the convergence rate is not enough. Another criterion for evaluating the performance of distributed algorithms is communication complexity because graph structures have different communication costs. The graph structure can be divided into four types, complete (Boyd et al., 2010), random (Mao et al., 2018), fixed subgraph (Shah & Avrachenkov, 2018), and cycle (West, 2001). The complete cannot preserve the private information of prosumers since all data will be shared. Random, fixed subgraphs and cycles can preserve privacy when optimising. According to the graph theory (West, 2001) and computation method in (Mao et al., 2018), the classical ADMM in a complete graph has a communication complexity as $O(\ln\left(\frac{1}{\epsilon}\right).\mathrm{P}^3)$, with the communication complexity.

Walkman ADMM and RW-ADMM have a better performance, with $O(\ln(\frac{1}{\epsilon}).\frac{\mathrm{P}\ln^3(\mathrm{P})}{(1-\rho_{\max}(\mathrm{Q}))^2})$ and $O(\ln(\frac{1}{\epsilon}).\frac{\mathrm{E}^2}{\mathrm{P}\sqrt{1-\rho_{\max}(\mathrm{Q})}})$. When Hamiltonian path P is cyclic, $1-\rho_{\max}(\mathrm{Q}) = O(1-\cos\frac{2\pi}{\mathrm{P}}) = O(\frac{1}{\mathrm{P}^2})$. In such a situation, our method can achieve a communication complexity as $O\left(\ln\left(\frac{1}{\epsilon}\right).\frac{\mathrm{P}}{\sqrt{1-\rho_{\max}(\mathrm{Q})}}\right) = O\left(\ln\left(\frac{1}{\epsilon}\right).\mathrm{P}^2\right)$, according to (Mao et al., 2018). When P is large but not limited to infinite, our method has lower

complexity than the Walkman and RW-ADMM. When P is limited to infinite, the Walkman ADMM can be more communication efficient as $\lim_{P\to\infty} \ln^3(P) \ll \lim_{P\to\infty} P$. For the aggregator trading problem in a community, the scale of optimisation is usually a limited number of prosumers, so our method can be considered more efficient.

5.4 Chapter summary

The penetration of DER and IoT technologies is transforming power systems' generation, transmission, consumption, and decision-making. The power flow has transitioned to bidirectional rather than unidirectional, but hierarchical control has not changed. Moreover, decentralised decision-making architecture is emerging to challenge the traditional centralised one in order to ensure data privacy and security and to allow prosumers to optimise their utility.

Thus, this chapter proposes an intelligent aggregation architecture to facilitate a more sophisticated energy transition. The architecture adopts distributed computing technologies to compute a multi-leader multi-follower complete information game with the novel graph-based consensus algorithm. This chapter proved the existence and uniqueness of the MLMFG model and convergence analysis of the proposed algorithm with a systematic convex approach. In addition, this chapter examined the applicability of the proposed intelligent aggregation framework on a distribution network, where the results showed the competitive game relationship among the aggregators. With a benchmark analysis, the proposed algorithm is compared with the state-of-the-art algorithm in terms of communication complexity, privacy preservation, and convergence rate. It is shown that the proposed algorithm has a communication complexity of $O(\ln\left(\frac{1}{\epsilon}\right).P^2)$, which means the proposed algorithm performs better than state-of-the-art algorithms in terms of communication complexity.

Future work could focus on inter-temporal decision-making and contractual agreements in electricity aggregation. The optimal strategy of the aggregation process could consider prosumers' decisions on electricity storage. The prosumers with storage units could store energy when the electricity price is low and sell stored electricity when the price is high. The optimal strategy requires inter-temporal decision-making. Moreover, the contractual agreement between prosumers and aggregators requires further research. In the conventional energy system, the contractual agreement of generation,

transmission, and distribution is centralised by the involved companies. In the decentralised energy system, the contractual agreements between agents are dynamic and hard to enforce. Blockchain technology could be a viable solution to establish contractual agreements among decentralised agents.

Chapter 6

6. Addressing evaluative complexity in hydrogen carrier selection with an integrated MCDM framework[5]

6.1 Introduction

The transition to sustainable energy systems has underscored green hydrogen as a pivotal solution for reducing dependency on fossil fuels. Green hydrogen carriers (GHC), including liquid hydrogen (LH_2), ammonia (NH_3), liquid-organic hydrogen carriers (LOHCs) such as dibenzyltoluene (DBT) or toluene (TOL), and methanol (MeOH), have emerged as pivotal energy vectors for large-scale storage and maritime transport. However, each carrier has distinct techno-economic performance, environmental impacts, and carrier efficiencies. The literature review in Chapter 2 shows that there is no GHC comparative study to systematically evaluate the GHCs, integrating key decision metrics, such as economic viability, environmental impact, and carrier efficiencies. Furthermore, the South Africa-UK hydrogen corridor is unexamined in the existing literature.

This chapter achieves **Objective 3** with a novel multi-criteria decision-making framework on an unexplored international hydrogen supply chain. The contributions of Chapter 6 are summarised as follows:

[5] This chapter is adapted from **Yao, R.**, Li, Y., Varga, L., & Hu, Y. (2025). A multi-criteria framework for evaluating hydrogen carriers for large-scale intercontinental exports. *Energy Policy*, 210, 115040, https://doi.org/10.1016/j.enpol.2025.115040

- Proposed a transparent MCDM framework that combines discounted techno-economic model, ISO-compliant life-cycle assessment and carrier-specific energy-efficiency metrics to produce a multi-criteria ranking of GHC options.
- Applies the framework to the previously unexamined South Africa-UK corridor, quantifying carrier performance under realistic supply-chain configurations.
- Conducts a structured sensitivity analysis (seven scenarios) to identify the dominant drivers of carrier ranking.

The rest of this chapter is organised as follows: Section 6.2 defines functional boundaries of international hydrogen-carrier supply chains. Section 6.3 sets out the mathematical formulation of the MCDM framework. Section 6.4 describes the South Africa-UK case-study configuration. Section 6.5 presents and discusses the results. Section 6.6 concludes this chapter.

6.2 System description

This section outlines the system definition of the large-scale international hydrogen supply chain system, as well as the key components of each hydrogen carrier delivery pathway. Figure 6-1 illustrates the hydrogen supply chain, which includes the exporting country, the importing country, and the maritime transportation between them. Green hydrogen is produced in the exporting country through water electrolysis using renewable energy sources, such as solar photovoltaic systems or wind turbines. The green hydrogen is then transported to conversion plants to be converted to GHCs. The GHCs are stored in the buffer storage before being loaded onto ships. The GHCs are then unloaded in the importing country at the buffer storage and then converted back to hydrogen.

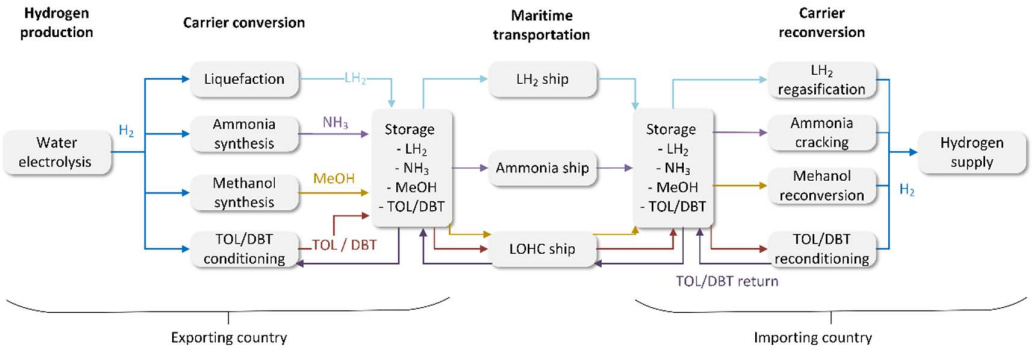

Figure 6-1 Schematic drawing of the international hydrogen supply chain.

It should be noted that some GHCs, such as green ammonia and methanol, could be delivered to the importing country directly without reconversion back to hydrogen, as they are already traded commodities. This chapter considers the reconversion of all GHCs to hydrogen, ensuring that the functional units of all GHCs are consistent in the LCA analysis. This practice can also be found in the literature (Dickson et al., 2022; Lee et al., 2022; Noh et al., 2023a). The rest of this section will describe the key technological components of each GHC delivery pathway.

The LH_2 delivery chain begins at the liquefaction plant, where green hydrogen is liquefied under extreme conditions. Given that hydrogen is the lightest known element, it must be cooled to cryogenic temperatures, approximately -253°C (Restelli et al., 2024). The liquefaction process requires multiple refrigeration cycles to achieve the desired state of liquefaction. After the production of LH_2, the LH_2 will be stored in the cryogenic tanks, where the boil-off rate can vary from 0.1% to 0.3% per day (Arrigoni et al., 2024). The maritime transportation of LH_2 is carried out by dedicated LH_2 tanker ships with refrigeration systems to reduce the LH_2 loss (Dickson et al., 2022). The LH_2 will be regasified in the importing port, and the regasification process is less energy-intensive than the liquefaction process (Dickson et al., 2022).

Ammonia is currently produced on an industrial scale using the Haber-Bosch process, which combines hydrogen and nitrogen at high temperatures, ranging from 400 to 600 °C, and high pressure, from 200 to 400 bar (IRENA, 2022). The conventional ammonia production method utilises natural gas or coal through gas reforming or coal gasification. Green ammonia production, on the other hand, does not rely on fossil fuels (natural gas and coal). Green ammonia is produced through an electrochemical nitrogen reduction reaction using nitrogen and hydrogen, and is supplied by electricity. The nitrogen required for ammonia production can be obtained directly from air with Air Separation Units (ASU). The produced liquid ammonia is also stored in refrigeration tanks, but the temperature requirement for liquid ammonia (-34 °C) (Lee et al., 2022) is less extreme than that of liquid hydrogen. Ammonia cracking is the reverse of ammonia synthesis. The ammonia cracking process requires energy input to break down ammonia into pure hydrogen and nitrogen (IPHE, 2023).

In contrast to LH_2 and NH_3, LOHCs are liquid at ambient temperature and pressure. Thus, LOHCs can leverage existing petrochemical infrastructure, reducing upfront

capital investments for specialised infrastructure. The LOHCs considered in this study include dibenzyltoluene (DBT), toluene (TOL), and methanol (MeOH). During the conversion process, DBT and TOL will be hydrogenated with green hydrogen to perhydro-dibenzyltoluene (H18-DBT) and methylcyclohexane (MCH), respectively (Raab et al., 2021). The hydrogen-rich carrier H18-DBT and MCH will be transported to importing countries, where the hydrogen-rich LOHCs will be dehydrogenated to release hydrogen. The unloaded LOHCs are then transported back to the hydrogenation facility in the export country.

Methanol is also a type of LOHC, which is a globally traded chemical commodity (Ortiz Cebolla et al., 2022). Green methanol differs from conventional fossil-based methanol because it uses a carbon source (CO_2) captured in exporting countries via direct air capture (DAC) (Ortiz Cebolla et al., 2022). Green methanol can also leverage existing transportation infrastructure, as it is liquid at ambient temperatures. The dehydrogenation of methanol differs from that of DBT and TOL, as the carrier CO_2 is re-emitted back into the atmosphere without a carbon capture facility. The GHCs covered in this section have various features that make the evaluation process complex. Section 6.3 will outline the methodology for developing a multi-criteria decision-making framework to rank hydrogen carriers.

6.3 Methodology

Figure 6-2 shows the proposed evaluation framework for GHC emissions in the international hydrogen supply chain. This framework compares GHC performances in three aspects: economic performance, environmental impacts, and carrier efficiency. Thus, the proposed framework integrates techno-economic analysis, LCA, and efficiency analysis results as criteria input for MCDM evaluation. Figure 6-2 also demonstrates the parameters required for evaluation. The proposed evaluation framework ranks GHCs based on the international hydrogen supply chain defined in Section 6.2.

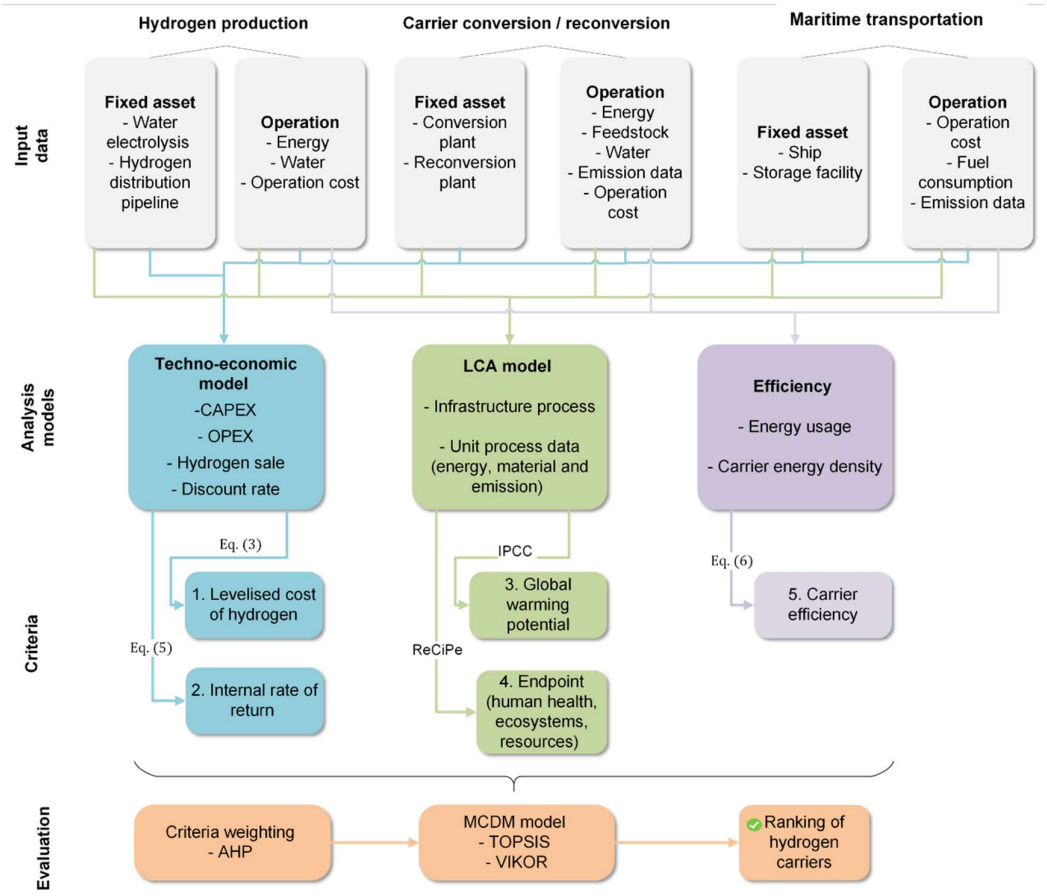

Figure 6-2 Proposed evaluation framework for green hydrogen carriers.

The rest of this section explains the methodology behind the proposed framework. Section 6.3.1 explains the techno-economic modelling methods. Section 6.3.2 explains the LCA modelling methodology, and Section 6.3.3 explains the MCDM methods.

6.3.1 Techno-economic analysis

The economic performance of green hydrogen delivery pathways is evaluated with the following performance indicators: LCOH and internal rate of return (IRR). A seminal work on the levelised cost models highlighted the importance of considering the discount rate and the inflation effect (Aldersey-Williams & Rubert, 2019). The conventional undiscounted levelised cost models divide the total capital and operation costs by the quantity of produced hydrogen. As a result, the conventional method does not provide insight into the impact of the time value of cash flow and hydrogen delivery. Therefore, this chapter adopts the weighted average cost of capital (WACC) as the discount factor (Rezaei et al., 2024). WACC is a key financial metric representing the

average cost of project financing, which is calculated from the capital investment structure. WACC is defined as Eq. (6.1) in regular terms:

$$WACC^{norm} = \frac{E}{E+D}R_e + \frac{D}{E+D}R_d \tag{6.1}$$

where E is the value of equity and D is the value of debt. The first term $\frac{E}{E+D}$ indicates the proportion of equity financing and $\frac{D}{E+D}$ represents the proportion of debt financing. R_e is the cost of equity that is required by the equity investors to compensate for risks. R_d is the cost of debt to pay out interest payments to debt financiers. To adjust for the inflation effect, the real term WACC can be calculated as:

$$WACC^{real} = \left(\frac{1 + WACC^{norm}}{1 + infl}\right) - 1 \tag{6.2}$$

where $infl$ is the inflation rate. By discounting with the real terms, the LCOH and IRR results can reflect the intrinsic performance of GHCs. Then, the real LCOH is calculated with the net present value of money by Eq. (6.3) (Aldersey-Williams & Rubert, 2019):

$$LCOH = \frac{CAPEX + \sum_{t=1}^{t=T} \frac{OPEX_t^{fixed} + OPEX_t^{variable}}{(1 + WACC^{real})}}{\sum_{t=1}^{t=T} \frac{M_{H_2}}{(1 + WACC^{real})^t}} \tag{6.3}$$

where $t \in [1, T]$ is the period from year 1 to year T. $CAPEX$ is the present value of capital expenditure on the project includes capital costs for plants, storage facilities, distribution pipeline, and carrier cost (for DBT and TOL). $OPEX_t^{fixed}$ is the fixed operation expense in period t, and $OPEX_t^{variable}$ is the variable operation expense in period t, including energy and feedstock costs.

The economies of scaling are considered in the techno-economic analysis to account for the impact of capacity scaling on CAPEX which can be calculated based on Eq. (6.4) (Rezaei et al., 2024):

$$CAPEX_{scale} = CAPEX_{base} \times \left(\frac{Capacity_{scale}}{Capacity_{base}}\right)^{\varepsilon} \tag{6.4}$$

where $CAPEX_{scale}$ is the capital expenditure for installed equipment after scaling to $Capacity_{scale}$ from $Capacity_{base}$. ε is the scaling exponent for considering the economics of scaling.

In addition to the LCOH, this study also calculates the IRR for economic performance evaluation. IRR is the discount rate that makes the net present value (NPV) of a project's future cash flow equal to zero, which accounts for the time value of money. In addition, IRR provides a single and annualised rate to reflect a GHC's profitability. The NPV for a green hydrogen project can be calculated by Eq. (6.5). In the context of a green hydrogen project, the cash flow at year t is calculated from the revenue of selling hydrogen Rev_t and operation expenses at year t (Nicita et al., 2020).

$$NPV = -CAPEX + \sum_{t=1}^{t+T} \frac{Rev_t - (OPEX_t^{fixed} + OPEX_t^{variable})}{(1+r)^t} \quad (6.5)$$

6.3.2 Life cycle assessment

The environmental impacts of each GHC pathway are evaluated using the LCA model in accordance with ISO 14040 and 14044 standards (ISO, 2006a, 2006b). The ISO standards define core principles and a framework for conducting LCA modelling, which consists of four phases: 1) defining the goal and scope, 2) performing life cycle inventory analysis, 3) conducting life cycle impact assessment, and 4) interpreting the life cycle results.

The goal of the LCA model is to provide quantitative environmental impact results for comparative evaluation with MCMD models. The system boundary of the LCA model is shown in Figure 6-1. The LCA model includes green hydrogen production with renewable energy, GHC conversion, the maritime transportation of GHCs, and reconversion of GHC to gaseous hydrogen. Hence, this system definition follows the cradle-to-gate structure (Dickson et al., 2022; IPHE, 2023). The functional unit of the LCA model is the delivery of 1 kg of gaseous hydrogen to the importing country.

Life cycle inventory (LCI) analysis is a core phase in an LCA model to quantify the unit process inputs (raw materials, energy, water) and the unit process outputs (products, emissions, and wastes). The life cycle inventory collection and reporting include the key information from input data of Figure 6-2. The input data includes the key

emissions from the production, conversion, and transportation processes. It should be noted that the environmental impacts related to business travel and employee commuting are not considered in this life cycle inventory analysis, as guided in (IPHE, 2023).

The LCI data are translated into the environmental impact scores using two complementary assessment methods, IPCC Global Warming Potential over a 100-year horizon (IPCC GWP 100) and ReCiPe Endpoint. IPCC GWP100 is a life cycle impact assessment that quantifies the climate impact of greenhouse gases, providing a focused metric that is highly relevant for energy policy (IPCC, 2023). The ReCiPe Endpoint method is adopted to provide a broad and aggregated assessment of environmental damage. In addition to the global warming potential, the ReCiPe method also calculates the environmental impact scores in the other 11 midpoint impact categories, such as stratospheric ozone depletion and fine particulate matter formation (Huijbregts et al., 2017). The midpoint impacts are subsequently translated to the endpoint impact of three areas of protection (human health, ecosystem, and resource availability). The endpoint results provide condensed information for decision-making, while being transparent about the environmental impact pathways and causes of damage (Hauschild et al., 2018). Hence, the proposed evaluation framework utilises the IPCC GWP100 and ReCiPe endpoint as input for MCDM analysis.

6.3.3 Carrier efficiency

The carrier efficiency η (%) for a GHC is defined in the Eq. (6.6). The numerator quantifies the output energy obtained from hydrogen, and the denominator aggregates all the energy input throughout the entire supply chain. A high value of η indicates that a significant proportion of the total energy is in the hydrogen output.

$$\eta = \frac{E_{H_2,output}}{E_{H_2,input} + E_{conversion} + E_{transport} + E_{reconversion}} \tag{6.6}$$

where $E_{H_2,output}$ is the energy content of delivered hydrogen at import country measured by low heating value. $E_{H_2,input}$ is the energy content of hydrogen to be transported in exporting country. $E_{conversion}$, $E_{transport}$, and $E_{reconversion}$ is the energy consumption in the conversion, transportation, and reconversion process of a GHC pathway respectively.

6.3.4 Multi-criteria decision-making framework

Building on the methods presented in Sections 6.3.1 to 6.3.3, five key criteria are identified for evaluating hydrogen carriers: LCOH, IRR, GWP, ReCiPe endpoint, and carrier efficiency. These criteria represent economic feasibility/profitability, environmental impacts, and energy efficiency, respectively. They collectively capture the economic, environmental, and operational dimensions for a comprehensive assessment.

In this section, MCDM methods are applied to evaluate and rank the hydrogen carriers based on these established criteria. The proposed framework integrates three decision-making tools with distinct objectives, including Analytic Hierarchy Process (AHP), TOPSIS (Technique for Order of Preference by Similarity to Ideal Solution), and VIKOR.

First, AHP is adopted to determine the relative importance of each criterion. Its structured pairwise comparison methodology provides a transparent and mathematically consistent approach to deriving the criteria weights (Y. Chen et al., 2013). Following the weight definition by AHP, both TOPSIS and VIKOR are applied to rank the GHCs based on the performance against the weighted criteria. It is important to note that TOPSIS and VIKOR have different methodological focuses. Specifically, TOPSIS aims to find the ideal solution by selecting the alternative that is geometrically closest to the best theoretical performance (Hwang & Yoon, 1981). This approach is valuable for decision-makers aiming to identify a carrier which excels on key metrics. In contrast, VIKOR is designed to find a compromise solution by focusing on minimising the regret in some criteria (San Cristóbal, 2011). This method is valuable for stakeholders seeking a balanced carrier that avoids significant underperformance in any single criterion. The combination of these methods ensures a comprehensive and clear rankings that reflect the carriers' overall suitability for the project, based on stakeholders' strategic priority. The details of MCDM implementation are explained in the following sections.

6.3.4.1 Criteria weighting with AHP

The AHP is a structured decision-making method that relies on pairwise comparisons to derive criteria weights, thereby reflecting the criteria's significance in the overall

decision (Y. Chen et al., 2013). It works by comparing criteria in pairs to establish priority rankings, assigning weightings based on their significance to the overall decision. Thereby, a hierarchical structure is first established, with the goal (i.e., evaluating GHCs) at the top level, the five criteria at the intermediate level, and the set of carrier options at the bottom. Each pairwise comparison quantifies how strongly one criterion is preferred over another, generating a comparison matrix whose elements a_{ij} capture the perceived importance of criterion i relative to criterion j. The matrix is then normalised, and its principal eigenvector is extracted to yield the criteria weights. These weights are checked for logical consistency using the Consistency Index (CI) and Consistency Ratio (CR) (Y. Chen et al., 2013). When CR values fall below 0.1, the matrix is deemed consistent. If the matrix fails the test, pairwise judgments would be revisited or revised to minimise subjectivity and bias. By consolidating expert inputs, project objectives, and technical requirements, AHP ensures that each criterion's weight corresponds to its true relevance in evaluating hydrogen carriers. The resulting weights will inform the evaluation stage with TOPSIS and VIKOR.

6.3.4.2 TOPSIS evaluation

TOPSIS is used to rank the GHCs by evaluating their proximity to both the ideal and worst solutions across multiple criteria (S.-J. Chen & Hwang, 1992; Hwang & Yoon, 1981). First, the decision matrix is normalised to eliminate unit dependence between the criteria. The normalised value r_{ij} is calculated as Eq. (6.7):

$$r_{ij} = \frac{x_{ij}}{\sqrt{\sum_{i=1}^{m} x_{ij}^2}} \tag{6.7}$$

where x_{ij} is the performance value of the i-th alternative for the j-th criterion. Then, weighted normalisation can be calculated with the normalized values r_{ij} which are multiplied by their respective weights w_j derived from AHP:

$$v_{ij} = w_j \cdot r_{ij} \tag{6.8}$$

Distance calculation is based on the Euclidean distance of each alternative from the ideal solution (A^+) and the worst solution (A^-):

$$D_i^+ = \sqrt{\sum_{j=1}^{n}\left(v_{ij} - v_j^+\right)^2}, D_i^- = \sqrt{\sum_{j=1}^{n}\left(v_{ij} - v_j^-\right)^2} \quad (6.9)$$

The distances, D_i^+ and D_i^-, are calculated using the weighted normalized values v_{ij} for each criterion. The ideal solution (v_j^+) is composed of the highest scores for all criteria, while the worst solution (v_j^-) is composed of the lowest scores. The distance calculations help measure how close each alternative iii is to the best or worst possible performance based on v_{ij}. Relative closeness to the ideal solution is calculated to rank the alternatives:

$$C_i^* = \frac{D_i^-}{D_i^+ + D_i^-} \quad (6.10)$$

The higher the C_i^*, the closer the hydrogen carrier is to the ideal solution. TOPSIS offers a balanced evaluation by considering both the ideal and worst scenarios, allowing for a robust ranking of alternatives. The method is suitable for complex decision-making problems, making it an ideal tool for evaluating GHCs based on diverse criteria. The application of TOPSIS in GHCs evaluation framework ensures that the ranking of carriers reflects their overall performance across all criteria, providing a clear path for selecting the most suitable carrier for hydrogen transport.

6.3.4.3 VIKOR evaluation

VIKOR is also an MCDM tool, but with a different focus than TOPSIS (San Cristóbal, 2011). While TOPSIS evaluates alternatives based on their distance from ideal and worst solutions, VIKOR emphasizes finding a compromise solution by balancing overall performance (utility) and the worst performance in any criterion (regret). This method is particularly valuable when criteria are conflicting, allowing for a more nuanced ranking by balancing the maximum group utility and individual regrets. For the utility (S), VIKOR calculates the overall utility of each hydrogen carrier based on its performance across all criteria, as follows:

$$S_i = \sum_{j=1}^{n} w_j \cdot \frac{f_j^* - f_{ij}}{f_j^* - f_j^-} \tag{6.11}$$

where f_j^* and f_j^- are the best and worst values for each criterion, respectively, and f_{ij} is the score of carrier i for criterion j. Regarding the regret (R), this captures the maximum regret for each alternative, calculated as:

$$R_i = \max_j \left[w_j \cdot \frac{f_j^* - f_{ij}}{f_j^* - f_j^-} \right] \tag{6.12}$$

Then, the final VIKOR score Q_i is calculated as:

$$\mathrm{Q}_i = v \cdot \frac{\mathrm{S_i} - \mathrm{S}^*}{\mathrm{S}^- - \mathrm{S}^*} + (1 - v) \cdot \frac{R_\mathrm{i} - R^*}{R^- - R^*} \tag{6.13}$$

where v is the weight assigned to utility, typically 0.5 in a balanced context. S^* and R^* are the best values for utility and regret. S^- and $R^-$and worst values for utility and regret.

VIKOR offers an advantage by accounting for compromises between conflicting criteria, such as balancing economic performance with environmental impacts. It evaluates not only the overall performance but also considers the carriers that might avoid extreme shortcomings in any single criterion (regret).

6.4 Case study

This section presents the assumptions and data input for an unexamined green hydrogen transportation case study from Port Elizabeth, South Africa, to the Thames Estuary, United Kingdom (UK). The green hydrogen project is assumed to commence in 2030 to supply 1 million tons of green hydrogen annually to the UK. Section 6.4.1 summarises the data input for techno-economic analysis, and Section 6.4.2 summarises the life cycle inventory for the LCA model, which also includes the data input for carrier efficiency analysis.

6.4.1 Techno-economic analysis data input

Table 6-1 shows the key economic parameters for all GHC supply pathways. The project is assumed to have a lifetime of 20 years. The annual operation is assumed to

be 330 days. The hydrogen sale price in the UK is assumed to be £8 $kg^{-1}H_2$ (Burgess, 2023). The chapter assumes that the project is entirely equity financed, and the techno-economic calculations are converted to USD using the conversion rates listed in Table 6-1. The following subsections summarise the techno-economic assumptions of green hydrogen production, GHC conversion/reconversion, and maritime transportation. In the base case assumption, the green hydrogen is generated by renewable wind electricity in South Africa. For the base case scenario, all electricity required for GHC conversion and reconversion processes is assumed to be sourced from the respective national grids at the prices listed in Table 6-1.

Table 6-1 South Africa-UK case study economic assumptions

Parameter	Value	Reference
Project lifetime (years)	20	Own assumption
Annual operation (days)	330	Own assumption
Hydrogen sale price (USD/kg)	10	(Burgess, 2023)
Inflation rate (%)	2.5%	(Office for National Statistics, 2025)
Cost of equity (%)	10%	(Mann, 2024)
ZAR/USD	0.053	(South Africa Reserve Bank, 2024)
GBP/USD	1.25	(South Africa Reserve Bank, 2024)
EUR/USD	1.04	(European Central Bank, 2024)
South Africa wind electricity (USD/MWh)	59.5	(IEA, 2022)
South Africa grid electricity (Rand/MWh)	3000	Own assumption
UK wind electricity (£/MWh)	39	(DESNZ, 2023a)
UK grid electricity (£/MWh)	90	Own assumption
UK heat source (£/MWh)	40	Own assumption

6.4.1.1 Green hydrogen production

The case study models green hydrogen production using the Polymer Electrolyte Membrane (PEM) water electrolysis powered by onshore wind. The PEM technology is selected due to its high operational flexibility, which is crucial for coupling with intermittent renewable energy sources, such as wind farms (Giampieri et al., 2024; Patel et al., 2022). The choice of onshore wind is based on South Africa's abundance of wind sources, particularly in Port Elizabeth (Rehman et al., 2022). Table 6-2 summarises the key assumptions for this production pathway. The CAPEX is obtained from the PEM cost prediction for 2030 (Reksten et al., 2022). The OPEX is expressed as a percentage

of initial CAPEX, where OPEX includes stack replacement, maintenance, and labour (Song et al., 2021).

The efficiency of the PEM system is assumed to be 60% (Bareiß et al., 2019). This resulted in an electricity consumption of 55.5 kWh to produce 1 kg of green hydrogen at the lower heating value (LHV). The capacity factory is assumed to be 40% for the onshore wind farm near Port Elizabeth. To meet the annual delivery of 1 million tons of green hydrogen, the rated installed capacity of the PEM electrolyser is approximately 17.5 GW. The cost of green electricity is modelled using the projected levelised cost of energy (LCOE) for South Africa's onshore wind in 2030, as shown in Table 6-1. It is also assumed that the distance between the green hydrogen plant and the hydrogen carrier production facility is 10 km. The hydrogen pipeline is assumed to be a distribution pipeline, as it is shorter and operates at a lower pressure than transmission pipelines (Wulf et al., 2018). The hydrogen distribution pipeline requires a CAPEX of 2.6 million USD and a 3% annual OPEX (Ortiz Cebolla et al., 2022).

Table 6-2 PEM production assumptions in South Africa

Parameter	Value	Reference
CAPEX $/kW	900	(Reksten et al., 2022)
OPEX	4%	(Ortiz Cebolla et al., 2022)
PEM system efficiency	60%	(Peterson et al., 2020)
Capacity factor	40%	Own assumption

6.4.1.2 Carrier conversion and reconversion

The techno-economic assumptions for the carrier conversion and reconversion stage are summarised in Table 6-3. The CAPEX includes the fixed plant and equipment for converting and reconverting GHCs, and in the case of NH3 and MeOH, the CAPEX data also include the capital costs for ASU and DAC facilities. The CAPEX data have been normalised to the unit capacity of plants. It should be noted that DBT and TOL can be re-hydrogenated in the exporting countries after the unloaded carrier is transported back to the exporting country. The initial purchase of carrier inventory is treated as an upfront cost, which includes 993,000 tons of DBT and 980,000 tons of TOL. The prices for the carriers are assumed to be 3.12 USD/kg for DBT and 0.88 USD/kg for TOL.

The complete derivation, including reference plant data, scaling calculations, and detailed energy consumption sources, is provided in the **Appendix A1: Detailed techno-economic data and assumptions**.

Table 6-3 GHC conversion and reconversion assumptions

	LH_2	NH_3	MeOH	DBT	TOL
Conversion					
Normalised unit CAPEX [$/(kg carrier/h)]	34,786.75 [$/(kg$H_2$/h)]	2,566.19 [$/(kg$NH_3$/h)]	2536.83 [$/(kgMeOH/h)]	445.6 [$/(kgH18-DBT/h)]	604.2 [$/(kgMCH/h)]
Electricity demand [kWh/kg GHC]	7	1.49	1.11	0.068	0.071
Heat demand [kWh/kg GHC]	0	0	1.5	0	0
OPEX (% of CAPEX)	3%	3%	3%	4%	4%
Reconversion					
Normalised unit CAPEX [$/(kg carrier/h)]	119.79 [$/(kg$H_2$/h)]	7,335.81 [$/(kg$H_2$/h)]	4,661.85 [$/(kg$H_2$/h)]	14,428.71 [$/(kg$H_2$/h)]	15,029.90 [$/(kg$H_2$/h)]
Electricity demand (kWh/kg H_2)	0.2	7	0.5	1.12	1.13
Heat demand (kWh/kg H_2)	0	0	0	9.79	10.25
OPEX (% of CAPEX)	2%	3%	3%	4%	4%
Reference	(Connelly et al., 2019; Heuser et al., 2019; IEA, 2020; IRENA, 2022; Restelli et al., 2024)	(IRENA, 2022; Nielsen & Topsoe, 2021; Ortiz Cebolla et al., 2022)	(Bos et al., 2020; Ortiz Cebolla et al., 2022; Papadias et al., 2019; Terlouw et al., 2021)	(Cho et al., 2024; IRENA, 2022; Niermann et al., 2021; Raab et al., 2021)	(Cho et al., 2024; IRENA, 2022; Niermann et al., 2021; Raab et al., 2021)

6.4.1.3 Maritime transportation

Table 6-4 shows the storage and shipping assumptions for the five GHCs. The maritime transport distance is assumed to be 14149 km from Port Elizabeth, South Africa, to the Thames Estuary, UK. In terms of the storage capacity, the storage capacity is determined by the maximum of two values: 1) the size of a single ship and 2) one week of equivalent production (IRENA, 2022). Additionally, the number of ships required for the GHC supply chain is determined based on ship capacity, speed, and project volumes. It is worth noting that the port infrastructure requires upgrading due to the cryogenic temperature requirements of LH_2. The CAPEX for the port upgrade is 52 million USD for both export and import ports (Raab et al., 2021). Losses during

transportation are accounted for based on the physical properties of GHCs. For carriers requiring cryogenic or refrigerated storage (LH_2 and NH_3), daily boil-off losses are assumed (Kawasaki, 2020; J. Kim et al., 2022). For the ambient liquid carriers (MeOH, DBT, and TOL), which utilise existing petrochemical infrastructure with steel tanks, a fixed material handling loss of 0.2% per cycle is adopted (Niermann et al., 2021). Additionally, a 1.2% loss for loading and unloading is considered for the LH_2 pathway, accounting for gasification caused by unavoidable temperature fluctuations during transfer (IRENA, 2022; Wijayanta et al., 2019).

Table 6-4 Storage and shipping assumptions for South Africa-UK case study

	LH_2	NH_3	MeOH	DBT	TOL
Storage					
Capacity (t)	25,200	130,000	149,000	340,400	340,400
Storage cost ($/t)	26000	2600	1050	275	275
Storage loss	0.10% day^{-1} (boil-off)	0.04% day^{-1} (boil-off)	no loss	no loss	no loss
OPEX (% of CAPEX)	2%	2%	2%	2%	2%
Reference	(Dickson et al., 2022; Kawasaki, 2020; Song et al., 2021)	(J. Kim et al., 2022; Song et al., 2021)	(Ortiz Cebolla et al., 2022)	(Ortiz Cebolla et al., 2022)	(Ortiz Cebolla et al., 2022)
Shipping					
Ship capacity (t)	11,000	52,000	52,560	110,000	110,000
CAPEX per ship (M$)	412	76	51	76	76
Average Speed (km/h)	30	30	30	30	30
Shipping loss (mechanism)	0.10% day^{-1} (boil-off)	0.04% day^{-1} (boil-off)	0.2% $cycle^{-1}$ (handling)	0.2% $cycle^{-1}$ (handling)	0.2% $cycle^{-1}$ (handling)
Load/unload time (day)	2	2	2	2	2
OPEX (% of CAPEX)	4%	4%	4%	4%	4%
Reference	(IEA, 2020; Kawasaki, 2020; Lee et al., 2022)	(IEA, 2020; J. Kim et al., 2022)	(Dickson et al., 2022; Niermann et al., 2021)	(IEA, 2020; Niermann et al., 2021)	(IEA, 2020; Niermann et al., 2021)

6.4.2 LCA modelling framework

The system boundary of the LCA model follows the definition in Figure 6-1, where South Africa is the exporting country, and the UK is the importing country. The functional unit of the LCA model is the delivery of 1 kg of green hydrogen at the Thames Estuary, UK at 99.9% purity in 2030. The background LCA processes, which are the processes outside the system boundary, are obtained with the Ecoinvent 3.10 database (Wernet et al., 2016). The foreground processes, which represent the core technological components of each GHC pathway, are modelled using life cycle inventory data from related literature and industry reports. In addition, it should be noted that the environmental impacts related to business travel and employee commuting are not considered in this life cycle inventory analysis, as guided by the IPHE guidelines (IPHE, 2023). The base case assumes that all electricity for carrier conversion and reconversion is supplied by the respective national grid. The 2030 electricity grid mixes for South Africa and the UK are based on (DESNZ, 2023b; IEA, 2024). A complete and detailed LCI for all unit processes is provided in **Appendix A2: Life Cycle Inventories**.

6.4.3 Application of MCDM framework

AHP is employed as the first step in the MCDM model. As mentioned in Section 6.3.4.1, its core strength lies in converting subjective comparisons into a structured pairwise matrix, thus yielding transparent and mathematically consistent weights. Table 6-5 below presents the pairwise comparison matrix constructed for the five criteria: LCOH, IRR, GWP, ReCiPe endpoint, and Carrier efficiency. Saaty's fundamental 1-9 scale is adopted to capture the relative importance of each criterion in the context of exporting hydrogen from South Africa to the UK (Saaty, 1987). By using AHP, these subjective views are systematically converted into numerical values, thereby clarifying the influence of each criterion on the final decision.

Table 6-5 AHP Pairwise comparison matrix for the five considered criteria

Criteria	LCOH	IRR	GWP	ReCiPe endpoint	Carrier Efficiency
LCOH	1	3	1	3	2
IRR	1/3	1	1/3	1/2	1/3

GWP100	1	3	1	3	1
ReCiPe endpoint	1/3	2	1/3	1	½
Carrier Efficiency	1/2	3	1	2	1

Based on the established AHP procedure, the comparison matrix is normalised, and the principal eigenvector is extracted to yield the final weights for each criterion. Then, a consistency check is performed by calculating the Consistency Ratio (CR) to ensure logical coherence among pairwise comparisons. The CR of the proposed pairwise comparisons is 0.02, which satisfies the below 0.1 requirements, and the resulting weights are validated (Saaty, 1987).

Figure 6-3 presents a radar chart illustrating the relative weights calculated by the AHP method for the LCOH, IRR, GWP, ReCiPe, and Carrier Efficiency. Each axis represents one criterion, and the numeric scale (0 to 0.40) indicates the weight assigned to the criterion. Larger values indicate a higher relative importance of that criterion.

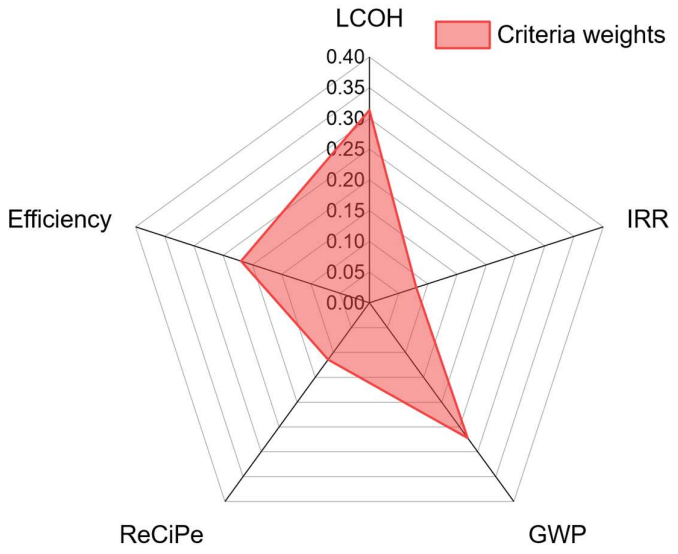

Figure 6-3 Radar chart illustrating the AHP weights of the five criteria.

It is essential to note that these weights are scenario-specific and are influenced by expert assessments of South Africa's hydrogen supply chain conditions to the UK. Different stakeholders or geographical contexts could yield distinct weight distributions, as priorities vary based on policy objectives, resource availability, and market structures. For instance, a region with more stringent environmental regulations might assign

substantially greater weight to GWP and ReCiPe. In contrast, a financially constrained project might emphasise LCOH and IRR to a larger degree.

Nevertheless, the AHP methodology provides a transparent mechanism for incorporating such subjectivity consistently and rigorously. By translating qualitative preferences into quantitative comparisons, the approach enables a clear justification for why certain criteria carry more weight than others in the final decision. The resulting weights serve as the input for the TOPSIS and VIKOR analyses in Section 6.5.4. This integrated and multi-criteria framework thus aligns with structured decision-making in energy and sustainability contexts.

6.5 Results and discussion

This section presents the criteria and MCDM results for the five GHCs. It includes techno-economic analysis results, life cycle impact assessments, and carrier efficiency. Section 6.5.5 presents the sensitivity analysis of the MCDM ranking based on the criteria results.

6.5.1 Techno-economic analysis results

Figure 6-4 compares the LCOH with the five GHCs. In all delivery pathways, the cost of hydrogen feedstock constitutes the most significant cost element. This reveals that hydrogen production remains a critical factor in determining overall carrier economics. Under the base case assumption, TOL demonstrates the most cost-effective route with an estimated total LCOH of \$7.07 $kg^{-1}H_2$, with MeOH and DBT ranking next. The NH_3 pathway shows a noticeably higher reconversion cost compared to the previous three pathways due to the energy-intensive ammonia cracking process. The LH_2 pathway has the highest carrier conversion cost for liquefaction (\$1.79 $kg^{-1}H_2$) and partially in the elevated transport and storage costs required to maintain cryogenic conditions. While LH_2 benefits from the lowest reconversion costs, it has the highest LCOH of \$8.16 $kg^{-1}H_2$.

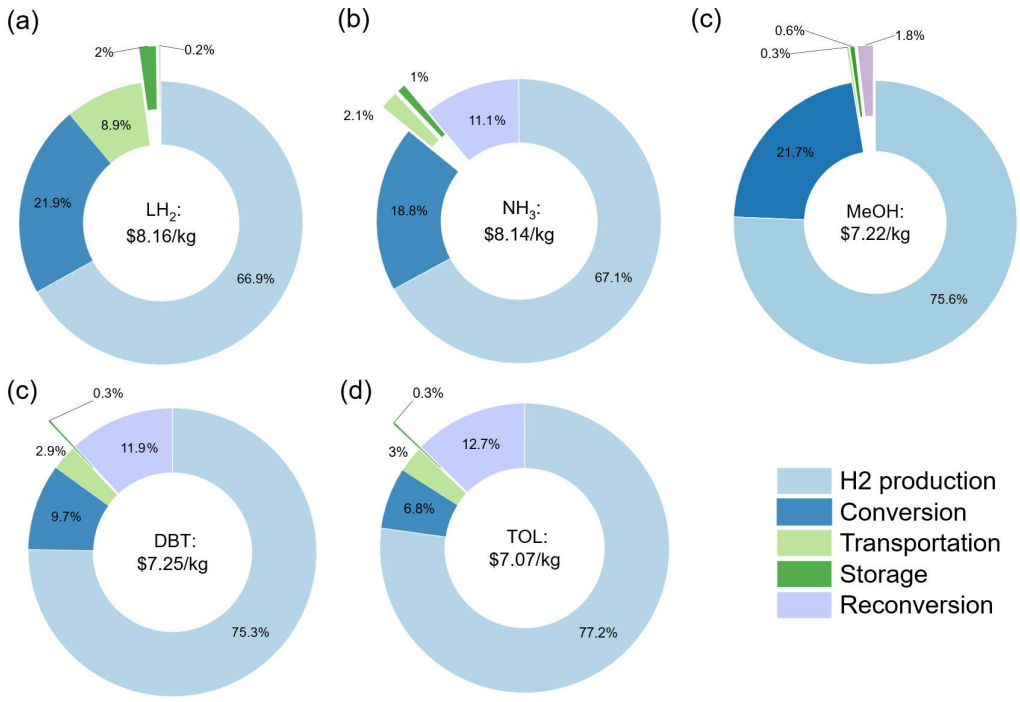

Figure 6-4 Breakdown of LCOH for the five GHC pathways: (a) LH2, (b) NH3, (c) MeOH, (d) DBT, and (e) TOL. The percentages represent the contribution of each stage to the total costs.

To contextualise the LCOH results, the imported carrier is benchmarked against on-site green hydrogen production in the UK. With data from the UK's National Energy System Operator (NESO), the LCOH of on-site production of a 2030 project using PEM electrolysers with a 10% discount factor can be estimated. Under the assumptions of a 40% capacity factor and a wind electricity price of £39/MWh, the projected domestic LCOH price is approximately £5.7 $kg^{-1}H_2$ (NESO, 2025). This is equivalent to \$7.13 $kg^{-1}H_2$ at the exchange rate assumption of £1=\$1.25.

This comparison reveals that the most economically viable pathway, TOL at \$7.07 $kg^{-1}H_2$, is cost-competitive with projected domestic UK production under the stated assumptions. In addition, other GHC pathways, such as MeOH (\$7.22 $kg^{-1}H_2$) and DBT (\$7.25 $kg^{-1}H_2$) could also be cost-competitive, providing further cost reductions of green hydrogen production in South Africa. This suggests that for the UK, importing green hydrogen from regions with superior renewable resources, like South Africa, could be an economically sound strategy to complement domestic production.

Table 6-6 shows the IRR results of the five GHCs under the base case assumptions. According to the table, MeOH exhibits the highest IRR (23.90%), followed by TOL (23.13%), DBT (21.18%), NH_3 (18.24%), and LH_2 (15.59%). MeOH's high IRR is due to the relatively low combined conversion/reconversion and transport costs. Although DBT and TOL have higher reconversion costs than MeOH, their lower conversion CAPEX and shipping benefits still yield healthy cash-flow profiles. NH_3's IRR of 18.2 % is lowered by the energy-intensive cracking step. LH_2 has the lowest IRR due to high liquefaction, transport, and storage costs.

Table 6-6 IRR of the five GHCs

	LH_2	NH_3	MeOH	DBT	TOL
IRR	15.59%	18.24%	23.90%	21.18%	23.13%

6.5.2 Life cycle impact assessment

The life cycle impacts were calculated using SimaPro 9.6, with results presented for both the IPCC GWP100 and ReCiPe endpoint method. Figure 6-5 breaks down the GWP results for the five carriers by supply chain stage: green H_2 production, carrier conversion, maritime transport, and carrier reconversion. The analysis reveals that the GWP of each carrier is directly linked to its fundamental chemistry and process energy requirements.

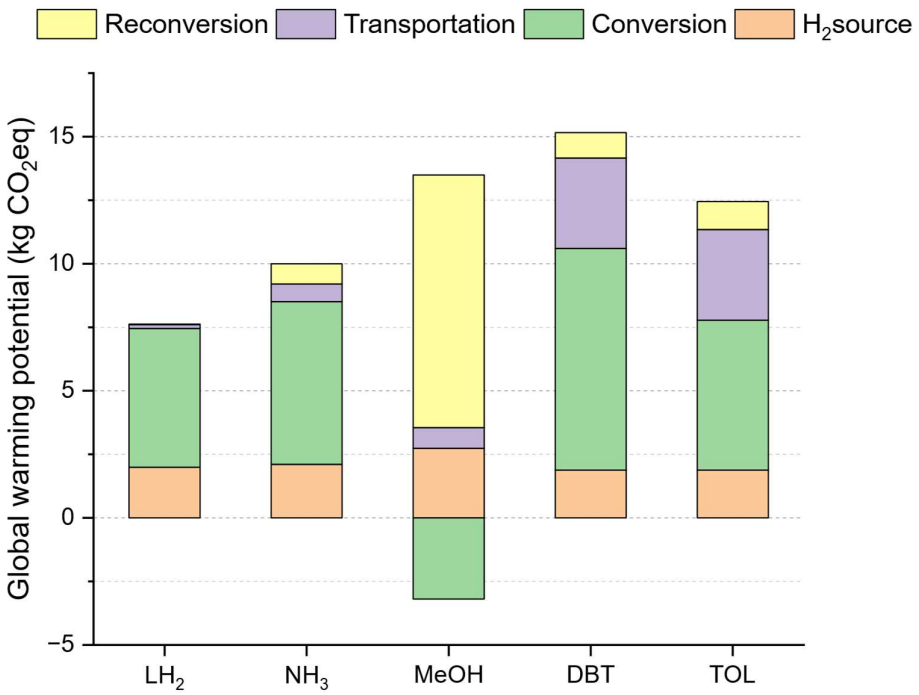

Figure 6-5 GWP100 results from green hydrogen supply from South Africa to the UK with liquid hydrogen, ammonia, methanol, DBT, and TOL.

LH_2 exhibits the lowest GWP (7.62 kg CO_2eq) among the five GHC pathways. The analysis shows that the electricity required for the cryogenic liquefaction process in South Africa is the primary contributor (5.42 kg CO_2eq), which accounts for over 71% of the total GWP. The hydrogen production contributes another 1.99 kg CO_2eq, while shipping and regasification have minimal impact. NH_3 have the second lowest GWP of 9.91 kg CO_2eq. The dominant GWP contributions are from the electricity used in South Africa for nitrogen production via the ASU (3.96 kg CO_2eq) and Haber-Bosch synthesis process (2.44 kg CO_2eq). The significant impact of electricity usage in South Africa reveals the critical role of the exporting country's grid decarbonisation in reducing the overall GWP of the green hydrogen supply chain. The effect of a greener grid and fully renewable energy supply is therefore investigated further in the sensitivity analysis in Section 6.5.5.

MeOH exhibits a mid-range GWP, for which carbon capture by DAC provides a net credit of 4.84 kg CO_2eq, after accounting for the energy consumed during capture and synthesis. The captured CO_2 is re-emitted when the fuel is reformed back to hydrogen, resulting in a total GWP of 10.3 kg CO_2eq kg. TOL and DBT have the highest carbon footprint (12.4 and 15.2 kg CO_2eq, respectively), due to the following reasons. First,

the LOHCs' impact needs to account for the life cycle impacts of producing the initial batch of the organic carrier itself and the markup for the dehydrogenation losses. Second, the dehydrogenation process of LOHCs is endothermic and requires heat supplies in the UK, adding 0.93 and 0.88 kg CO_2eq, respectively, at the destination port. Finally, as the unloaded LOHCs must be shipped back to South Africa, the round-trip maritime transportation contributes 3.57 and 3.56 kg CO_2eq, respectively, to the total GWP.

To validate the LCA model results, the GWP results are compared with recent publications on international green hydrogen carrier supply chains. While specific assumptions regarding system definitions (such as shipping distance and energy supply) and impact assessment methods may vary slightly, the functional unit of 1 kg of delivered hydrogen is consistent, enabling a direct comparison.

The result for the LH_2 (7.62 kg CO_2eq) pathway is higher than the 3.8 kg CO_2eq reported by Lee et al, (2022). This difference is expected and can be attributed to their assumption of a fully renewable energy system in a 2050 scenario, whereas our base case models a partially decarbonised 2030 grid. The high GWP for TOL (12.4 kg CO_2eq) and DBT (15.2 kg CO_2eq) is consistent with broader literature, which identifies LOHCs as having the highest environmental impacts among common carriers (Dickson et al., 2022; Noh et al., 2023a). However, it is important to note that using renewable and biomass-derived TOL and DBT can lower the GWP to 10.21 to 10.61 kg CO_2eq for 11,000 km marine transport (Cho et al., 2024). Overall, the GWP results and relative performance of carriers are consistent with the findings of a recent publication.

Beyond global warming, the ReCiPe endpoint method was used to assess a broader range of environmental impacts with a single score, which includes three areas of protection: human health, ecosystems, and resource availability (Huijbregts et al., 2017). Figure 6-6 compares the ReCiPe endpoint results of the five GHCS across the three areas of protection. Among the carriers, LH_2 has the smallest aggregated impact at 0.77 Pt $kg^{-1}H_2$, followed by TOL (0.97 Pt $kg^{-1}H_2$) and NH_3 (0.99 Pt $kg^{-1}H_2$), MeOH (1.11 Pt $kg^{-1}H_2$) and DBT (1.20 Pt $kg^{-1}H_2$). The ReCiPe results show that the aggregated environmental damage score is primarily driven by impacts on human health for all GHCs. The human health endpoint score is calculated by summing the damages of all midpoint categories that can affect human health, as measured in Disability-Adjusted

Life Years (DALY). In particular, Fine Particulate Matter Formation (FPMF) and Human Carcinogenic Toxicity (HCT) are the two main contributors to human health damage, surpassing the global warming potential for all GHC pathways. The full details of ReCiPe results are provided in **Appendix A3 ReCiPe impacts**.

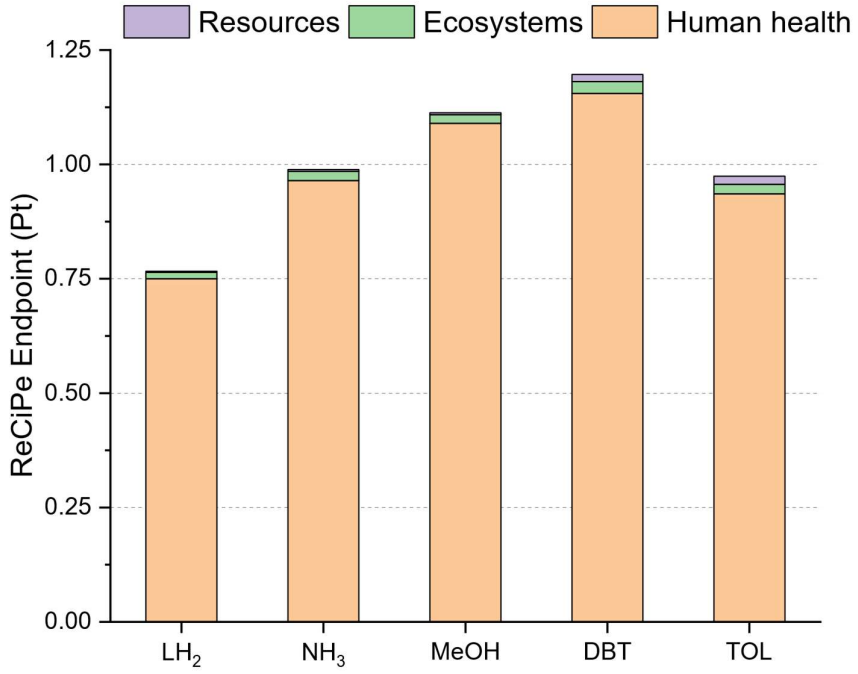

Figure 6-6 ReCiPe endpoint on three areas of protection by the five GHCs.

The FPMF are primarily linked to the energy consumption and maritime transportation. For the LH_2 and NH_3 pathways, the dominant contributor is the process electricity consumption in South Africa for carrier conversion. Specifically, the electricity consumption accounts for 74% of fine particulate matter impact for LH_2 and 59% for NH_3, as shown in Table 6-7. For the LOHC, the impact is driven by the maritime transport, responsible for 46% and 62% of the impact for DBT and TOL, respectively.

Table 6-7 Top process contributions to key midpoint impacts

Carrier	Rank	Contributing Process	Impact Disability-Adjusted Life Years (DALY)	Contribution
Impact category: Fine particulate matter formation				
LH_2	1	Electricity, medium voltage {ZA} -2030	9.41E-06	74%

	2	Wind turbine, onshore {GLO}	2.31E-06	18%
NH_3	1	Electricity, medium voltage {ZA} - 2030	1.04E-05	59%
	2	Wind turbine, onshore {GLO}	2.49E-06	14%
MeOH	1	Electricity, medium voltage {ZA} - 2030	1.00E-05	55%
	2	Wind turbine, onshore {GLO}	3.16E-06	17%
DBT	1	Transport, freight, sea, tanker for liquid goods other than petroleum and liquefied natural gas {GLO}	1.23E-05	46%
	2	Electricity, medium voltage {ZA} - 2030	7.21E-06	27%
TOL	1	Transport, freight, sea, tanker for liquid goods other than petroleum and liquefied natural gas {GLO}	1.23E-05	62%
	2	Toluene production, liquid - 2030 {ZA}	3.11E-06	16%
Impact category: Human carcinogenic toxicity				
LH_2	1	Wind turbine, onshore {GLO}	1.69E-05	79%
	2	Electricity, high voltage {ZA}	4.28E-06	20%
NH_3	1	Wind turbine, onshore {GLO}	1.82E-05	71%
	2	Electricity, medium voltage {ZA} - 2030	4.78E-06	19%
MeOH	1	Wind turbine, onshore {GLO}	2.31E-05	73%
	2	Electricity, medium voltage {ZA} - 2030	4.59E-06	14%
DBT	1	Wind turbine, onshore {GLO}	1.59E-05	65%
	2	Electricity, medium voltage {ZA} - 2030	3.28E-06	13%
TOL	1	Wind turbine, onshore {GLO}	1.57E-05	72%
	2	Toluene production, liquid	2.90E-06	13%

In contrast, the HCT category is not driven by the operation, but by the upstream infrastructure processes. For each carrier, the most extensive contributing process is the wind turbine infrastructure, which accounts for 79% of the impact for LH_2, 71% for NH_3, 73% for MeOH, 65% for DBT, and 72% for TOL. This indicates that the materials required to build wind farms are the primary sources of carcinogenic impacts in this case study. Overall, the ReCiPe provides critical insights into the broader environmental impacts beyond global warming potential, identifying the key demanding processes including energy consumption, maritime transportation, and wind turbine infrastructure.

6.5.3 Carrier efficiency

Table 6-8 shows that LH_2 achieves the highest efficiency at 77.62%, because this pathway does not require any chemical conversion steps after the liquefaction stage. NH_3 has the second-highest carrier efficiency of 70.05%. MeOH, DBT, and TOL cluster near 63%, reflecting the high energy requirements for hydrogenation and dehydrogenation of carbon-based hydrogen carriers. Overall, these efficiencies capture the extent of energy penalties arising from liquefaction, synthesis, hydrogenation/dehydrogenation, and storage constraints, highlighting LH_2's advantage in retaining a larger fraction of the initial energy content despite the high cost of cryogenic processes.

Table 6-8 Carrier efficiency results of the five GHCs

Carrier	LH_2	NH_3	MeOH	DBT	TOL
Carrier efficiency η	77.62%	70.05%	63.57%	63.27%	63.45%

6.5.4 MCDM ranking

The results in Sections 6.5.1 to 6.5.3 show that no single hydrogen carrier achieves the best performance in terms of economic, environmental, and efficiency simultaneously. As a result, the application of MCDM offers insights and decision support for choosing the appropriate hydrogen carrier. Table 6-9 presents the final rankings of the five hydrogen carriers (LH_2, NH_3, MeOH, DBT, and TOL) based on the AHP-derived weights and the subsequent evaluations using TOPSIS and VIKOR. As discussed in Sections 6.3.4.2 and 6.3.4.3, the higher TOPSIS score and the lower VIKOR score demonstrate better performance, respectively. The utility weight v is set to 0.5 for AHP-VIKOR method.

As shown in Table 6-9, the two MCDM methods yield different top rankings. The AHP-TOPSIS method, which identifies the alternative closest to an ideal solution, ranks LH_2 first with a score of 0.78. This is because LH_2 performs best in three of the five criteria (GWP, ReCiPe, and Efficiency), making it the technically ideal choice. It is followed by NH_3 (0.61), MeOH (0.59), TOL (0.40), and DBT (0.17).

Table 6-9 AHP-TOPSIS and AHP-VIKOR results of the five GHCs

	LH_2	NH_3	MeOH	DBT	TOL
AHP-TOPSIS score	0.78	0.61	0.59	0.17	0.40
AHP-TOPSIS ranking	1	2	3	5	4
AHP-VIKOR score	0.50	0.84	0.09	0.79	0.12
AHP-VIKOR ranking	3	5	1	4	2

The AHP-VIKOR method focuses on finding a compromise candidate option that has a balanced overall performance and minimises the worst criterion regret. MeOH ranks first with the lowest Q value of 0.09. Its good economic performance (LCOH and IRR) combined with moderate environmental impacts makes it the most balanced choice. It is followed by TOL (0.11), which also demonstrates a strong compromise profile. LH_2's high LCOH increases the regret in this criterion and then makes LH_2 rank third in the AHP-VIKOR method. NH_3 drops from second place in AHP-TOPSIS to fifth place in the AHP-VIKOR method with a score of 0.84. It indicates that the high reconversion costs and low IRR create regret that outweighs good environmental and efficiency performance. It should be noted that the MCDM ranking results are based on the base case assumption of the economic and environmental parameters. The parameters may change due to project assumptions, which can alter the MCDM ranking results. The following section presents a sensitivity analysis on seven alternative cases for South Africa compared to the UK case study.

6.5.5 Sensitivity analysis on the MCDM results

An additional sensitivity analysis was conducted to understand how changes in the parameter inputs could affect the MCMD ranking of the GHCs, as shown in Table 6-10. Case 0 serves as the base case in this chapter, utilising the economic assumptions outlined in Tables 6-1 and 6-2, and incorporating electricity for carrier conversion/reconversion based on electricity grid mix projections for 2030, as detailed in (DESNZ, 2023b; IEA, 2024). Cases 1 and 2 investigate the sensitivities of results by the capacity factor assumption in the green hydrogen production, compared with the base case capacity factor of 40%. Cases 3 and 4 investigate the changes in the utility prices, which include the grid electricity price in South Africa (3000 Rand/MWh) and the UK (£ 90/MWh), as well as the heat prices in the UK (£ 40/MWh). Cases 5 and 6

investigate how the electricity grid decarbonisation in 2035 and 2040 will affect the MCDM ranking, with country-specific projections of the electricity grid mix (DESNZ, 2023b; IEA, 2024). Case 7 investigated the MCDM results with the process energy from renewable wind.

Table 6-10 Sensitivity analysis cases for the five GHC pathways

	Parameter varied	Changes applied		Parameter varied	Changes applied
Case 0	Base case	-	Case 4	Utility prices	-20%
Case 1	Capacity factor	+20%	Case 5	Process energy	Grid mix, 2035
Case 2	Capacity factor	-20%	Case 6	Process energy	Grid mix, 2040
Case 3	Utility prices	+20%	Case 7	Process energy	Wind

The details of the criteria results and MCDM scores of sensitivity analysis are shown in the **Appendix A4**. Table 6-11 demonstrates carrier ranking results from the sensitivity analysis. The AHP-VIKOR method is responsive to the alternative case assumptions. Because it penalises carriers on the single worst criterion (regret). In the base case (Case 0), MeOH is ranked first, establishing it as the best initial compromise solution. This top ranking is reinforced in other scenarios where economic factors are the primary driver, such as variations in the capacity factor (Cases 1 and 2) and lower utility prices (Case 4).

Table 6-11 Sensitivity analysis results of AHP-TOPSIS and AHP-VIKOR

	AHP-TOPSIS					AHP-VIKOR				
	LH_2	NH_3	MeOH	DBT	TOL	LH_2	NH_3	MeOH	DBT	TOL
Case 0	1	2	3	5	4	3	5	1	4	2
Case 1	1	2	3	5	4	3	5	1	4	2
Case 2	1	2	3	5	4	3	5	1	4	2
Case 3	1	2	3	5	4	3	5	2	4	1
Case 4	1	2	3	5	4	4	3	1	5	2
Case 5	1	2	3	5	4	4	1	2	5	3

Case 6	1	2	3	5	4	4	1	2	5	3
Case 7	1	2	3	5	4	3	1	2	5	4

In contrast, the AHP-TOPSIS rankings demonstrate robustness across all scenarios. LH_2 consistently ranks first, maintaining its position as the ideal solution regardless of variations in capacity factor, utility prices, or grid carbon intensity. The robustness stems from LH_2's good performance in three of the five criteria: GWP, ReCiPe, and Efficiency. Similarly, the rankings for the other carriers remain unchanged across all cases, with NH_3 at second, MeOH at third, TOL at fourth, and DBT at fifth under the case study assumptions. Therefore, AHP-TOPSIS provides a stable and consistent recommendation, which can be a suitable method for long-term decision-making, such as energy infrastructure decisions.

The sensitivity analysis also reveals a critical change as the energy system decarbonises. NH_3's position as the best compromise solution strengthens significantly as the electricity supply becomes cleaner. In Cases 5 and 6 (2035 and 2040 grid mix) and Case 7 (wind), NH_3 ranks first. When all the process energy is from wind (Case 7), NH_3's GWP falls to 3.66 kg CO_2eq kg and its LCOH drops to \$6.89 $kg^{-1}H_2$, making NH_3 the first and MeOH the second. The combination makes it the top compromised solution in a deeply decarbonised energy system.

6.5.6 Criteria weight analysis

To address the potential subjectivity of the criteria weighting, a criteria weight analysis was performed. In addition to the Balanced Priority scenario used as the base case, three alternative weighting scenarios were developed. The Economic Priority focuses on the financial metrics that determine a project's bankability and profitability. The Environmental Priority scenario focuses on the environment-related performance. The Equal Weight scenario assumes no a priori preference and treats all five criteria as equally important.

Table 6-12 shows the pairwise comparison matrix for calculating the criteria weights of each alternative scenario. For the Economic Priority, LCOH and IRR are set as very strongly more important (7) than GWP and ReCiPe, and strongly more important (5) than Efficiency. LCOH is moderately more important (3) than IRR. For the

Environmental Priority scenario, GWP and ReCiPe are set as very strongly more important (7) than LCOH and IRR. GWP is moderately more important (3) than ReCiPe and Efficiency. For the Equal Weight scenario, all pairwise comparisons are 1. Table 6-13 shows the MCDM scores of weight analysis.

Table 6-12 Pairwise comparison matrix for alternative scenarios

Economic Priority					
Criteria	LCOH	IRR	GWP	ReCiPe	Efficiency
LCOH	1	3	7	7	5
IRR	1/3	1	5	5	3
GWP	1/7	1/5	1	1	1/3
ReCiPe	1/7	1/5	1	1	1/3
Efficiency	1/5	1/3	3	3	1
Environmental Priority					
Criteria	LCOH	IRR	GWP	ReCiPe	Efficiency
LCOH	1	1	1/7	1/5	1/3
IRR	1	1	1/7	1/5	1/3
GWP	7	7	1	3	3
ReCiPe	5	5	1/3	1	1
Efficiency	3	3	1/3	1	1
Equal Weight					
Criteria	LCOH	IRR	GWP	ReCiPe	Efficiency
LCOH	1	1	1	1	1
IRR	1	1	1	1	1
GWP	1	1	1	1	1
ReCiPe	1	1	1	1	1
Efficiency	1	1	1	1	1

Table 6-13 MCDM results of the weight analysis

	AHP-TOPSIS					AHP-VIKOR				
	LH_2	NH_3	MeOH	DBT	TOL	LH_2	NH_3	MeOH	DBT	TOL
Balanced Priority (Based case)	0.78	0.61	0.59	0.17	0.40	0.50	0.84	0.09	0.79	0.11

Economic Priority	0.32	0.23	0.73	0.54	0.72	0.99	0.98	0.04	0.17	0.00
Environmental Priority	0.93	0.67	0.59	0.03	0.37	0.00	0.31	0.41	1.00	0.60
Equal Weights	0.64	0.54	0.53	0.17	0.45	0.50	0.31	0.19	1.00	0.34

Table 6-14 shows the ranking of the alternative weighting scenarios. The results provide key insights into the implementation of the proposed framework. The shift in ranking shows the proposed framework's responsiveness to stakeholder priorities. When economic factors are dominant, the cost-effective MeOH and TOL rise to the top as the preferred carriers. The assigned decision weight to LCOH and IRR (over 76%) penalises the high-cost LH_2 and NH_3 pathways, resulting in them being ranked at the bottom. Conversely, when environmental performance is the priority, LH_2 is the best carrier in both AHP-TOPSIS and AHP-VIKOR due to its good performance in GWP, ReCiPe and Efficiency criteria. The equal weights scenario reveals the results without any priority. Overall, the weighting analysis shows that the best hydrogen carrier is not absolute but subject to the strategic priorities of the decision-maker. The analysis demonstrates that the proposed framework is effective and transparent for evaluating the critical trade-offs between key criteria in the development of green hydrogen.

Table 6-14 GHC ranking across different weighting scenarios

	AHP-TOPSIS					AHP-VIKOR				
	LH_2	NH_3	MeOH	DBT	TOL	LH_2	NH_3	MeOH	DBT	TOL
Balanced Priority (Based case)	1	2	3	5	4	3	5	1	4	2
Economic Priority	4	5	1	3	2	5	4	2	3	1
Environmental Priority	1	2	3	5	4	1	2	3	5	4
Equal Weights	1	2	3	5	4	4	2	1	5	3

6.6 Chapter summary

This chapter proposed and applied a novel computational framework to address the gap in existing research on hydrogen carrier comparative studies, where carriers exhibit distinct performances across multiple criteria. The proposed framework compares green hydrogen carriers in terms of techno-economic performance (LCOH and IRR),

environmental impacts (IPCC GWP100 and ReCiPe endpoint), and carrier efficiency using AHP-TOPSIS and AHP-VIKOR methods. The proposed framework can provide detailed ranking results for GHCS, facilitating informed decision-making.

The utility of the proposed framework is demonstrated with a South Africa–UK hydrogen supply chain. The LCOH results show that importing green hydrogen can be cost-competitive with domestic production. The levelised cost of the most economical carrier, TOL \$7.07 $kg^{-1}H_2$, is on par with the projections for domestic UK production (\$7.13 $kg^{-1}H_2$). This validates international hydrogen trade as an economically rational strategy for an importing country to enhance energy security and achieve its decarbonisation goals. The case study results show that no individual GHC wins on economic, environmental impacts and carrier efficiency simultaneously. LH_2 was consistently identified by the AHP-TOPSIS method as the ideal solution, ranking first in all scenarios due to its superior performance on environmental criteria and carrier efficiency.

Policy decisions that lower the levelised cost of hydrogen production and carbon intensity of the electricity grid will impact the GHCs' competitiveness significantly. Across five GHC pathways analysed, green hydrogen production accounts for 66.4% to 77.2% of the delivered costs. Therefore, policy measures that can lower the levelised costs of green hydrogen, such as production tax credits to renewable energy farms in the exporting countries, can increase IRR for all carriers and narrow the cost gaps. In addition, the life-cycle results show that the further decarbonisation of the grid could alter the ranking of GHCs. When the process energy originates from a 2035 grid mix or a more decarbonised grid, NH3 benefits greatly, as it becomes the best compromised carrier. Moreover, renewable utilisation and grid energy price matter. Variations in renewable capacity factors and grid energy prices move MeOH and NH_3 up or down by one place in the MCDM ranking. Therefore, a technology-neutral but performance-based policy design that focuses on cheap, clean electricity and grid decarbonisation will allow the most cost-effective and climate-aligned carrier to scale first while keeping national decarbonisation goals firmly on track.

In addition to the carbon footprint of carriers, the ReCiPe results show that a significant percentage of human health damage induced by the hydrogen supply chain is driven by the fine particulate matter formation and human carcinogenic toxicity, which originates

from the upstream manufacturing of the infrastructure, such as the materials for wind turbines. This finding demonstrates that a holistic green hydrogen policy needs to extend beyond ensuring a renewable energy supply to include sustainable procurement procedures for capital equipment.

However, there are some limitations to the case study results. First, the case study results are limited to the system defined in Section 6.2. A change in system definition will result in different project factors for the green hydrogen supply chain. Factors such as shipping distance, available infrastructure, environmental regulations, and policy incentives can shift the relative importance of each criterion. Hence, the criteria configuration and weight will be different. Second, the economic and environmental results are sensitive to assumptions. The current proposed framework considers the steady state of commodity prices, energy prices, and energy consumption. Therefore, future studies can investigate a multi-criteria decision-making framework from a dynamic system perspective, where prices and energy consumption are dynamic. To sum up, this chapter provides an effective evaluation framework for stakeholders in the green hydrogen supply chain to gain more insights into the viable hydrogen carriers.

Chapter 7

7. Conclusion

7.1 Thesis summary

This thesis was motivated by the revelation that the global energy transition is driving three fundamental shifts in decision-making, making traditional computational frameworks inadequate. The first is the shift in operational uncertainty, where the integration of intermittent renewables and novel storage assets creates deep uncertainty. The second is a structural shift from centralised control to decentralised coordination, in which the emergence of prosumers and aggregators requires privacy-preserving, competitive market interactions. The third is the shift in strategic evaluation, where decision-makers must move from a single objective on cost minimisation to a multi-dimensional assessment. As outlined in Chapter 3, these shifts create a nested hierarchy of complexity, spanning uncertainty complexity at the operational scale, interactional complexity at the transactional scale, and evaluative complexity at the strategic scale. The overarching research question of this thesis asked how computational frameworks must be developed to manage these emergent complexities. By systematically addressing each layer of this hierarchy, this thesis advances this field by establishing new computational frameworks that collectively address the nest complexities.

At the foundational layer of this hierarchy, this thesis addresses uncertainty complexity at the operational scale. Traditional stochastic programming assumes that probability distributions accurately describe market conditions. However, this assumption will not hold when the market is under severe volatility introduced by renewable penetration. To resolve this, Chapter 4 contributed a novel hybrid framework that integrates IGDT with STA. By applying the proposed framework to the scheduling of LAES-equipped micro-grids, this thesis demonstrates that the proposed framework allows operators to quantify the risks the systems can tolerate while meeting performance targets. This contribution fills the critical methodological gap by providing a non-probabilistic

computational framework for managing risks associated with novel storage assets in volatile markets.

Building on the operational scale, this thesis addressed interactional complexity at the transactional scale as the energy system becomes more decentralised in energy generation. This shift creates challenges in managing the competitive interactions between autonomous agents. Existing centralised optimisation methods cannot preserve privacy, and single-leader game models fail to capture horizontal competition among multi-aggregators. Chapter 5 addresses this gap by formulating an MLMFG and solving it via a novel graph-based consensus algorithm. This contribution advances the field by moving beyond a single-leader architecture towards a multi-leader architecture. By proving that market equilibrium can be achieved through decentralised, privacy-preserving edge computing, this framework provides the decision-making tool for future competitive energy markets.

Finally, at the strategic scale, this thesis addressed evaluative complexity. The selection of long-term technology pathways, such as international green hydrogen carriers, involves trade-offs that cannot be resolved by a single metric alone. Existing studies often rely on simplified economic models or focus exclusively on global warming potential. Chapter 6 contributed a new MCDM framework that synthesises discounted techno-economic analysis, comprehensive ReCiPe endpoint environmental assessment, and carrier efficiency metrics. By applying the proposed framework to a previously unexamined South Africa-to-UK hydrogen corridor, this thesis provides the first detailed techno-economic and environmental assessment of the green hydrogen route, with sensitivity analysis of the GHC evaluation.

Collectively, these three studies constitute a coherent research design that develops the decision-making in multi-energy systems. Therefore, the primary contribution of this work is the development of these computational frameworks, which together provide a foundation for future decision-support tools to navigate the complexities of a sustainable energy future.

7.2 Socio-technical and ethical implications

The computational framework developed in this thesis is primarily a set of mathematical tools designed to optimise the energy system. However, energy systems

are not just physical infrastructures. They are socio-technical systems within economic, political, and social contexts. Although the focus of this thesis has been the development of computational frameworks, it is necessary to reflect on their socio-technical implications for the principles of fairness, equity, and sustainability. This reflection mirrors the nested hierarchy of complexity established in this thesis, examining the ethical dimensions at the operational, transactional, and strategic scales.

At the operational scale, the development of the hybrid IGDT-STA framework in Chapter 4 highlights an ethical tension between system robustness and energy affordability. The framework enables micro-grid operators to adopt risk-averse strategies by accepting higher operational costs. It raises questions about distributive costs: who will pay the extra cost of resilience? In a community micro-grid setting, a highly risk-averse operating strategy will drive up energy costs. If these costs are passed down uniformly to end users, they may cause energy poverty, particularly for vulnerable households. Therefore, the deployment of such an optimisation framework is not just a mathematical exercise. It requires further definition on the acceptable level of risk a community should bear.

Moving to the transactional scale, the intelligent aggregation framework proposed in Chapter 5 introduces socio-technical considerations regarding inclusivity. The proposed aggregation framework relies heavily on advanced digital infrastructure, including edge computing nodes and smart metering. The reliance creates a technological barrier to entry. In a decentralised market where participation requires both hardware and algorithmic competence, there is a risk of excluding prosumers who lack the financial means to upgrade their digital infrastructure to participate with automated agents. Furthermore, the aggregation framework assumes that every prosumer aims to maximise utility by maximising profits. However, in a real-world setting, the utility is not the same for all prosumers. A household with life-sustaining medical equipment has fundamentally different priorities than profit-maximising prosumers. Hence, the utility setting of the aggregation framework could incorporate fairness constraints into the optimisation model.

Finally, at the strategic scale, the evaluation of the South Africa-UK green hydrogen corridor in Chapter 6 raises questions about global equity and the geopolitics of the energy transition. The techno-economic analysis reveals that carriers such as LH_2,

LOHCs and Ammonia offer viable pathways for export. However, ownership of the intellectual property for these GHC pathways is concentrated in the Global North (e.g., Germany and Japan), while the Global South (South Africa) provides the primary land and renewable energy resources. If South Africa exports green hydrogen but imports the expensive liquefaction plants and specialised vessels required to transport it, the local economic benefit may be limited.

7.3 Limitations and recommendations for future research

In addition to the socio-technical discussion and future research recommendations in the previous section, Section 7.3 examines methodological and technical limits.

7.3.1 Methodological and validation limits

The key methodological limitation of this thesis is the reliance on computational simulation rather than empirical validation in operational environments. The proposed algorithms, such as the hybrid IGDT-STA and the graph-based consensus mechanism, have demonstrated numerical applicability against benchmarks. They have not yet undergone the physical experiment of hardware-in-the-loop testing or pilot deployment. Consequently, while the thesis provides frameworks that can support decision-making, the transition to deployed decision-support tools would require further validation to account for real-world communication latency, sensor noise, and hardware applicability.

Furthermore, the computational frameworks developed in this thesis depend on the quality of the input data. The case studies utilised standard benchmark datasets (e.g., SimBench) and historical market data (e.g., Nord Pool). In a real operational context, data availability is often imperfect, characterised by missing values and measurement errors. Additionally, while the research aims to support stakeholders such as micro-grid operators and policymakers, the validation process did not include qualitative feedback or usability testing with these human stakeholders. Therefore, the practical adoption of these frameworks would require a socio-technical validation phase to ensure the outputs are interpretable and actionable for human decision-makers.

7.3.2 Technical simplification in system modelling

Some specific technical simplifications were adopted in this thesis. In Chapter 4, the LAES system was treated as a steady-state system. The charging and discharging phases

were modelled with linearised equations assuming time-invariance. This approach neglects the complex thermodynamic transients in the compressor and expander, particularly during start-up and shut-down.

In Chapter 5, the intelligent aggregation framework solves a single-period decision-making problem. While this effectively demonstrates the graph-based consensus algorithm's ability to reach a market equilibrium, it does not fully capture prosumers' inter-temporal strategic behaviour. In reality, prosumers with storage capacity would likely engage in intertemporal arbitrage, storing energy when prices are low to sell in future periods when prices are high. By limiting the game to a single period, the current model may not fully reveal the potential economic benefits of storage assets in a competitive market.

Finally, the strategic evaluation of hydrogen carriers in Chapter 6 is centred on intrinsic techno-economic and environmental criteria. It does not explicitly model extrinsic factors such as geopolitical risks or evolving policy landscapes. Extrinsic geopolitical risks in the exporting country or along the maritime transportation route could lead to a higher risk premium when discounting the project's cash flows. In addition, the implementation of a carbon border adjustment mechanism (CBAM) by the importing country, such as the UK, would significantly change the economic performance of carbon-based carriers, especially methanol, by taxing the re-emission of captured CO_2. The absence of these dynamic policy and risk factors means the current ranking reflects a technocratic ideal rather than a fully risk-adjusted geopolitical reality.

7.3.3 Recommendations for Future Research

Building on these limitations, several future research directions are recommended to further advance the field. Future work could move from pure simulation to emulation using digital twins or hardware-in-the-loop setups. This would allow testing of the proposed algorithms under physical constraints, such as communication delay, which are critical for decentralised systems.

Regarding the specific models, future research should aim to relax the current simplifications. For the micro-grid scheduling framework, the IGDT formulation could be expanded to handle coupled uncertainties, investigating the simultaneous impact of renewable generation intermittency and price volatility, rather than treating them in

isolation. For the aggregation framework, extending the MLMFG to a multi-period horizon would entail analysing complex inter-temporal strategies, thereby providing a more accurate reflection of storage value in local markets.

Finally, integrating extrinsic risk factors into the MCDM criteria is a vital next step for strategic hydrogen research. Future work could expand the proposed framework to include criteria such as supply chain resilience, policy alignment, and geopolitical stability. In addition, incorporating further consideration of carbon pricing and border adjustment mechanisms would enable the framework to produce time-dependent rankings that quantify carrier selection under plausible future policy scenarios. This would enhance the practical relevance of the framework for investors and policymakers navigating the uncertainties of the global energy transition.

7.4 Concluding remarks

By moving from deterministic to risk-included robust optimisation, from centralised to decentralised coordination, and from single-objective to multi-criteria evaluation, this thesis advances the field of decision-making strategies in multi-energy systems by introducing new computational frameworks. These frameworks demonstrate that the emergent complexities of uncertainty, interaction and evaluation can be addressed with quantitative methods. While acknowledging its limitations, this thesis provides a foundation for future research that aims at developing dynamic, robust, and equitable decision-support systems required for a net-zero future.

Appendix

This appendix provides supplementary information to Chapter 5 on green hydrogen carrier evaluation, which includes life cycle inventories, life cycle impact assessment results, and sensitivity analysis results by case.

A1 Detailed techno-economic data and assumptions

This section presents the detailed techno-economic calculation and data sources of green hydrogen carriers (GHC) conversion and reconversion. The GHCs considered include liquid hydrogen (LH_2), ammonia (NH_3), methanol (MeOH), dibenzyltoluene (DBT), and toluene (TOL). The currency is converted based on the exchange rate assumed in Table 6-1. It should be noted that in addition to the CAPEX for the hydrogenation and dehydrogenation plant, the DBT and TOL pathway also considers the upfront purchase of the carrier, due to the closed-loop nature of DBT and TOL. This study considers the initial purchase of 993,000 t and 980,000 t of DBT and TOL, respectively, based on the annual green hydrogen delivery. Table A2 illustrates the energy consumption data sources for the conversion and reconversion of GHC. It should be noted that the waste heat for CO_2 capture with DAC is assumed to be supplied by industrial plants in the Coega Industrial Development Zone at Port Elizabeth.

Table A1. Detailed techno-economic input calculation. C: Conversion, R: Reconversion.

Carrier	Process	System lifetime [year]	Reference CAPEX [original currency]	Reference capacity	Scaling exponent	Final scaled CAPEX [Million $]	Normalised unit CAPEX[1]	Reference
LH_2	C	20	See Note[2]	See Note[2]	See Note[2]	5192.64	34,786.75 [$/(kg$H_2$/h)]	(Connelly et al., 2019)
	R	20	0.81 M€	42.7 tH_2/d	0.67	15.12	119.79 [$/(kg$H_2$/h)]	Table 17 of (Restelli et al., 2024)
NH_3	C	20	2373.3 M€[3]	24,627 t$NH_{3,product}$/d	0.67	1938.0	2,566.19 [$/(kg$NH_3$/h)]	(Ortiz Cebolla et al., 2022)
	R	20	1,100 M€	24,627 t$NH_{3,feed}$/d	0.67	926.24	7,335.81 [$/(kg$H_2$/h)]	(Ortiz Cebolla et al., 2022)

MeOH	C	20	106 M€[4]	65,000 tMeOH/y	0.67	2,540.23	2864.52 [$/(kgMeOH/h)]	(Bos et al., 2020)
	R	20	138.6 M$	115,500t H_2/y	0.67	588.62	4,661.85 [$/(kg$H_2$/h)]	(Papadias et al., 2019)
DBT	C	20	319.6 M€	3610931.5 tH18-DBT/y	0.67	902.77	445.6 [$/(kgH18-DBT/h)]	(Raab et al., 2021)
	R	20	640 M€	225,500 tH_2/y	0.67	1821.81	14,428.71 [$/(kg$H_2$/h)]	(Raab et al., 2021)
TOL	C	20	439.41 M€	3,662,120 tMCH/y	0.67	1241.30	604.2 [$/(kgMCH/h)]	(Raab et al., 2021)
	R	20	666.67 M€	225,500 tH_2/y	0.67	1897.71	15,029.90 [$/(kg$H_2$/h)]	(Raab et al., 2021)

[1] Normalised unit CAPEX is defined as the total installed CAPEX [$] divided by the hourly capacity of the plants (kg carrier/h), assuming 7,920 annual operating hours

[2] The CAPEX for the LH2 liquefaction plant was not scaled from reference but was calculated directly using the liquefier capital cost equation of (Connelly et al., 2019). For this study, the daily liquefied hydrogen production considers the 6.4% loss during the supply chain. A cost index adjustment of 1.33 was applied to adjust the liquefier cost estimation.

[3] The CAPEX of green ammonia conversion includes the Air Separation Unit (ASU) and the ammonia synthesis plant (Ortiz Cebolla et al., 2022).

[4] The CAPEX for Direct Air Capture (DAC) and methanol synthesis plant are 95 and 11 million € respectively (Bos et al., 2020).

Table A2. Energy consumption reference. C: Conversion, R: Reconversion.

Carrier	Process		Energy consumption	Reference
LH_2	C	Hydrogen liquefaction	7 kWh/kgH_2	(Heuser et al., 2019)
	R	Hydrogen regasification	0.2 kWh/kgH_2	(IRENA, 2022)
NH_3	C	Electricity consumption by ASU	1.03 kWh/kgN_2	(Althaus et al., 2007)
		Electricity consumption by the Haber-Bosch process	0.464 kWh/kgNH_3	(D'Angelo et al., 2021)
	R	Ammonia cracking	7 kWh/kgH_2	(Nielsen & Topsoe, 2021)
MeOH	C	Electricity consumption by DAC	0.614 kWh/kgCO_2	(Terlouw et al., 2021)

	C	Waste heat consumption by DAC	1.5 kWh/kgCO_2	(Terlouw et al., 2021)
	C	Methanol synthesis	0.217 kWh/kgMeOH	(Badger et al., 2024)
	R	Methanol dehydrogenation	0.501 kWh/kgH_2	(MAHLER, 2024)
DBT	C	DBT hydrogenation	0.068 kWh/kgH18-DBT	(Cho et al., 2024)
	R	H18-DBT dehydrogenation – electricity	1.12 kWh/kgH_2	(Cho et al., 2024)
		H18-DBT dehydrogenation – heat	9.79 kWh/kgH_2	(Cho et al., 2024)
TOL	C	TOL hydrogenation	0.071 kWh/kgMCH	(Cho et al., 2024)
	R	MCH dehydrogenation – electricity	1.13 kWh/kgH_2	(Cho et al., 2024)
		MCH dehydrogenation – heat	10.25 kWh/kgH_2	(Cho et al., 2024)

A2 Life cycle inventories

This section presents for the life cycle inventories in the LCA modelling. It should be noted that the employees' travel and commuting are not considered in this LCA model.

A2.1 Green hydrogen production

Table A3 explains the life cycle inventories for green hydrogen production. The quantity of water and electricity consumption is obtained by assuming the PEM system efficiency of 60% (Bareiß et al., 2019). The inventory for the PEM gasket and cell stack construction is presented in Tables A4 and A5. It should be noted that the green hydrogen produced by PEM water electrolysis must be transported to a hydrogen carrier production facility, such as a hydrogen liquefaction plant. It is assumed that the distance between the green hydrogen production plant and the hydrogen carrier conversion facility is 10 km. The hydrogen pipeline is assumed to be a distribution pipeline, as it is shorter and operates at a lower pressure than transmission pipelines (Wulf et al., 2018). Table A6 presents the life cycle inventories for hydrogen distribution pipeline construction at Port Elizabeth, which has a lifetime of 20 years, based on the data from (Wulf et al., 2018).

Table A3 Life cycle inventory for green hydrogen production

Green hydrogen production (Bareiß et al., 2019)		
Input, material & energy		
Water, deionised, from tap water, at user	9.00E+00	kg
Electricity, solar	5.55E+01	kWh
Hydrogen pipeline	5.37E-07	km
PEM cell stack construction	1	p*
Output, product		
H2 - PEM water electrolysis operation	1	kg

*p is a normalised unit in SimaPro with respect to the infrastructure process's production capacity.

Table A4 Life cycle inventory of gasket construction

Gasket construction, cell stack (D'Angelo et al., 2021)		
Input, materials		
Tetrafluoroethylene	7.63E-02	kg
Acrylonitrile	1.56E-01	kg
Aniline	4.79E-02	kg
Acetic anhydride	5.28E-02	kg
Purifies terephthalic acid	8.61E-02	kg
Nitric acid, without water, in 50% solution state	3.23E-02	kg
Hydrochloric acid, without water, in 30% solution state	1.27E-01	kg
Graphite	4.21E-01	kg
Lubricating oil	4.69E-01	kg
Output, product		
Materials for gasket construction, cell stack	1	Kg

Table A5 Life cycle inventory of PEM cell stack construction

PEM cell stack construction (D'Angelo et al., 2021)		
Input, materials & energy		
Iridium	6.37E-07	kg
Platinum	6.73E-08	kg

Copper	1.43E-06	kg
Steel, unalloyed	3.14E-05	kg
Titanium, primary	4.74E-04	kg
Aluminium, primary, ingot	2.42E-05	kg
Tetrafluoroethylene	1.43E-05	kg
Activated carbon	8.07E-06	kg
Precious metal from electronics scrap	7.40E-07	kg
Gasket construction, cell stack	1.13E-04	kg
Water, decarbonised, at user	1.21E-06	t
Water, deionised, from tap water, at user	9.45E-06	t
Electricity, grid	3.98E-06	GJ
Heat, district or industrial, natural gas	9.72E-06	GJ
Heat, from steam, in chemical industry	7.73E-05	MJ
Industrial machine, heavy	1.77E-08	kg
Plaster mixing	8.61E-05	kg
Calendering, rigid sheets	8.61E-05	kg
Output, product		
H2 - Cell stack construction, PEM water electrolysis	1	p/kgH2

Table A6 Life cycle inventory of hydrogen distribution pipeline construction

Hydrogen distribution pipeline (Wulf et al., 2018)		
Input, material		
Primary aluminium	1.94E+01	kg
Silica sand	1.20E+02	t
Steel, low-alloyed	5.34E+03	kg
Silicon	5.70E+02	g
Zinc	1.53E+01	kg
Drawing of pipe steel	5.34E+03	kg
Excavation, hydraulic digger	1.20E+03	m^3
Excavation, skid-steer loader	9.00E+03	m^3
Zinc coating	5.34E+03	kg
Output, product		
hydrogen distribution pipeline	1	km
Output, waste to treatment		
Pipeline decommissioning	2.70E+03	kg

A2.2 Liquid hydrogen pathway

The life cycle inventory data for the LH_2 pathway is presented in Tables A7 and A8, considering a hydrogen loss of 1.6% during the liquefaction process (Heuser et al., 2019) and a 0.2 kWh energy consumption for LH_2 regasification (IRENA, 2022). The primary energy consumption in the liquid hydrogen supply chain occurs during the liquefaction process, which is energy-intensive due to the extremely low temperatures required and the need to maintain the hydrogen in its liquid state to prevent boil-off. Energy consumption for hydrogen liquefaction varies across different sources in the literature. An energy requirement of 7 kWh per kilogram of hydrogen is assumed in this chapter based on (IRENA, 2022). The life cycle inventories of the hydrogen liquefaction plant are scaled linearly based on the data from (IdealHY, 2013).

The maritime transportation of liquid hydrogen is carried out by dedicated liquid hydrogen tanker ships with an average speed of 30 km/h (IEA, 2020) and a boil-off rate of 0.1% per day during transportation (Dickson et al., 2022). Since the liquid hydrogen ships are currently in the prototype stage, the background Ecoinvent data from the liquid natural gas tankers is used as a conservative proxy for liquid hydrogen ships. It should be noted that the environmental footprint from the ballast voyage is implicitly considered in the Ecoinvent database (Wernet et al., 2016). Additionally, the hydrogen could be lost during the transfer operation from the port storage tanks to the transporting ships due to unavoidable temperature fluctuations. As a result, a total of 1.3% hydrogen loss is assumed during the loading and unloading of LH_2 (Wijayanta et al., 2019).

Table A7 Hydrogen liquefaction inventories

Hydrogen liquefaction (Heuser et al., 2019; IRENA, 2022)		
Input, materials & energy		
Hydrogen, gaseous	1.016	kg
Electricity	7.00E+0	kWh
Hydrogen liquefaction plant	5.34E-11	p
Output, product		
Hydrogen, liquid	1	kg
Output, emission		
Hydrogen, gaseous	1.60E-02	kg

Table A8 Life cycle inventory of liquefaction plant construction

Liquefaction plant construction (IdealHY, 2013)		
Input, materials		
Carbon steel	2.17E+04	tons
Stainless steel	3.39E+04	tons
Copper	8.55E+03	tons
Aluminium	7.98E+03	tons
Concrete	2.66E+06	tons
Output, product		
Liquefaction plant	1	p

A2.3 Green ammonia pathway

Table A9 presents the life cycle inventory of nitrogen production, indicating that 1.03 kWh of electricity is required to produce 1 kg of nitrogen. The synthesis catalyst for the electrified Haber-Bosch process consists of magnetite, lime, and zeolite, as shown in Table A10. Another key data point for ammonia production is the electricity consumption of the Haber-Bosch process, which includes the electricity used by the refrigeration compressor, feed compressor, recycle compressor, and electric heater (IRENA, 2022). The electricity consumption of 0.464 kWh for ammonia production is obtained from (Chisalita et al., 2020). In addition, emission data is sourced from (D'Angelo et al., 2021). The infrastructure data of a chemical factory from the Ecoinvent database is used to approximate the infrastructure processes in green ammonia production (Althaus et al., 2007). Overall, the life cycle inventory of green ammonia production is shown in Table A11. After production at the ammonia synthesis plant, ammonia is stored in refrigerated tanks. This chapter assumes a daily loss rate of 0.036% (Noh et al., 2023b).

Ammonia cracking, which is the reverse of ammonia synthesis, involves breaking down ammonia into pure hydrogen and nitrogen. The life cycle inventory for ammonia cracking is detailed in Table A12, with the catalyst composed of nickel and magnesium oxide (Noh et al., 2023b). The life cycle inventory data for electrified ammonia crackers is based on (Nielsen & Topsoe, 2021). Producing 1 kg of gaseous hydrogen requires 5.93 kg of ammonia and 8 kWh of electricity, assuming a cracker efficiency of 95%. It should be noted that the electrified ammonia cracker is currently in the pilot project stage, and its system and energy efficiency may evolve as the technology advances. The

infrastructure for ammonia cracking is modelled using generic chemical factory data from the Ecoinvent database.

Table A9 Life cycle inventory of the nitrogen production

Nitrogen production with ASU (Althaus et al., 2007)		
Input from nature		
Air	1.28E+00	kg
Input from the techno space		
Air separation facility	6.30E-10	P
Electricity	1.03E+00	kWh
Water, cooling	2.70E-03	m^3
Output, product		
Nitrogen	1.00E+00	kg
Output, emissions/wastes		
Waste heat to air	3.69E+00	MJ
Waste water	1.15E+00	kg

Table A10 Life cycle inventory of the ammonia synthesis catalyst

Ammonia synthesis catalyst (D'Angelo et al., 2021)		
Input, material and energy		
Magnetite	9.17E-01	kg
Lime	3.00E-02	kg
Zeolite, powder	5.25E-02	kg
Electricity	3.14E-05	kWh
Output, product		
NH3 synthesis catalyst	1	kg

Table A11 Life cycle inventory for green ammonia production

Green ammonia by Haber-Bosch process (Chisalita et al., 2020; D'Angelo et al., 2021)		
Input, material and energy		
Hydrogen	1.89E-01	kg
Nitrogen	8.74E-01	kg
Electricity, for HB process	4.64E-01	kWh
Ammonia synthesis catalyst	2.00E-04	kg

Water, cooling	8.31E-01	kg
Chemical factory	4.00E-10	p
Output, product		
Ammonia	1	kg
Output, emissions/wastes		
Hydrogen (to air)	7.67E-04	kg
Ammonia (to air)	1.63E-03	kg
Nitrogen oxide (to air)	1.00E-03	kg
water, cooling (to water)	8.31E-01	kg
Spent catalyst (to treatment or inert material landfill)	2.00E-04	kg

Table A12 Life cycle inventory for ammonia cracking

Ammonia cracking (Nielsen & Topsoe, 2021)		
Input, material & energy		
Ammonia	5.93E+00	kg
Electricity, UK	8.00E+00	kWh
Nickel	1.20E-4	kg
Magnesium oxide	1.88E-3	kg
Ammonia cracker (chemical factory proxy)	4.00E-10	p
Output, product		
Hydrogen, Gaseous	1	kg
Output, waste		
Spent catalyst	2.00E-3	kg

A2.4 Methanol pathway

The life cycle inventory analysis of methanol as a hydrogen carrier encompasses three primary stages: carbon dioxide (CO_2) production via direct air capture (DAC), methanol synthesis, and methanol dehydrogenation to release hydrogen at the point of use. In the CO_2 production stage, as shown in Table A13, capturing 1 kg of CO_2 requires 1.50 kWh of waste heat, 0.614 kWh of electricity, and 3 grams of sorbent material. The Methanol synthesis data is obtained from Badger et al., 2024 (Badger et al., 2024), as shown in Table A14. The Ecoinvent data of a liquid goods tanker ship is used for modelling the transportation of methanol. No boil-off loss is considered for methanol transportation. In the methanol dehydrogenation stage, as shown in Table A15, 7.01 kg of methanol and 3.78 kg of demineralised water are consumed to produce 1 kg of hydrogen gas,

utilising 0.5 kWh of electricity and 222.52 L of cooling water (MAHLER, 2024). The CO_2 is assumed to be released back into the atmosphere during the methanol dehydrogenation stage (Arrigoni et al., 2024; Dickson et al., 2022).

Table A13 Life cycle inventories for CO2 production

CO_2 production (Badger et al., 2024; Terlouw et al., 2021)		
Input, material & energy		
Waste heat	1.50E+00	kWh
Electricity	6.14E-01	kWh
Sorbent	3.00E-03	kg
Chemical factory	4.00E-10	p
Output, product		
CO_2, captured	1	kg
Output, emissions		
CO_2, emission to air	-1	kg

Table A14 Life cycle inventories for green methanol synthesis

Methanol synthesis (Badger et al., 2024)		
Input, material & energy		
Copper oxide	1.67E-05	kg
CO2, captured	1.45E+00	kg
Hydrogen	2.08E-01	kg
Water, cooling	5.64E-01	kg
Electricity	2.17E-01	kWh
Methanol factory	3.71E-11	p
Output, product		
Methanol	1	kg
Output, Emissions/Waste		
CO_2, to air	7.26E-02	kg
Hydrogen, to air	1.93E-02	kg
Waste water	5.64E-04	m^3
Spent catalyst (to treatment or inert material landfill)	1.67E-05	kg

Table A15 Life cycle inventories for methanol dehydrogenation

Methanol dehydrogenation (Arrigoni et al., 2024; MAHLER, 2024)		
Input, material & energy		
Methanol	7.01E+00	kg
Demineralised water	3.78E+00	kg
Cooling water	2.23E+02	L
Electricity	5.01E-01	kWh
Copper oxide	3.02E-06	kg
Zinc oxide	3.10E-06	kg
Output, product		
Hydrogen, gaseous	1	kg
Output, emissions/waste		
Carbon dioxide	9.7E+00	kg
Water, cooling	2.23E+00	m^3
Spent catalyst	6.12E-06	kg

A2.5 DBT and TOL pathway

Table A16 shows the production data for DBT from toluene, where the electricity and heat consumption data are from (Cho et al., 2024). The environmental impacts of the DBT production process are attributed to DBT (Arrigoni et al., 2024). Table A17 shows the hydrogenation process where hydrogen molecules are chemically bonded to DBT, forming perhydro-dibenzyltoluene (H18-DBT). Since DBT carriers can be recycled more than 750 times, it is assumed that the DBT are returned to the hydrogenation facility (Arrigoni et al., 2024). Therefore, the environmental impacts of the initial batch of purchasing / producing DBT are credited based on the maritime transportation assumptions in Table 6-4. As a result, 9.39% of impacts should be credited to the South Africa case study in the UK.

The transportation process of H18-DBT is modelled using Ecoinvent data of liquid goods other than petroleum, with consideration of transporting unloaded DBT back to South Africa. The ship transport of crude oil shows losses of around 0.2%, which is also assumed for DBT transport (Niermann et al., 2021). Table A18 shows the dehydrogenation process, where the H18-DBT is unloaded to supply green hydrogen with an efficiency of 97% (IRENA, 2022). The hydrogenation facility will purchase or

produce additional LOHCs to compensate for the loss. Similar processes apply to toluene as an LOHC, where toluene is hydrogenated to methylcyclohexane (MCH) and later dehydrogenated to release hydrogen, as shown in Table A19 and Table A20. The dehydrogenation efficiency of TOL is assumed to be 95% (IRENA, 2022).

Table A16 Life cycle inventories for DBT production

DBT Production (Cho et al., 2024; Wulf et al., 2018)		
Input, materials & energy		
Toluene	1.03E+00	Kg
Decarbonised water	1.20E+00	kg
Chlorine gas	2.60E-01	Kg
Iron (III) chloride	2.00E-06	Kg
Electricity	2.42E+00	kWh
Heat	2.70E+00	MJ
Chemical factory	4.00E-10	p
Output, product		
DBT	1	Kg
Hydrochloric acid	0.535	Kg

Table A17 Life cycle inventory of DBT hydrogenation

DBT Hydrogenation (Cho et al., 2024; Dickson et al., 2022; Niermann et al., 2021; Wulf et al., 2018)		
Input, materials & energy		
DBT	15.013	Kg
Electricity	1.091	kWh
Hydrogen	1	Kg
Water, cooling	1.4	L
Platinum	0.161	mg
Aluminium oxide	32	mg
Output, product & energy		
H18 DBT	16.013	kg
Output, emissions & waste		
Heat	11	kWh
Water, cooling	1.4	L
Spent catalyst	32.161	mg

Table A18 Life cycle inventory of DBT dehydrogenation

DBT dehydrogenation (Wulf et al., 2018)		
Input, material & energy		
H18-DBT	16.013	kg
Electricity	1.119	kWh
Heat	9.79	kWh
Platinum	0.161	mg
Aluminium oxide	32	mg
Water, cooling	358	L
Output, product		
Hydrogen	1	kg
Output, emission, waste		
Water, cooling (to water)	358	l
Spent catalyst	32.161	mg

Table A19 Life cycle inventory of Toluene hydrogenation

Toluene hydrogenation (Dickson et al., 2022; Niermann et al., 2021)		
Input, materials & energy		
Toluene	15.24	kg
Electricity	1.16	kWh
Hydrogen	1	kg
Water, cooling	1.4	L
Platinum	0.161	mg
Aluminium oxide	32	mg
Output, product		
Methylcyclohexane (MCH)	16.24	kg
Output, emissions & wastes		
Heat	13.2	kWh
Water, cooling (to water)	1.4	L
Spent catalyst	32.161	mg

Table A20 Life cycle inventory of Toluene dehydrogenation

Toluene dehydrogenation(Dickson et al., 2022; Niermann et al., 2021)		
Input, material & energy		

MCH	16.24	kg
Electricity	1.13	kWh
Water, cooling	1.4	L
Platinum	0.161	mg
Aluminium oxide	32	mg
Heat	10.25	kWh
Output, product		
Hydrogen	1	kg
Output, emissions & waste		
Water, cooling (to water)	1.4	L
Spent catalyst	32.161	mg

A3 ReCiPe impacts

Tables A21 and A22 present the ReCiPe midpoint and endpoint impact characterisation of the base case, respectively. The specific methods are ReCiPe 2016 Midpoint (H) V1.09 / World (2010) H and ReCiPe 2016 Endpoint (H) V1.09 / World (2010) H/A. Table A23 shows quantitative process contributions to the Fine particulate matter formation and Human carcinogenic toxicity.

Table A21 ReCiPe midpoint impact characterisation of the five GHCs

Impact category	Unit	LH_2	NH_3	MeOH	DBT	TOL
Global warming	kg CO2 eq	7.70E+00	1.00E+01	1.04E+01	1.55E+01	1.29E+01
Stratospheric ozone depletion	kg CFC11 eq	5.92E-06	8.01E-06	7.46E-06	7.78E-06	4.58E-06
Ionizing radiation	kBq Co-60 eq	3.69E-01	7.54E-01	5.15E-01	4.70E-01	4.37E-01
Ozone formation, Human health	kg NOx eq	3.20E-02	4.89E-02	4.90E-02	9.41E-02	8.11E-02
Fine particulate matter formation	kg PM2.5 eq	2.02E-02	2.80E-02	2.90E-02	4.16E-02	3.16E-02
Ozone formation, Terrestrial ecosystems	kg NOx eq	3.24E-02	5.39E-02	4.97E-02	9.68E-02	8.43E-02
Terrestrial acidification	kg SO2 eq	6.17E-02	9.34E-02	8.60E-02	1.24E-01	9.20E-02
Freshwater eutrophication	kg P eq	7.51E-03	8.84E-03	9.28E-03	7.25E-03	3.28E-03
Marine eutrophication	kg N eq	3.73E-04	4.60E-04	4.92E-04	5.54E-04	3.52E-04
Terrestrial ecotoxicity	kg 1,4-DCB	2.02E+02	2.50E+02	3.15E+02	2.73E+02	2.62E+02

Freshwater ecotoxicity	kg 1,4-DCB	1.14E+00	1.48E+00	1.86E+00	1.27E+00	1.11E+00
Marine ecotoxicity	kg 1,4-DCB	1.67E+00	2.14E+00	2.68E+00	1.90E+00	1.68E+00
Human carcinogenic toxicity	kg 1,4-DCB	6.48E+00	7.75E+00	9.57E+00	7.36E+00	6.54E+00
Human non-carcinogenic toxicity	kg 1,4-DCB	1.55E+01	2.12E+01	2.44E+01	1.78E+01	1.13E+01
Land use	m2a crop eq	2.56E-01	8.41E-01	4.50E-01	4.58E-01	3.70E-01
Mineral resource scarcity	kg Cu eq	6.78E-02	9.38E-02	1.22E-01	9.08E-02	8.73E-02
Fossil resource scarcity	kg oil eq	2.19E+00	2.86E+00	2.93E+00	6.32E+00	6.32E+00
Water consumption	m3	5.07E-02	7.07E-02	8.06E-02	8.06E-02	5.53E-02

Table A22 ReCiPe Endpoint impact characterisation of the five GHCs.

Impact category	**Unit**	**LH_2**	**NH_3**	**MeOH**	**DBT**	**TOL**
Global warming, Human health	DALY	7.14E-06	9.30E-06	9.65E-06	1.44E-05	1.20E-05
Global warming, Terrestrial ecosystems	species.yr	2.16E-08	2.81E-08	2.91E-08	4.35E-08	3.62E-08
Global warming, Freshwater ecosystems	species.yr	5.89E-13	7.67E-13	7.95E-13	1.19E-12	9.89E-13
Stratospheric ozone depletion	DALY	3.14E-09	4.25E-09	3.96E-09	4.13E-09	2.43E-09
Ionizing radiation	DALY	3.13E-09	6.40E-09	4.37E-09	3.98E-09	3.70E-09
Ozone formation, Human health	DALY	2.91E-08	4.54E-08	4.45E-08	8.56E-08	7.38E-08
Fine particulate matter formation	DALY	1.27E-05	1.76E-05	1.82E-05	2.62E-05	1.99E-05
Ozone formation, Terrestrial ecosystems	species.yr	4.18E-09	7.08E-09	6.42E-09	1.25E-08	1.09E-08
Terrestrial acidification	species.yr	1.31E-08	1.98E-08	1.82E-08	2.63E-08	1.95E-08
Freshwater eutrophication	species.yr	5.03E-09	5.92E-09	6.22E-09	4.86E-09	2.20E-09
Marine eutrophication	species.yr	6.34E-13	7.82E-13	8.37E-13	9.41E-13	5.98E-13
Terrestrial ecotoxicity	species.yr	2.30E-09	2.85E-09	3.59E-09	3.11E-09	2.99E-09
Freshwater ecotoxicity	species.yr	7.92E-10	1.02E-09	1.29E-09	8.80E-10	7.69E-10
Marine ecotoxicity	species.yr	1.75E-10	2.25E-10	2.82E-10	2.00E-10	1.77E-10
Human carcinogenic toxicity	DALY	2.15E-05	2.57E-05	3.18E-05	2.44E-05	2.17E-05
Human non-carcinogenic toxicity	DALY	3.53E-06	4.82E-06	5.55E-06	4.06E-06	2.57E-06

Land use	species.yr	2.27E-09	7.46E-09	3.99E-09	4.06E-09	3.29E-09
Mineral resource scarcity	USD2013	1.57E-02	0.0216781	2.82E-02	2.10E-02	2.02E-02
Fossil resource scarcity	USD2013	3.36E-01	0.5240146	5.47E-01	2.14E+00	2.42E+00
Water consumption, Human health	DALY	5.66E-08	4.99E-08	9.90E-08	1.05E-07	-9.48E-08
Water consumption, Terrestrial ecosystem	species.yr	6.93E-10	1.01E-09	1.04E-09	1.01E-09	9.89E-10
Water consumption, Aquatic ecosystems	species.yr	7.75E-14	1.32E-13	1.11E-13	1.06E-13	2.25E-13

A4 Sensitivity analysis results

This section presents the results of the sensitivity analysis of the 7 alternative cases. Table A24 shows the criteria results based on the case definition, and Table A25 shows the VIKOR and TOPSIS results.

Table A24 The criteria result of the sensitivity analysis

		LH_2	NH_3	MeOH	DBT	TOL
Case 0	LCOH (USD/kg)	8.17	8.14	7.22	7.25	7.07
	IRR	15.59%	18.24%	23.90%	21.18%	23.13%
	GWP (kg CO2eq)	7.62	9.91	10.30	15.16	12.45
	ReCiPe (Pt)	0.77	0.98	1.11	1.20	0.97
	Efficiency	77.62%	70.05%	63.57%	63.27%	63.45%
Case 1	LCOH (USD/kg)	7.81	7.78	6.86	6.89	6.71
	IRR	18.00%	21.84%	28.47%	24.60%	27.10%
	GWP (kg CO2eq)	7.62	9.91	10.30	15.16	12.45
	ReCiPe (Pt)	0.77	0.98	1.11	1.20	0.97
	Efficiency	77.62%	70.05%	63.57%	63.27%	63.45%
Case 2	LCOH (USD/kg)	8.71	8.68	7.76	7.79	7.61
	IRR	12.62%	14.13%	18.84%	17.18%	18.59%
	GWP (kg CO2eq)	7.62	9.91	10.30	15.16	12.45
	ReCiPe (Pt)	0.77	0.98	1.11	1.20	0.97
	Efficiency	77.62%	70.05%	63.57%	63.27%	63.45%
Case 3	LCOH (USD/kg)	9.07	9.22	8.14	8.07	7.89
	IRR	11.77%	12.33%	18.85%	17.40%	19.05%
	GWP (kg CO2eq)	7.62	9.91	10.30	15.16	12.45

	ReCiPe (Pt)	0.77	0.98	1.11	1.20	0.97
	Efficiency	77.62%	70.05%	63.57%	63.27%	63.45%
Case 4	LCOH (USD/kg)	7.27	7.07	6.30	6.43	6.24
	IRR	19.21%	23.81%	28.81%	24.86%	27.11%
	GWP (kg CO2eq)	7.62	9.91	10.30	15.16	12.45
	ReCiPe (Pt)	0.77	0.98	1.11	1.20	0.97
	Efficiency	77.62%	70.05%	63.57%	63.27%	63.45%
Case 5	LCOH (USD/kg)	8.17	8.14	7.22	7.25	7.07
	IRR	15.59%	18.24%	23.90%	21.18%	23.13%
	GWP (kg CO2eq)	6.89	9.10	9.49	14.56	12.31
	ReCiPe (Pt)	0.72	0.93	1.06	1.16	0.96
	Efficiency	77.62%	70.05%	63.57%	63.27%	63.45%
Case 6	LCOH (USD/kg)	8.17	8.14	7.22	7.25	7.07
	IRR	15.59%	18.24%	23.90%	21.18%	23.13%
	GWP (kg CO2eq)	5.60	7.68	8.12	13.62	11.99
	ReCiPe (Pt)	1.24	0.83	0.96	1.09	0.95
	Efficiency	77.62%	70.05%	63.57%	63.27%	63.45%
Case 7	LCOH (USD/kg)	7.41	6.89	6.40	7.07	6.88
	IRR	18.65%	24.71%	28.25%	22.00%	24.04%
	GWP (kg CO2eq)	2.43	3.66	4.72	11.20	11.44
	ReCiPe (Pt)	0.45	0.62	0.78	0.96	0.91
	Efficiency	77.62%	70.05%	63.57%	63.27%	63.45%

Table A25 AHP-TOPSIS and AHP-VIKOR score of sensitivity analysis

	AHP-TOPSIS					AHP-VIKOR				
	LH_2	NH_3	MeOH	DBT	TOL	LH_2	NH_3	MeOH	DBT	TOL
Case 0	0.78	0.61	0.59	0.17	0.40	0.50	0.84	0.09	0.79	0.11
Case 1	0.77	0.61	0.59	0.18	0.41	0.50	0.83	0.09	0.79	0.12
Case 2	0.79	0.62	0.59	0.17	0.40	0.50	0.86	0.09	0.79	0.11
Case 3	0.77	0.60	0.59	0.20	0.42	0.33	0.96	0.17	0.79	0.15
Case 4	0.77	0.63	0.59	0.17	0.40	0.50	0.44	0.04	0.79	0.12
Case 5	0.79	0.67	0.61	0.07	0.31	0.50	0.04	0.20	0.87	0.48
Case 6	0.76	0.72	0.66	0.09	0.25	0.68	0.03	0.20	0.87	0.53
Case 7	0.85	0.82	0.70	0.05	0.07	0.54	0.01	0.20	0.85	0.79

References

Abeynaike, A., & Barbenel, Y. (2024). Energy carrier exports from New Zealand to Japan – A comparative life cycle assessment of hydrogen and ammonia. *International Journal of Hydrogen Energy*, S0360319924028209. https://doi.org/10.1016/j.ijhydene.2024.07.146

Aghbalou, N., Charki, A., Elazzouzi, S. R., & Reklaoui, K. (2018). A probabilistic assessment approach for wind turbine-site matching. *International Journal of Electrical Power and Energy Systems*, *103*, 497–510. https://doi.org/10.1016/j.ijepes.2018.06.018

Ahrens, M., Kern, F., & Schmeck, H. (2021). Strategies for an adaptive control system to improve power grid resilience with smart buildings. *Energies*, *14*(15). https://doi.org/10.3390/en14154472

Aldersey-Williams, J., & Rubert, T. (2019). Levelised cost of energy – A theoretical justification and critical assessment. *Energy Policy*, *124*, 169–179. https://doi.org/10.1016/j.enpol.2018.10.004

Alishavandi, A. M., & Moghaddas-Tafreshi, S. M. (2019). Interactive decentralized operation with effective presence of renewable energies using multi-agent systems. *International Journal of Electrical Power and Energy Systems*, *112*(December 2018), 36–48. https://doi.org/10.1016/j.ijepes.2019.04.023

Althaus, H.-J., Hischier, R., Osses, M., Primas, A., Hellweg, S., Jungbluth, N., & Chudacoff, M. (2007). *Life Cycle Inventories of Chemicals*.

Anvari-Moghaddam, A., Rahimi-Kian, A., Mirian, M. S., & Guerrero, J. M. (2017). A multi-agent based energy management solution for integrated buildings and microgrid system. *Applied Energy*, *203*, 41–56. https://doi.org/10.1016/j.apenergy.2017.06.007

Arrigoni, A., Dolci, F., Ortiz Cebolla, R., Weidner, E., D'Agostini, T., Eynard, U., Santucci, V., & Mathieux, F. (2024). *Environmental life cycle assessment (LCA) comparison of hydrogen delivery options within Europe*.

Badger, N., Boylu, R., Ilojianya, V., Erguvan, M., & Amini, S. (2024). A cradle-to-gate life cycle assessment of green methanol production using direct air capture. *Energy Advances*, *3*(9), 2311–2327. https://doi.org/10.1039/D4YA00316K

Bareiß, K., De La Rua, C., Möckl, M., & Hamacher, T. (2019). Life cycle assessment of hydrogen from proton exchange membrane water electrolysis in future energy systems. *Applied Energy*, *237*, 862–872. https://doi.org/10.1016/j.apenergy.2019.01.001

Behboodi, S., Chassin, D. P., Djilali, N., & Crawford, C. (2018). Transactive control of fast-acting demand response based on thermostatic loads in real-time retail electricity markets. *Applied Energy*, *210*, 1310–1320. https://doi.org/10.1016/j.apenergy.2017.07.058

Ben-Haim, Y. (2006). *Info-Gap Decision Theory Decisions Under Severe Uncertainty*. Elsevier. https://doi.org/10.1016/B978-0-12-373552-2.X5000-0

Bergen, A. R., & Vittal, V. (2000). *Power Systems Analysis*. Pearson.

Bertsekas, D. P. (1997). Nonlinear Programming. *Journal of the Operational Research Society*, *48*(3), 334–334. https://doi.org/10.1057/palgrave.jors.2600425

Bhandari, D. (2025, April 16). *Article: Negative Prices in CAISO*. https://resurety.com/article-negative-prices-in-caiso/

Blaauwbroek, N., Nguyen, P. H., Konsman, M. J., Shi, H., Kamphuis, R. I. G., & Kling, W. L. (2015). Decentralized Resource Allocation and Load Scheduling for Multicommodity Smart Energy Systems. *IEEE Transactions on Sustainable Energy*, *6*(4), 1506–1514. https://doi.org/10.1109/TSTE.2015.2441107

Borri, E., Tafone, A., Romagnoli, A., & Comodi, G. (2017). A preliminary study on the optimal configuration and operating range of a “microgrid scale” air liquefaction plant for Liquid Air Energy Storage. *Energy Conversion and Management*, *143*, 275–285. https://doi.org/10.1016/j.enconman.2017.03.079

Borri, E., Tafone, A., Romagnoli, A., & Comodi, G. (2021). A review on liquid air energy storage: History, state of the art and recent developments. *Renewable and Sustainable Energy Reviews*, *137*. https://doi.org/10.1016/j.rser.2020.110572

Bos, M. J., Kersten, S. R. A., & Brilman, D. W. F. (2020). Wind power to methanol: Renewable methanol production using electricity, electrolysis of water and CO2 air capture. *Applied Energy*, *264*, 114672. https://doi.org/10.1016/j.apenergy.2020.114672

Bowling, M., & Veloso, M. (2002). Multiagent learning using a variable learning rate. *Artificial Intelligence*, *136*(2), 215–250. https://doi.org/10.1016/S0004-3702(02)00121-2

Boyd, S., Parikh, N., Chu, E., Peleato, B., & Eckstein, J. (2010). Distributed optimization and statistical learning via the alternating direction method of multipliers. *Foundations and Trends in Machine Learning*, *3*(1), 1–122. https://doi.org/10.1561/2200000016

Bünning, F., Wetter, M., Fuchs, M., & Müller, D. (2018). Bidirectional low temperature district energy systems with agent-based control: Performance comparison and operation optimization. *Applied Energy*, *209*, 502–515. https://doi.org/10.1016/j.apenergy.2017.10.072

Burger, S., Chaves-Ávila, J. P., Batlle, C., & Pérez-Arriaga, I. J. (2017). A review of the value of aggregators in electricity systems. *Renewable and Sustainable Energy Reviews*, *77*, 395–405. https://doi.org/10.1016/j.rser.2017.04.014

Burgess. (2023, December 14). *First UK green hydrogen funding round awards just half of 250 MW capacity*. S&P Global Commodity Insights. https://www.spglobal.com/commodity-insights/en/news-research/latest-news/energy-transition/121423-first-uk-green-hydrogen-funding-round-awards-just-half-of-250-mw-capacity

Cai, J., Kim, D., Jaramillo, R., Braun, J. E., & Hu, J. (2016). A general multi-agent control approach for building energy system optimization. *Energy and Buildings*, *127*, 337–351. https://doi.org/10.1016/j.enbuild.2016.05.040

Chen, S.-J., & Hwang, C.-L. (1992). Fuzzy Multiple Attribute Decision Making Methods. In M. Beckmann & W. Krelle (Eds.), *Fuzzy Multiple Attribute Decision Making* (Vol. 375, pp. 289–486). Springer Berlin Heidelberg. https://doi.org/10.1007/978-3-642-46768-4_5

Chen, Y., Yu, J., & Khan, S. (2013). The spatial framework for weight sensitivity analysis in AHP-based multi-criteria decision making. *Environmental Modelling & Software*, *48*, 129–140. https://doi.org/10.1016/j.envsoft.2013.06.010

Chisalita, D.-A., Petrescu, L., & Cormos, C.-C. (2020). Environmental evaluation of european ammonia production considering various hydrogen supply chains. *Renewable and Sustainable Energy Reviews*, *130*, 109964. https://doi.org/10.1016/j.rser.2020.109964

Cho, H. H., Strezov, V., & Evans, T. J. (2024). Life cycle assessment of renewable hydrogen transport by liquid organic hydrogen carriers. *Journal of Cleaner Production*, *469*, 143130. https://doi.org/10.1016/j.jclepro.2024.143130

Claessens, B. J., Vanhoudt, D., Desmedt, J., & Ruelens, F. (2018). Model-free control of thermostatically controlled loads connected to a district heating network. *Energy and Buildings*, *159*, 1–10. https://doi.org/10.1016/j.enbuild.2017.08.052

Connelly, E., Penev, M., Elgowainy, A., & Hunter, C. (2019). *Current Status of Hydrogen Liquefaction Costs*.

Conte, G., Morganti, G., Perdon, A. M., & Scaradozzi, D. (2009). Multi-agent system theory for resource management in home automation systems. *Journal of Physical Agents*, *3*(2), 15–19. https://doi.org/10.14198/JoPha.2009.3.2.04

CSIS. (2022). *South Africa's Hydrogen Strategy*. https://www.csis.org/analysis/south-africas-hydrogen-strategy

Čuček, L., Martin, M., & Kravanja, Z. (2021). Sustainable renewable energy supply networks optimization – The gradual transition to a renewable energy system within the European Union by 2050. *Renewable and Sustainable Energy Reviews*, *146*, 111186. https://doi.org/10.1016/j.rser.2021.111186

Cui, S., He, Q., Liu, Y., Wang, T., Shi, X., & Du, D. (2021). Techno-economic analysis of multi-generation liquid air energy storage system. *Applied Thermal Engineering*, *198*. https://doi.org/10.1016/j.applthermaleng.2021.117511

Damak, C., Leducq, D., Hoang, H. M., Negro, D., & Delahaye, A. (2020). Liquid Air Energy Storage (LAES) as a large-scale storage technology for renewable energy integration – A review of investigation studies and near perspectives of LAES. *International Journal of Refrigeration*, *110*, 208–218. https://doi.org/10.1016/j.ijrefrig.2019.11.009

D'Angelo, S. C., Cobo, S., Tulus, V., Nabera, A., Martín, A. J., Pérez-Ramírez, J., & Guillén-Gosálbez, G. (2021). Planetary Boundaries Analysis of Low-Carbon Ammonia Production Routes. *ACS Sustainable Chemistry & Engineering*, *9*(29), 9740–9749. https://doi.org/10.1021/acssuschemeng.1c01915

Dantzig, G. B., & Wolfe, P. (1961). *The Decomposition Algorithm for Linear Programs* (Vol. 29, Issue 4, pp. 767–778).

Deng, W., Lai, M.-J., Peng, Z., & Yin, W. (2017). Parallel Multi-Block ADMM with o(1 / k) Convergence. *Journal of Scientific Computing*, *71*(2), 712–736. https://doi.org/10.1007/s10915-016-0318-2

DESNZ. (2023a). *Electricity generation costs 2023*.

DESNZ. (2023b). *Energy and emissions projections 2023 to 2050*. The Department for Energy Security & Net Zero.

DESNZ. (2024). *UK hydrogen strategy*. GOV.UK. https://www.gov.uk/government/publications/uk-hydrogen-strategy/uk-hydrogen-strategy-accessible-html-version

Devia, W., Agbossou, K., & Cardenas, A. (2021). An evolutionary approach to modeling and control of space heating and thermal storage systems. *Energy and Buildings*, *234*, 110674. https://doi.org/10.1016/j.enbuild.2020.110674

Dickson, R., Akhtar, M. S., Abbas, A., Park, E. D., & Liu, J. (2022). Global transportation of green hydrogen via liquid carriers: Economic and environmental sustainability analysis, policy implications, and future directions. *Green Chemistry*, *24*(21), 8484–8493. https://doi.org/10.1039/D2GC02079C

Duffie, J. A., & Beckman, W. A. (2013). *Solar Engineering of Thermal Processes*. John Wiley & Sons, Inc. https://doi.org/10.1002/9781118671603

Erbach, G., & Jensen, L. (2021). *EU hydrogen policy*.

European Central Bank. (2024, December 27). *Euro exchange rates charts*. https://www.ecb.europa.eu/stats/policy_and_exchange_rates/euro_reference_exchange_rates/html/eurofxref-graph-usd.en.html

Farinis, G., & Kanellos, F. D. (2021). Integrated energy management system for Microgrids of building prosumers. *Electric Power Systems Research*, *198*. https://doi.org/10.1016/j.epsr.2021.107357

Farshidian, B., Rajabi-Ghahnavieh, A., & Haghi, E. (2021). Planning of multi-hub energy system by considering competition issue. *International Journal of Sustainable Energy Planning and Management*, *30*, 5–20. https://doi.org/10.5278/ijsepm.6190

Firouzi, H., Ahmadabadi, M. N., Araabi, B. N., Amizadeh, S., Mirian, M. S., & Siegwart, R. (2012). Interactive Learning in Continuous Multimodal Space: A Bayesian Approach to Action-Based Soft Partitioning and Learning. *IEEE Transactions on Autonomous Mental Development*, *4*(2), 124–138. https://doi.org/10.1109/TAMD.2011.2170213

Franceschelli, M., Pilloni, A., & Gasparri, A. (2021). Multi-Agent Coordination of Thermostatically Controlled Loads by Smart Power Sockets for Electric Demand Side Management. *IEEE Transactions on Control Systems Technology*, *29*(2), 731–743. https://doi.org/10.1109/TCST.2020.2974181

Gao, Y., & Ai, Q. (2018). Hierarchical Coordination Control for Interconnected Operation of Electric-thermal-gas Integrated Energy System with Micro-energy Internet Clusters. *IEEE Journal of Emerging and Selected Topics in Power Electronics*, *6777*(c). https://doi.org/10.1109/JESTPE.2018.2838144

Geidl, M., & Andersson, G. (2007a). Integrated Modeling and Optimization of Multi-Carrier Energy Systems. *Power Systems Laboratory*, *Doctor of*(17141), 143.

Geidl, M., & Andersson, G. (2007b). Optimal power flow of multiple energy carriers. *IEEE Transactions on Power Systems*, *22*(1), 145–155. https://doi.org/10.1109/PESGM.2016.7741940

Giampieri, A., Ling-Chin, J., & Roskilly, A. P. (2024). Techno-economic assessment of offshore wind-to-hydrogen scenarios: A UK case study. *International Journal of Hydrogen Energy*, *52*, 589–617. https://doi.org/10.1016/j.ijhydene.2023.01.346

Giesen, J., & Laue, S. (2016). *Distributed Convex Optimization with Many Convex Constraints*. http://arxiv.org/abs/1610.02967

Godinho, J., Hoefnagels, R., Braz, C. G., Sousa, A. M., & Granjo, J. F. O. (2023). An economic and greenhouse gas footprint assessment of international maritime transportation of hydrogen using liquid organic hydrogen carriers. *Energy*, *278*, 127673. https://doi.org/10.1016/j.energy.2023.127673

Gonzalez De Durana, J. M., Barambones, O., Kremers, E., & Varga, L. (2014). Agent based modeling of energy networks. *Energy Conversion and Management*, *82*, 308–319. https://doi.org/10.1016/j.enconman.2014.03.018

González-Briones, A., Prieto, J., De La Prieta, F., Herrera-Viedma, E., & Corchado, J. M. (2018). Energy optimization using a case-based reasoning strategy. *Sensors (Switzerland)*, *18*(3), 1–27. https://doi.org/10.3390/s18030865

Green Hydrogen Organisation. (2025). *Accelerating the truly low-carbon hydrogen transition in Japan*.

Guerrero, J., Gebbran, D., Mhanna, S., Chapman, A. C., & Verbič, G. (2020). Towards a transactive energy system for integration of distributed energy resources: Home energy management, distributed optimal power flow, and peer-to-peer

energy trading. *Renewable and Sustainable Energy Reviews*, *132*. https://doi.org/10.1016/j.rser.2020.110000

Han, L., Wang, S., Wang, D., & Fan, X. (2013). Optimal planning of distributed generations with the combination of genetic algorithm and interval numbers TOPSIS. *IEEE Power and Energy Society General Meeting*. https://doi.org/10.1109/PESMG.2013.6672576

Haque, A. N. M. M., Nguyen, P. H., Vo, T. H., & Bliek, F. W. (2017). Agent-based unified approach for thermal and voltage constraint management in LV distribution network. *Electric Power Systems Research*, *143*, 462–473. https://doi.org/10.1016/j.epsr.2016.11.007

Harb, H., Paprott, J.-N., Matthes, P., Schütz, T., Streblow, R., & Müller, D. (2015). Decentralized scheduling strategy of heating systems for balancing the residual load. *Building and Environment*, *86*, 132–140. https://doi.org/10.1016/j.buildenv.2014.12.015

Hauschild, M. Z., Olsen, S. I., & Rosenbaum, R. K. (Eds). (2018). *Life Cycle Assessment Theory and Practice*. Springer.

He, C., Wu, L., Liu, T., & Shahidehpour, M. (2017). Robust Co-Optimization Scheduling of Electricity and Natural Gas Systems via ADMM. *IEEE Transactions on Sustainable Energy*, *8*(2), 658–670. https://doi.org/10.1109/TSTE.2016.2615104

Henwood, T. G. M. I. (1996). An algorithm for combined heat and power economic dispatch. *IEEE Transactions on Power Systems*, *11*(4), 1778–1784. https://doi.org/10.1109/59.544642

Heo, J. Y., Park, J. H., & Lee, J. I. (2022). Experimental investigation of tank stratification in liquid air energy storage (LAES) system. *Applied Thermal Engineering*, *202*. https://doi.org/10.1016/j.applthermaleng.2021.117841

Heuser, P.-M., Ryberg, D. S., Grube, T., Robinius, M., & Stolten, D. (2019). Techno-economic analysis of a potential energy trading link between Patagonia and Japan based on CO2 free hydrogen. *International Journal of Hydrogen Energy*, *44*(25), 12733–12747. https://doi.org/10.1016/j.ijhydene.2018.12.156

Homer Energy. (2016). *Homer user manual*.

Hong, Q., Meng, F., Liu, J., & Bo, R. (2023). A bilevel game-theoretic decision-making framework for strategic retailers in both local and wholesale electricity markets. *Applied Energy*, *330*. https://doi.org/10.1016/j.apenergy.2022.120311

Hori, A., Tsuyuguchi, D., & Fukuda, E. H. (2023). *A method for multi-leader-multi-follower games by smoothing the followers' response function*. http://arxiv.org/abs/2311.18601

Hu, J., & Wellman, M. P. (2003). Nash Q-Learning for General-Sum Stochastic Games. In *Journal of Machine Learning Research* (Vol. 4, pp. 1039–1069).

Hu, M., & Fukushima, M. (2011). Variational Inequality Formulation of a Class of Multi-Leader-Follower Games. *Journal of Optimization Theory and Applications*, *151*(3), 455–473. https://doi.org/10.1007/s10957-011-9901-8

Hu, M., & Fukushima, M. (2015). Multi-Leader-Follower games: Models, methods, and applications. *Journal of the Operations Research Society of Japan*, *58*(1), 1–23.

Huijbregts, M. A. J., Steinmann, Z. J. N., Elshout, P. M. F., Stam, G., Verones, F., Vieira, M., Zijp, M., Hollander, A., & Van Zelm, R. (2017). ReCiPe2016: A harmonised life cycle impact assessment method at midpoint and endpoint level. *The*

International Journal of Life Cycle Assessment, *22*(2), 138–147. https://doi.org/10.1007/s11367-016-1246-y

Hutty, T. D. T. D., Dong, S., & Brown, S. (2020). Suitability of energy storage with reversible solid oxide cells for microgrid applications. *Energy Conversion and Management*, *226*(October), 113499. https://doi.org/10.1016/j.enconman.2020.113499

Hwang, C.-L., & Yoon, K. (1981). Methods for Multiple Attribute Decision Making. In M. Beckmann & H. P. Künzi (Eds.), *Multiple Attribute Decision Making* (Vol. 186, pp. 58–191). Springer Berlin Heidelberg. https://doi.org/10.1007/978-3-642-48318-9_3

IdealHY. (2013). *Hydrogen liquefaction report* (Fuel Cells and Hydrogen Joint).

IEA. (2020). *The Future of Hydrogen Assumption annex*.

IEA. (2022). *Africa Energy Outlook 2022*.

IEA. (2024). *South Africa electricity generation by technology in the Africa Case, 2010-2040 – Charts – Data and Statistics*. IEA. https://www.iea.org/data-and-statistics/charts/south-africa-electricity-generation-by-technology-in-the-africa-case-2010-2040

IPCC. (2023). *Climate Change 2021 – The Physical Science Basis: Working Group I Contribution to the Sixth Assessment Report of the Intergovernmental Panel on Climate Change* (1st edn). Cambridge University Press. https://doi.org/10.1017/9781009157896

IPHE. (2023). *Methodology for determining the greenhouse gas emissions association with the production of hydrogen*. International Partnership for Hydrogen and Fuel Cells in the Economy.

IRENA. (2019). *Hydrogen: A renewable energy perspective*. International Renewable Energy Agency.

IRENA. (2022). *Global hydrogen trade to meet the 1.5 °C climate goal part II - Technology review of hydrogen carriers*. International Renewable Energy Agency.

Iria, J., Scott, P., Attarha, A., Gordon, D., & Franklin, E. (2022). MV-LV network-secure bidding optimisation of an aggregator of prosumers in real-time energy and reserve markets. *Energy*, *242*. https://doi.org/10.1016/j.energy.2021.122962

ISO. (2006a). *Environmental management—Life cycle assessment—Principles and framework* (No. 14040:2006).

ISO. (2006b). *Environmental management—Life cycle assessment—Requirements and guidelines* (No. 14044:2006).

Jafari, M., & Akbari Foroud, A. (2020). A medium/long-term auction-based coalition-forming model for a virtual power plant based on stochastic programming. *International Journal of Electrical Power and Energy Systems*, *118*. https://doi.org/10.1016/j.ijepes.2019.105784

Jain, R. K., Qin, J., & Rajagopal, R. (2017). Data-driven planning of distributed energy resources amidst socio-technical complexities. *Nature Energy*, *2*(8). https://doi.org/10.1038/nenergy.2017.112

Jin, J., Gubbi, J., Marusic, S., & Palaniswami, M. (2014). An information framework for creating a smart city through internet of things. *IEEE Internet of Things Journal*, *1*(2), 112–121. https://doi.org/10.1109/JIOT.2013.2296516

Jin, S., Wang, S., & Fang, F. (2021). Game theoretical analysis on capacity configuration for microgrid based on multi-agent system. *International Journal*

of Electrical Power and Energy Systems, *125*(August 2020), 106485. https://doi.org/10.1016/j.ijepes.2020.106485

Karavas, C. S., Arvanitis, K., & Papadakis, G. (2017). A game theory approach to multi-agent decentralized energy management of autonomous polygeneration microgrids. *Energies*, *10*(11). https://doi.org/10.3390/en10111756

Karavas, C. S., Kyriakarakos, G., Arvanitis, K. G., & Papadakis, G. (2015). A multi-agent decentralized energy management system based on distributed intelligence for the design and control of autonomous polygeneration microgrids. *Energy Conversion and Management*, *103*, 166–179. https://doi.org/10.1016/j.enconman.2015.06.021

Kardakos, E. G., Simoglou, C. K., & Bakirtzis, A. G. (2016). Optimal Offering Strategy of a Virtual Power Plant: A Stochastic Bi-Level Approach. *IEEE Transactions on Smart Grid*, *7*(2), 794–806. https://doi.org/10.1109/TSG.2015.2419714

Kawasaki. (2020). *Kawasaki Completes Basic Design for World's Largest Class (11,200-cubic-meter) Spherical Liquefied Hydrogen Storage Tank*. https://global.kawasaki.com/en/corp/newsroom/news/detail/?f=20201224_8018

Kennedy, J., & Eberhart, R. (1995). Particle swarm optimization. *Proceedings of ICNN'95 - International Conference on Neural Networks*, *4*, 1942–1948. https://doi.org/10.1109/ICNN.1995.488968

Kenny, J., Timoney, D., & Syron, E. (2024). A techno-economic analysis of global renewable hydrogen value chains. *International Journal of Hydrogen Energy*, *79*, 690–701. https://doi.org/10.1016/j.ijhydene.2024.06.377

Khan, M. W., Wang, J., & Xiong, L. (2021). Optimal energy scheduling strategy for multi-energy generation grid using multi-agent systems. *International Journal*

of Electrical Power and Energy Systems, *124*(August 2020), 106400. https://doi.org/10.1016/j.ijepes.2020.106400

Kim, H. J., & Kim, M. K. (2021). Risk-based hybrid energy management with developing bidding strategy and advanced demand response of grid-connected microgrid based on stochastic/information gap decision theory. *International Journal of Electrical Power and Energy Systems*, *131*. https://doi.org/10.1016/j.ijepes.2021.107046

Kim, J., Huh, C., & Seo, Y. (2022). End-to-end value chain analysis of isolated renewable energy using hydrogen and ammonia energy carrier. *Energy Conversion and Management*, *254*, 115247. https://doi.org/10.1016/j.enconman.2022.115247

Kolen, S., Molitor, C., Wagner, L., & Monti, A. (2017). Two-level agent-based scheduling for a cluster of heating systems. *Sustainable Cities and Society*, *30*, 273–281. https://doi.org/10.1016/j.scs.2017.01.014

Kou, Y., Bie, Z., Li, G., Liu, F., & Jiang, J. (2021). Reliability evaluation of multi-agent integrated energy systems with fully distributed communication. *Energy*, *224*. https://doi.org/10.1016/j.energy.2021.120123

Kou, Y., Wang, Y., Bie, Z., Wang, X., & Ding, T. (2021). Distributed accelerated descent algorithm for energy resource coordination in multi-agent integrated energy systems. *IET Generation, Transmission and Distribution*, *15*(12), 1884–1896. https://doi.org/10.1049/gtd2.12142

Kumari, A., & Tanwar, S. (2021). Multiagent-based secure energy management for multimedia grid communication using Q-learning. *Multimedia Tools and Applications*. https://doi.org/10.1007/s11042-021-11491-x

Kyriakarakos, G., Piromalis, D. D., Dounis, A. I., Arvanitis, K. G., & Papadakis, G. (2013). Intelligent demand side energy management system for autonomous polygeneration microgrids. *Applied Energy*, *103*, 39–51. https://doi.org/10.1016/j.apenergy.2012.10.011

Lee, J.-S., Cherif, A., Yoon, H.-J., Seo, S.-K., Bae, J.-E., Shin, H.-J., Lee, C., Kwon, H., & Lee, C.-J. (2022). Large-scale overseas transportation of hydrogen: Comparative techno-economic and environmental investigation. *Renewable and Sustainable Energy Reviews*, *165*, 112556. https://doi.org/10.1016/j.rser.2022.112556

Li, C., Jia, X., Zhou, Y., & Li, X. (2020). A microgrids energy management model based on multi-agent system using adaptive weight and chaotic search particle swarm optimization considering demand response. *Journal of Cleaner Production*, *262*, 121247. https://doi.org/10.1016/j.jclepro.2020.121247

Li, G., Bie, Z., Kou, Y., Jiang, J., & Bettinelli, M. (2016). Reliability evaluation of integrated energy systems based on smart agent communication. *Applied Energy*, *167*, 397–406. https://doi.org/10.1016/j.apenergy.2015.11.033

Li, W., Li, H., & Wang, S. (2021). An event-driven multi-agent based distributed optimal control strategy for HVAC systems in IoT-enabled smart buildings. *Automation in Construction*, *132*. https://doi.org/10.1016/j.autcon.2021.103919

Li, Y.-S., Zhang, H.-G., Huang, B.-N., & Teng, F. (2016). Distributed Optimal Economic Dispatch Based on Multi-Agent System Framework in Combined Heat and Power Systems. *Applied Sciences*, *6*(10), 308. https://doi.org/10.3390/app6100308

Lin, B., Wu, W., Bai, M., & Xie, C. (2019). Liquid air energy storage: Price arbitrage operations and sizing optimization in the GB real-time electricity market. *Energy Economics*, *78*, 647–655. https://doi.org/10.1016/j.eneco.2018.11.035

Lin, H., Liu, Y., Sun, Q., Xiong, R., Li, H., & Wennersten, R. (2018). The impact of electric vehicle penetration and charging patterns on the management of energy hub – A multi-agent system simulation. *Applied Energy*, *230*, 189–206. https://doi.org/10.1016/j.apenergy.2018.08.083

Liu, C., Wang, Y., & Chen, Z. (2019). Degradation model and cycle life prediction for lithium-ion battery used in hybrid energy storage system. *Energy*, *166*, 796–806. https://doi.org/10.1016/j.energy.2018.10.131

Liu, H., Li, J., & Ge, S. (2020). Research on hierarchical control and optimisation learning method of multi-energy microgrid considering multi-agent game. *IET Smart Grid*, *3*(4), 479–489. https://doi.org/10.1049/iet-stg.2019.0268

Loose, N., Thommessen, C., Mehlich, J., Derksen, C., & Eicker, S. (2020). Unified energy agents for combined district heating and electrical network simulation. *Sustainability (Switzerland)*, *12*(21), 1–16. https://doi.org/10.3390/su12219301

MAHLER. (2024). Hydrogen plant Hydroform. *Welcome to Mahler AGS – Advanced Gas Systems*. https://www.mahler-ags.com/plants/hydrogen-plant-hydroform-m/

Majidi, M., Mohammadi-Ivatloo, B., & Soroudi, A. (2019). Application of information gap decision theory in practical energy problems: A comprehensive review. *Applied Energy*, *249*, 157–165. https://doi.org/10.1016/j.apenergy.2019.04.144

Makhdoumi, A., & Ozdaglar, A. (2017). Convergence Rate of Distributed ADMM over Networks. *IEEE Transactions on Automatic Control*, *62*(10), 5082–5095. https://doi.org/10.1109/TAC.2017.2677879

Mancarella, P. (2014). MES (multi-energy systems): An overview of concepts and evaluation models. *Energy*, *65*, 1–17. https://doi.org/10.1016/j.energy.2013.10.041

Mann, C. L. (2024). *Cost of Capital and UK Business Investment: Measurement Challenges and Research Opportunities*. Bank of England. https://www.bankofengland.co.uk/-/media/boe/files/speech/2024/may/cost-of-capital-and-uk-business-investment-slides-by-catherine-l-mann.pdf

Mao, X., Yuan, K., Hu, Y., Gu, Y., Sayed, A. H., & Yin, W. (2018). *Walkman: A Communication-Efficient Random-Walk Algorithm for Decentralized Optimization*. http://arxiv.org/abs/1804.06568

Martinez-Mares, A., & Fuerte-Esquivel, C. R. (2013). A Robust Optimization Approach for the Interdependency Analysis of Integrated Energy Systems Considering Wind Power Uncertainty. *IEEE Transactions on Power Systems*, *28*(4), 3964–3976. https://doi.org/10.1109/TPWRS.2013.2263256

Mehdizadeh, A., Taghizadegan, N., & Salehi, J. (2018). Risk-based energy management of renewable-based microgrid using information gap decision theory in the presence of peak load management. *Applied Energy*, *211*, 617–630. https://doi.org/10.1016/j.apenergy.2017.11.084

Mei, J., Zuo, Y., Lee, C. H. T., Wang, X., & Kirtley, J. L. (2021). Stochastic optimization of multi-energy system operation considering hydrogen-based vehicle applications. *Advances in Applied Energy*, *2*, 100031. https://doi.org/10.1016/j.adapen.2021.100031

Meinecke, S., Sarajlić, D., Drauz, S. R., Klettke, A., Lauven, L. P., Rehtanz, C., Moser, A., & Braun, M. (2020). SimBench-A benchmark dataset of electric power

systems to compare innovative solutions based on power flow analysis. *Energies*, *13*(12). https://doi.org/10.3390/en13123290

Mirzaei, M. A., Nazari-Heris, M., Mohammadi-Ivatloo, B., Zare, K., Marzband, M., Shafie-Khah, M., Anvari-Moghaddam, A., & Catalao, J. P. S. (2021). Network-constrained joint energy and flexible ramping reserve market clearing of power-And heat-based energy systems: A two-stage hybrid igdt-stochastic framework. *IEEE Systems Journal*, *15*(2), 1547–1556. https://doi.org/10.1109/JSYST.2020.2996952

Mnih, V., Badia, A. P., Mirza, M., Graves, A., Lillicrap, T. P., Harley, T., Silver, D., & Kavukcuoglu, K. (2016). *Asynchronous Methods for Deep Reinforcement Learning*. http://arxiv.org/abs/1602.01783

Moghaddas-Tafreshi, S. M., Mohseni, S., Karami, M. E., & Kelly, S. (2019). Optimal energy management of a grid-connected multiple energy carrier micro-grid. *Applied Thermal Engineering*, *152*, 796–806. https://doi.org/10.1016/j.applthermaleng.2019.02.113

Mohamed, M. A., Jin, T., & Su, W. (2020). Multi-agent energy management of smart islands using primal-dual method of multipliers. *Energy*, *208*, 118306. https://doi.org/10.1016/j.energy.2020.118306

Monteiro, C., Ramirez-Rosado, I. J., Fernandez-Jimenez, L. A., & Ribeiro, M. (2018). New probabilistic price forecasting models: Application to the Iberian electricity market. *International Journal of Electrical Power and Energy Systems*, *103*, 483–496. https://doi.org/10.1016/j.ijepes.2018.06.005

Morgan, R., Nelmes, S., Gibson, E., & Brett, G. (2015). Liquid air energy storage—Analysis and first results from a pilot scale demonstration plant. *Applied Energy*, *137*, 845–853. https://doi.org/10.1016/j.apenergy.2014.07.109

Mota, J. F. C., Xavier, J. M. F., Aguiar, P. M. Q., & Püschel, M. (2013). D-ADMM: A communication-efficient distributed algorithm for separable optimization. *IEEE Transactions on Signal Processing*, *61*(10), 2718–2723. https://doi.org/10.1109/TSP.2013.2254478

Nash, J. F. (1950). Equilibrium points in n-person games. *Proceedings of the National Academy of Sciences*, *36*(1), 48–49. https://doi.org/10.1073/pnas.36.1.48

Nasr, M. A., Nasr-Azadani, E., Nafisi, H., Hosseinian, S. H., & Siano, P. (2020). Assessing the Effectiveness of Weighted Information Gap Decision Theory Integrated with Energy Management Systems for Isolated Microgrids. *IEEE Transactions on Industrial Informatics*, *16*(8), 5286–5299. https://doi.org/10.1109/TII.2019.2954706

Nasr, M. A., Nasr-Azadani, E., Rabiee, A., & Hosseinian, S. H. (2019). Risk-averse energy management system for isolated microgrids considering generation and demand uncertainties based on information gap decision theory. *IET Renewable Power Generation*, *13*(6), 940–951. https://doi.org/10.1049/iet-rpg.2018.5856

Nelder, J. A., & Mead, R. (1965). A Simplex Method for Function Minimization. *The Computer Journal*, *7*(4), 308–313. https://doi.org/10.1093/comjnl/8.1.27

Nemhauser, G., & Wolsey, L. (1988). *Integer and Combinatorial Optimization*. John Wiley & Sons, Inc. https://doi.org/10.1002/9781118627372

NESO. (2025, March 21). *Levelised cost of green hydrogen | National Energy System Operator*. https://www.neso.energy/data-portal/levelised-cost-green-hydrogen

Nguyen, D. H., & Ishihara, T. (2021). Distributed peer-to-peer energy trading for residential fuel cell combined heat and power systems. *International Journal of Electrical Power and Energy Systems*, *125*. https://doi.org/10.1016/J.IJEPES.2020.106533

Nicita, A., Maggio, G., Andaloro, A. P. F., & Squadrito, G. (2020). Green hydrogen as feedstock: Financial analysis of a photovoltaic-powered electrolysis plant. *International Journal of Hydrogen Energy*, *45*(20), 11395–11408. https://doi.org/10.1016/j.ijhydene.2020.02.062

Nielsen, R., & Topsoe, H. (2021). *Topsoes Ammonia cracking technology – Delivering green Hydrogen*. https://www.ammoniaenergy.org/wp-content/uploads/2021/11/Rasmus-Topsoe-NH3-cracking-AEA-2021.pdf

Niermann, M., Timmerberg, S., Drünert, S., & Kaltschmitt, M. (2021). Liquid Organic Hydrogen Carriers and alternatives for international transport of renewable hydrogen. *Renewable and Sustainable Energy Reviews*, *135*, 110171. https://doi.org/10.1016/j.rser.2020.110171

Nikmehr, N., Najafi-Ravadanegh, S., & Khodaei, A. (2017). Probabilistic optimal scheduling of networked microgrids considering time-based demand response programs under uncertainty. *Applied Energy*, *198*, 267–279. https://doi.org/10.1016/j.apenergy.2017.04.071

Nocedal, J., & Wright, S. J. (2006). *Numerical Optimization*. Springer.

Noh, H., Kang, K., & Seo, Y. (2023a). Environmental and energy efficiency assessments of offshore hydrogen supply chains utilizing compressed gaseous hydrogen, liquefied hydrogen, liquid organic hydrogen carriers and ammonia. *International Journal of Hydrogen Energy*, *48*(20), 7515–7532. https://doi.org/10.1016/j.ijhydene.2022.11.085

Noh, H., Kang, K., & Seo, Y. (2023b). Environmental and energy efficiency assessments of offshore hydrogen supply chains utilizing compressed gaseous hydrogen, liquefied hydrogen, liquid organic hydrogen carriers and ammonia.

International Journal of Hydrogen Energy, *48*(20), 7515–7532. https://doi.org/10.1016/j.ijhydene.2022.11.085

Nojavan, S., Zare, K., & Ashpazi, M. A. (2015). A hybrid approach based on IGDT-MPSO method for optimal bidding strategy of price-taker generation station in day-ahead electricity market. *International Journal of Electrical Power and Energy Systems*, *69*, 335–343. https://doi.org/10.1016/j.ijepes.2015.01.006

Nord Pool. (2024). *Nord Pool Day Ahead Auction Prices*. https://www.nordpoolgroup.com/en/market-data12/GB/Auction-prices/UK/Hourly/

Obi, M., Slay, T., & Bass, R. (2020). Distributed energy resource aggregation using customer-owned equipment: A review of literature and standards. *Energy Reports*, *6*, 2358–2369. https://doi.org/10.1016/j.egyr.2020.08.035

Office for National Statistics. (2025). *CPI Annual rate*. https://www.ons.gov.uk/economy/inflationandpriceindices/timeseries/d7g7/mm23

Oltean, M. (2008). Solving the Hamiltonian path problem with a light-based computer. *Natural Computing*, *7*(1), 57–70. https://doi.org/10.1007/s11047-007-9042-z

Ortiz Cebolla, R., Dolci, F., & Weidner, E. (2022). *Assessment of hydrogen delivery options: Feasibility of transport of green hydrogen within Europe.* Publications Office of the European Union. https://data.europa.eu/doi/10.2760/869085

Pan, J., & McElhannon, J. (2018). Future Edge Cloud and Edge Computing for Internet of Things Applications. *IEEE Internet of Things Journal*, *5*(1), 439–449. https://doi.org/10.1109/JIOT.2017.2767608

Papadias, D. D., Peng, J., & Ahluwalia, R. K. (2019). *H2@Scale: Outlook of Hydrogen Carriers at Different Scales*. Argonne National Laboratory.

https://stage.energy.gov/sites/prod/files/2020/03/f72/fcto-hydrogen-carriers-workshop-2019-anl.pdf

Patel, M., Roy, S., Roskilly, A. P., & Smallbone, A. (2022). The techno-economics potential of hydrogen interconnectors for electrical energy transmission and storage. *Journal of Cleaner Production*, *335*, 130045. https://doi.org/10.1016/j.jclepro.2021.130045

Petcu, A., & Faltings, B. (2005). *A Scalable Method for Multiagent Constraint Optimization*. http://liawww.epfl.ch/

Peterson, D., Vickers, J., & DeSantis, D. (2020). *Hydrogen Production Cost From PEM Electrolysis—2019*. Department of Energy.

Powell, W. B., & Meisel, S. (2016). Tutorial on Stochastic Optimization in Energy—Part I: Modeling and Policies. *IEEE Transactions on Power Systems*, *31*(2), 1459–1467. https://doi.org/10.1109/TPWRS.2015.2424974

Qi, M., Park, J., Lee, I., & Moon, I. (2022). Liquid air as an emerging energy vector towards carbon neutrality: A multi-scale systems perspective. *Renewable and Sustainable Energy Reviews*, *159*, 112201. https://doi.org/10.1016/j.rser.2022.112201

Raab, M., Maier, S., & Dietrich, R.-U. (2021). Comparative techno-economic assessment of a large-scale hydrogen transport via liquid transport media. *International Journal of Hydrogen Energy*, *46*(21), 11956–11968. https://doi.org/10.1016/j.ijhydene.2020.12.213

Rahimiyan, M., & Baringo, L. (2016). Strategic Bidding for a Virtual Power Plant in the Day-Ahead and Real-Time Markets: A Price-Taker Robust Optimization Approach. *IEEE Transactions on Power Systems*, *31*(4), 2676–2687. https://doi.org/10.1109/TPWRS.2015.2483781

Rahman, M. S., & Kaykobad, M. (2005). On hamiltonian cycles and hamiltonian paths. *Information Processing Letters*, *94*(1), 37–41. https://doi.org/10.1016/j.ipl.2004.12.002

Rehman, S., Natarajan, N., Mohandes, M. A., Meyer, J. P., Alam, M. M., & Alhems, L. M. (2022). Wind and wind power characteristics of the eastern and southern coastal and northern inland regions, South Africa. *Environmental Science and Pollution Research*, *29*(57), 85842–85854. https://doi.org/10.1007/s11356-021-14276-9

Reksten, A. H., Thomassen, M. S., Møller-Holst, S., & Sundseth, K. (2022). Projecting the future cost of PEM and alkaline water electrolysers; a CAPEX model including electrolyser plant size and technology development. *International Journal of Hydrogen Energy*, *47*(90), 38106–38113. https://doi.org/10.1016/j.ijhydene.2022.08.306

Ren, H., Ma, Z., Ming Lun Fong, A., & Sun, Y. (2022). Optimal deployment of distributed rooftop photovoltaic systems and batteries for achieving net-zero energy of electric bus transportation in high-density cities. *Applied Energy*, *319*, 119274. https://doi.org/10.1016/j.apenergy.2022.119274

Restelli, F., Spatolisano, E., Pellegrini, L. A., Cattaneo, S., De Angelis, A. R., Lainati, A., & Roccaro, E. (2024). Liquefied hydrogen value chain: A detailed techno-economic evaluation for its application in the industrial and mobility sectors. *International Journal of Hydrogen Energy*, *52*, 454–466. https://doi.org/10.1016/j.ijhydene.2023.10.107

Rezaei, M., Akimov, A., & Gray, E. MacA. (2024). Cost-competitiveness of green hydrogen and its sensitivity to major financial and technical variables.

International Journal of Hydrogen Energy, *90*, 1365–1377. https://doi.org/10.1016/j.ijhydene.2024.10.068

Ruiz, N., Cobelo, I., & Oyarzabal, J. (2009). A direct load control model for virtual power plant management. *IEEE Transactions on Power Systems*, *24*(2), 959–966. https://doi.org/10.1109/TPWRS.2009.2016607

Saaty, R. W. (1987). The analytic hierarchy process—What it is and how it is used. *Mathematical Modelling*, *9*(3–5), 161–176. https://doi.org/10.1016/0270-0255(87)90473-8

Samadi, E., Badri, A., & Ebrahimpour, R. (2020). Decentralized multi-agent based energy management of microgrid using reinforcement learning. *International Journal of Electrical Power and Energy Systems*, *122*. https://doi.org/10.1016/j.ijepes.2020.106211

San Cristóbal, J. R. (2011). Multi-criteria decision-making in the selection of a renewable energy project in spain: The Vikor method. *Renewable Energy*, *36*(2), 498–502. https://doi.org/10.1016/j.renene.2010.07.031

Scholvin, S., Black, A., & Robbins, G. (2025). De-risking green hydrogen? Insights from Chile and South Africa. *Energy Policy*, *198*, 114485. https://doi.org/10.1016/j.enpol.2024.114485

Shabani, M. J., & Moghaddas-Tafreshi, S. M. (2020). Fully-decentralized coordination for simultaneous hydrogen, power, and heat interaction in a multi-carrier-energy system considering private ownership. *Electric Power Systems Research*, *180*(April 2019), 106099. https://doi.org/10.1016/j.epsr.2019.106099

Shabanzadeh, M., Sheikh-El-Eslami, M. K., & Haghifam, M. R. (2016). A medium-term coalition-forming model of heterogeneous DERs for a commercial virtual

power plant. *Applied Energy*, *169*, 663–681. https://doi.org/10.1016/j.apenergy.2016.02.058

Shah, S. M., & Avrachenkov, K. E. (2018). *Linearly Convergent Asynchronous Distributed ADMM via Markov Sampling*. http://arxiv.org/abs/1810.05067

Shapley, L. S. (1971). Cores of convex games. *International Journal of Game Theory*, *1*(1), 11–26. https://doi.org/10.1007/BF01753431

She, X., Peng, X., Nie, B., Leng, G., Zhang, X., Weng, L., Tong, L., Zheng, L., Wang, L., & Ding, Y. (2017). Enhancement of round trip efficiency of liquid air energy storage through effective utilization of heat of compression. *Applied Energy*, *206*, 1632–1642. https://doi.org/10.1016/j.apenergy.2017.09.102

Sheikhi, A., Rayati, M., & Ranjbar, A. M. (2016). Dynamic load management for a residential customer; Reinforcement Learning approach. *Sustainable Cities and Society*, *24*, 42–51. https://doi.org/10.1016/j.scs.2016.04.001

Shen, X., Luo, Z., Xiong, J., Liu, H., Lv, X., Tan, T., Zhang, J., Wang, Y., & Dai, Y. (2021). Optimal Hybrid Energy Storage System Planning of Community Multi-Energy System Based on Two-Stage Stochastic Programming. *IEEE Access*, *9*, 61035–61047. https://doi.org/10.1109/ACCESS.2021.3074151

Sherson, T., Heusdens, R., & Kleijn, W. B. (2017). *Derivation and Analysis of the Primal-Dual Method of Multipliers Based on Monotone Operator Theory*. http://arxiv.org/abs/1706.02654

Shomalzadeh, K., Scherpen, J. M. A., & Camlibel, M. K. (2022). Bilevel aggregator-prosumers' optimization problem in real-time: A convex optimization approach. *Operations Research Letters*, *50*(5), 568–573. https://doi.org/10.1016/j.orl.2022.08.008

Sirojan, T., Lu, S., Phung, B. T., & Ambikairajah, E. (2019). Embedded Edge Computing for Real-time Smart Meter Data Analytics. *2019 International Conference on Smart Energy Systems and Technologies (SEST)*, 1–5. https://doi.org/10.1109/SEST.2019.8849012

Skarvelis-Kazakos, S., Papadopoulos, P., Grau Unda, I., Gorman, T., Belaidi, A., & Zigan, S. (2016). Multiple energy carrier optimisation with intelligent agents. *Applied Energy*, *167*, 323–335. https://doi.org/10.1016/j.apenergy.2015.10.130

Song, S., Lin, H., Sherman, P., Yang, X., Nielsen, C. P., Chen, X., & McElroy, M. B. (2021). Production of hydrogen from offshore wind in China and cost-competitive supply to Japan. *Nature Communications*, *12*(1), 6953. https://doi.org/10.1038/s41467-021-27214-7

Soroudi, A., Aien, M., & Ehsan, M. (2012). A probabilistic modeling of photo voltaic modules and wind power generation impact on distribution networks. *IEEE Systems Journal*, *6*(2), 254–259. https://doi.org/10.1109/JSYST.2011.2162994

South Africa Reserve Bank. (2024). *Current Market Rates*. South African Reserve Bank. https://www.resbank.co.za/en/home/what-we-do/statistics/key-statistics/current-market-rates

Su, K., Du, H., Zhao, X., Wang, X., Zhang, X., Lu, Y., She, X., & Wang, C. (2023). Tech-economic analysis of liquid air energy storage—A promising role for carbon neutrality in China. *Journal of Energy Storage*, *72*. https://doi.org/10.1016/j.est.2023.108786

Sutton, R. S., & Barto, A. G. (2018). *Reinforcement learning: An introduction*. MIT Press.

Tafone, A., Romagnoli, A., Borri, E., & Comodi, G. (2019). New parametric performance maps for a novel sizing and selection methodology of a Liquid Air

Energy Storage system. *Applied Energy*, *250*, 1641–1656. https://doi.org/10.1016/j.apenergy.2019.04.171

Terlouw, T., Treyer, K., Bauer, C., & Mazzotti, M. (2021). Life Cycle Assessment of Direct Air Carbon Capture and Storage with Low-Carbon Energy Sources. *Environmental Science & Technology*, *55*(16), 11397–11411. https://doi.org/10.1021/acs.est.1c03263

Tezer, T., Yaman, R., & Yaman, G. (2017). Evaluation of approaches used for optimization of stand-alone hybrid renewable energy systems. *Renewable and Sustainable Energy Reviews*, *73*, 840–853. https://doi.org/10.1016/j.rser.2017.01.118

Wahbah, M., Mohandes, B., EL-Fouly, T. H. M., & El Moursi, M. S. (2022). Unbiased cross-validation kernel density estimation for wind and PV probabilistic modelling. *Energy Conversion and Management*, *266*(May), 115811. https://doi.org/10.1016/j.enconman.2022.115811

Wang, H., Zhang, C., Li, K., & Ma, X. (2021). Game theory-based multi-agent capacity optimization for integrated energy systems with compressed air energy storage. *Energy*, *221*. https://doi.org/10.1016/j.energy.2021.119777

Wang, T., & Zhang, L. (2021). Coordinated scheduling of integrated energy microgrid with multi-energy hubs based on MADDPG and two-layer game. *Journal of Renewable and Sustainable Energy*, *13*(6). https://doi.org/10.1063/5.0051840

Wei, Q., Liu, D., & Shi, G. (2015). A novel dual iterative Q-learning method for optimal battery management in smart residential environments. *IEEE Transactions on Industrial Electronics*, *62*(4), 2509–2518. https://doi.org/10.1109/TIE.2014.2361485

Wernet, G., Bauer, C., Steubing, B., Reinhard, J., Moreno-Ruiz, E., & Weidema, B. (2016). The ecoinvent database version 3 (part I): Overview and methodology. *The International Journal of Life Cycle Assessment*, *21*(9), 1218–1230. https://doi.org/10.1007/s11367-016-1087-8

West, D. B. (2001). *Introduction to graph theory* (Vol. 2).

Wijayanta, A. T., Oda, T., Purnomo, C. W., Kashiwagi, T., & Aziz, M. (2019). Liquid hydrogen, methylcyclohexane, and ammonia as potential hydrogen storage: Comparison review. *International Journal of Hydrogen Energy*, *44*(29), 15026–15044. https://doi.org/10.1016/j.ijhydene.2019.04.112

Wulf, C., Reuß, M., Grube, T., Zapp, P., Robinius, M., Hake, J.-F., & Stolten, D. (2018). Life Cycle Assessment of hydrogen transport and distribution options. *Journal of Cleaner Production*, *199*, 431–443. https://doi.org/10.1016/j.jclepro.2018.07.180

Xi, L., Yu, L., Xu, Y., Wang, S., & Chen, X. (2020). A Novel Multi-Agent DDQN-AD Method-Based Distributed Strategy for Automatic Generation Control of Integrated Energy Systems. *IEEE Transactions on Sustainable Energy*, *11*(4), 2417–2426. https://doi.org/10.1109/TSTE.2019.2958361

Xiao, Y., Xiao, Y., Wang, X., Pinson, P., & Wang, X. (2020). Transactive Energy Based Aggregation of Prosumers as a Retailer. *IEEE Transactions on Smart Grid*, *11*(4), 3302–3312. https://doi.org/10.1109/TSG.2020.2976130

Xiong, Z., Kang, J., Niyato, D., Wang, P., & Poor, H. V. (2020). Cloud/Edge Computing Service Management in Blockchain Networks: Multi-Leader Multi-Follower Game-Based ADMM for Pricing. *IEEE Transactions on Services Computing*, *13*(2), 356–367. https://doi.org/10.1109/TSC.2019.2947914

Yan, C., Wang, C., Hu, Y., Yang, M., & Xie, H. (2021). Optimal operation strategies of multi-energy systems integrated with liquid air energy storage using information gap decision theory. *International Journal of Electrical Power and Energy Systems*, *132*. https://doi.org/10.1016/j.ijepes.2021.107078

Yang, L., Zhang, X., & Gao, P. (2018). Research on heat and electricity coordinated dispatch model for better integration of wind power based on electric boiler with thermal storage. *IET Generation, Transmission and Distribution*, *12*(15), 3736–3743. https://doi.org/10.1049/iet-gtd.2017.2032

Ye, Y., Chen, H., Ma, Z., & Xiao, M. (2020). Decentralized Consensus Optimization Based on Parallel Random Walk. *IEEE Communications Letters*, *24*(2), 391–395. https://doi.org/10.1109/LCOMM.2019.2955442

Yu, L., Sun, Y., Xu, Z., Shen, C., Yue, D., Jiang, T., & Guan, X. (2021). Multi-Agent Deep Reinforcement Learning for HVAC Control in Commercial Buildings. *IEEE Transactions on Smart Grid*, *12*(1), 407–419. https://doi.org/10.1109/TSG.2020.3011739

Zamani, A. G., Zakariazadeh, A., Jadid, S., & Kazemi, A. (2016). Stochastic operational scheduling of distributed energy resources in a large scale virtual power plant. *International Journal of Electrical Power and Energy Systems*, *82*, 608–620. https://doi.org/10.1016/j.ijepes.2016.04.024

Zeng, C., Jiang, Y., Liu, Y., Tan, Z., He, Z., & Wu, S. (2019). Optimal dispatch of integrated energy system considering energy hub technology and multi-agent interest balance. *Energies*, *12*(16). https://doi.org/10.3390/en12163112

Zhang, J., Zhu, L., Wang, Y., Sun, Y., Yan, Z., & Zhou, B. (2023). Global sensitivity analysis and stochastic optimization of multi-energy complementary distributed

energy system considering multiple uncertainties. *Journal of Cleaner Production*, *389*, 136120. https://doi.org/10.1016/j.jclepro.2023.136120

Zhang, N., Sun, Q., Wang, J., & Yang, L. (2021). Distributed Adaptive Dual Control via Consensus Algorithm in the Energy Internet. *IEEE Transactions on Industrial Informatics*, *17*(7), 4848–4860. https://doi.org/10.1109/TII.2020.3031437

Zhang, R., Li, G., Jiang, T., Chen, H., Li, X., Pei, W., & Xiao, H. (2021). Incorporating Production Task Scheduling in Energy Management of an Industrial Microgrid: A Regret-Based Stochastic Programming Approach. *IEEE Transactions on Power Systems*, *36*(3), 2663–2673. https://doi.org/10.1109/TPWRS.2020.3037831

Zhang, X., & Yu, T. (2019). Fast Stackelberg equilibrium learning for real-time coordinated energy control of a multi-area integrated energy system. *Applied Thermal Engineering*, *153*, 225–241. https://doi.org/10.1016/j.applthermaleng.2019.02.053

Zhao, P., Suryanarayanan, S., & Simoes, M. G. (2013). An energy management system for building structures using a multi-agent decision-making control methodology. *IEEE Transactions on Industry Applications*, *49*(1), 322–330. https://doi.org/10.1109/TIA.2012.2229682

Zhou, X., Yang, C., & Gui, W. (2012). State transition algorithm. *Journal of Industrial and Management Optimization*, *8*(4), 1039–1056. https://doi.org/10.3934/jimo.2012.8.1039

Zhou, X., Yang, C., & Gui, W. (2019). A Statistical Study on Parameter Selection of Operators in Continuous State Transition Algorithm. *IEEE Transactions on Cybernetics*, *49*(10), 3722–3730. https://doi.org/10.1109/TCYB.2018.2850350

Zhou, Y., Duan, L., Ding, X., Bao, Y., & Tian, F. (2023). Economic feasibility assessment of a solar aided liquid air energy storage system with different operation strategies. *Journal of Energy Storage*, *72*. https://doi.org/10.1016/j.est.2023.108812

Zhu, J., Jing, Z., Ji, T., & Larik, N. A. (2020). Energy-economy coupled simulation approach and simulator based on individual-based model. *Energies*, *13*(11). https://doi.org/10.3390/en13112771